VECTOR VORTEX MODES IN FEW MODE OPTICAL FIBERS: GENERATION AND CHARACTERIZATION

Submitted in partial fulfilment of the requirements
for the award of the degree of

DOCTOR OF PHILOSOPHY

by

C. Hari Krishna

Roll no. 701441

Supervisor

Dr. Sourabh Roy

DEPARTMENT OF PHYSICS
NATIONAL INSTITUTE OF TECHNOLOGY
WARANGAL, INDIA
JULY, 2019.

राष्ट्रीय प्रौद्योगिकी संस्थान, वारांगल
NATIONAL INSTITUTE OF TECHNOLOGY
WARANGAL-506 004
DEPARTMENT OF PHYSICS

Date: 16 - 03 -2020

APPROVAL OF THE VIVA-VOCE BOARD

Certified that the thesis entitled **"Vector Vortex Modes in Few Mode Optical Fibers: Generation and Characterization"** submitted by **C. Hari Krishna** (Roll No. 701441) to the National Institute of Technology, Warangal, for the award of the degree ***Doctor of Philosophy*** has been accepted by the external examiners and that the student has successfully defended the thesis in the viva-voce examination held today.

(Member of the DSC) (Member of the DSC) (Member of the DSC)

(External Examiner) (Supervisor)

(HOD & Chairman of DSC)

NATIONAL INSTITUTE OF TECHNOLOGY
DEPARTMENT OF PHYSICS

CERTIFICATE

This is to certify that the thesis entitled **"Vector vortex modes in few mode optical fibers: Generation and characterization"** is being submitted by **Mr. C. Hari Krishna** to the Department of Physics, National Institute of Technology, Warangal, India, is a record of Bonafide research work carried out by him under my supervision and it has not been submitted elsewhere for award of any degree.

(Dr. SOURABH ROY)
Associate Professor
Thesis Supervisor

DECLARATION

This is to certify that the work presented in the thesis entitled **" Vector vortex modes in few mode optical fibers: Generation and characterization**" is a Bonafide work done by me under the supervision of **Dr. Sourabh Roy,** Associate Professor, Department of Physics, National Institute of Technology, Warangal, and was not submitted elsewhere for the award of any degree.

I declare that this written submission represents my ideas in my own words and where others' ideas or words have been included, I have adequately cited and referenced the original sources. I also declare that I have adhered to all principles of academic honesty and integrity and have not miss represented or fabricated or falsified any idea/ data/ fact/ source in my submission. I understand that any violation of the above will be a cause for disciplinary action by the institute and can also evoke penal action from the sources which have thus not been properly cited or from whom proper permission has not been taken when needed.

(C. Hari Krishna)

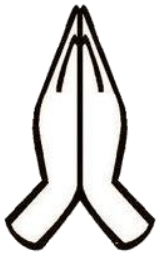

The tribute to my parents

Jyothi & Ráma Chary

Dare to be free,

Dare to go as far as your thought leads,

And, Dare to carry that out in your life.

-Swami Vivekananda

ACKNOWLEDGEMENTS

I take this opportunity to thank the people who have been involved in my efforts directly or indirectly, to complete this dissertation. The words mentioned here may not be sufficient to express my gratitude towards them.

Foremost, I sincerely thank my supervisor, **Dr. Sourabh Roy**, for his valuable guidance, motivation and encouragement throughout my work. It has been great pleasure for me to work under his guidance. I am thankful to my supervisor for believing in me, giving me freedom in pursuing my own ideas and also patiently bearing me. This thesis wouldn't have been possible without his immense support, academically and personally.

I am thankful to my Doctoral Scrutiny Committee members, **Prof. K. Venu Gopal Reddy** (Head of the department), **Prof. M. Sai Shankar**, **Prof. R.L.N. Sai Prasad**, **Prof. S.V.S. Ramana Reddy** and **Prof. Debashish Dutta** (Mathematics department) for constantly reviewing my progress and providing valuable suggestions in a constructive way that helped me to carry forward my work successfully. I am very thankful to **Prof. M. Raja Vishwanathan** for his help in proof reading the thesis. I would like to extend my sincere thanks to all the faculty members, office staff and students of Physics department for their support, whenever necessary.

I am deeply indebted to **Dr. Shankar Pidishety** and **Dr. Vijay Kumar** for helping me in understanding the concepts of the problem chosen and also for the technical support given whenever needed. I am extremely thankful to **Dr. P. Kishore** and **Dr. Onkar Nath Verma** for constant support and endless discussions. These people have had a great impact on my thought process and research work.

I have great respect for the worldwide research community who had contributed a lot and have been contributing to science and constantly inspiring young minds.

It would be ungrateful on my part if I forget to recall my teachers **Mr. T. Rama Krishna, Mr. Veerendra Babu,** and **Mr. Vishveshwar,** who inspired me in my graduation days to take up this career.

I enjoyed the company of my seniors, **Dr. Vengal Rao, Dr. Rajeshwar Rao, Dr. Nanda Kishore, Dr. Hima Mahesh** and **Dr. Raj Kumar** and had wonderful time working with them. I am deeply indebted to my dearest friend **Dr. Venkat Reddy** for his affection and suggestions in my academics. I had great time with my friends **Mr. Mohan Babu, Dr. Suman, Mr. Ashish,** and **Mr. Ramarajan** during my stay at NIT Warangal. It has been a great pleasure working with my lab mates, **Ms. Sravanthi, Mr. Pavan, Mr. Koustav Dey,** and **Mr. Rajesh** who had been very supportive in all aspects. The time spent with all these people was full of joy and reenergized me to work with more determination.

I thank OSA, the optical society for travel grants to attend international conference.

No words can adequately express my gratitude towards the love, support and patience that I received from my family. It is the constant motivation from my mother that has guided me through the odds and helped me in completing the work. I thank my sisters for their support in all aspects. Finally, I would like to thank my wife for the love and affection showered on me all the time.

CONTENTS

NOTATIONS

n_{co}	Core refractive index
n_{cl}	Cladding refractive index
$n(r)$	Transverse refractive index profile
Δ	Relative refractive index
(r, ϕ, z)	Cylindrical coordinates
(x, y, z)	Cartesian coordinates
ρ	Core radius
$E(x, y, z)$	Electric field
$H(x, y, z)$	Magnetic field
ε_o	Permittivity of free-space
μ_o	Permeability of free-space
J	Current density
ρ	Charge density
$\nabla \times$	Curl operator
$\nabla.$	Divergence operator
∇^2	Laplacian operator
k	Wave number
ω	Angular frequency
λ	Wavelength
β	Propagation constant
$\tilde{\beta}$	Scalar propagation constant
$U, V, and\ W$	Dimensionless fiber parameter
J_l	Bessel function of first kind
K_l	Bessel function of second kind
α	Anisotropy parameter
δ, γ	Relative phase differences

ABBREVIATIONS

LG	Laguerre Gaussian
HG	Hermite Gaussian
BG	Bessel Gaussian
OVB	Optical vortex beam
CVB	Cylindrical vector beam
VVM	Vector vortex mode
OAM	Orbital angular momentum
SAM	Spin angular momentum
SPP	Spiral phase plate
SLM	Spatial light modulator
FMF	Few mode fiber
LP	Linearly polarized
SOP	State of polarization
HWP	Half wave plate
QWP	Quarter wave plate
ND	Neutral density
CL	Cylindrical lens
MO	Microscope objective
BS	Beam splitter
CCD	Charge coupled device
TE	Transverse electric
TM	Transverse magnetic
TEM	Transverse electromagnetic
HOPS	Higher order Poincare sphere
SVB	Spiral vector beam
CW	Clockwise
CCW	Counter clockwise
SOI	Spin orbit interactions

LIST OF FIGURES

ABSTRACT

Phase, polarization and intensity are the most important features of an electromagnetic beam field, which helps us in understanding the field distribution across the beam, its interactions with other fields and also with matter. Recently, optical beams with complex or inhomogeneous phase and polarization topology are gaining much importance over beams with homogeneous phase and polarization states, leading to a new branch of optics known as *singular optics*. It deals with complex light beams that are either phase or polarization singular, which are referred to as scalar and vector vortex modes respectively. The advent of laser technology paved the path for generation of such complex light beams by modifying the cavity so as to generate modes of desired phase and polarization. Later, many methods are reported on the generation and study of the characteristics of such complex fields thereby hinting at possible applications. In early 90's, it was reported that beams with helical phase structure are associated with orbital angular momentum of light which are in recent days finding applications in optical tweezing and advanced optical communication via orbital angular momentum mode multiplexing. Additionally, beams with inhomogeneous polarization states are found to be useful in microscopy, data encoding, lithography and laser machining.

There are numerous active and passive methods proposed to generate phase and polarization structured beams in order to address the stability and controllability of such fields as well as aiming at various applications. Most of the methods use bulk optical setups, which include complex micro-structured devices to generate complex optical beams that increase the cost of experiments. One of the most convenient and cost-effective methods of generating such fields is optical fibers. Optical fiber is an inhomogeneous, dielectric, cylindrical optical waveguide whose eigen modes have spatially inhomogeneous polarization and are known as cylindrical vector beams or zeroth order vector modes. These modes includes radial, azimuthal and hybridly polarized vector modes.

In this thesis, we are devoted to generate and characterize such complex vector fields using a few mode optical fiber by controlling the coupling conditions of fiber with input Gaussian beam. Our method fully relies on precise control over coupling conditions and the input state of polarization which has the potential to switch between various vector fields. We begin the thesis with a brief introduction to phase and polarization structured beams with their generation schemes and possible applications. Further, we analyze the wave propagation mechanism in optical fibers with the help of Maxwell's equations to understand the origin of

polarization inhomogeneity of the modes. Various vector modes in optical fiber are generated and characterized using standard Stokes polarimetry. An attempt has been made to represent linearly polarized modes of optical fiber and their combinational vector modes onto standard and higher order Poincare sphere respectively. We have also generated polarization singular beams that are a combination of Gaussian and vortex modes of orthogonal polarizations within the fiber by selective excitation of modes. Complex polarization topologies such as lemon, star and monstar are generated and also the formation of dipoles is studied. The behavior of polarization singular beams under the action of half wave plate and cylindrical lens are studied.

CHAPTER

1

Introduction

Contents

CHAPTER 1

Introduction

1.1 Introduction

Singular optics, the branch of optics that deals with light beams having complex phase and polarization topology, is fast developing owing to its promising features and fundamental nature of scientific interest [1]. Phase and polarization, in addition to intensity are the skeleton of an electromagnetic beam field, which helps one in understanding the properties of the field and also its interactions with itself and matter. The complex nature of light beams leads to singular regions (undetermined state) across the beams either in phase or polarization. Such beams are popularly known as vortex beams and are classified as scalar and vector vortices depending on whether the singularity is in phase or in polarization respectively [2,3]. Generally, scalar vortices or phase singularities can be observed in null intensity regions of higher order Laguerre-Gaussian (LG) and Bessel-Gaussian (BG) beams with annular intensity profile. These beams are usually homogeneously polarized and are often referred to as optical vortex beams (OVBs), which have phase circulation of 0 to 2π around the center of the beam resulting from the helicity of wave front and are generally known as phase vortices. The vortex nature was first identified by Nye in electromagnetic waves, which is analogous to dislocations in crystals [4]. Later, Allen et al. reported that the phase singularity of these beams has a direct connection with their orbital angular momentum (OAM) which kickstarted the massive research in the respective areas for a better understanding of the nature of beams and their possible applications [5,6].

On the other hand, vector vortices are beams with similar intensity profile as that of OVBs but with spatial inhomogeneous polarization and are known as cylindrical vector beams (CVBs) due to their cylindrically symmetric polarization distribution [7]. Radial and azimuthal vector beams are popularly known CVBs, which are the solutions to vector wave equation and have exceptional focusing properties when focused under high numerical aperture lens [8]. This unique sharp focusing feature enables the beams to be useful in laser machining, lithography, and also in the generation of optical needles [9,10]. Additionally, CVBs along with OVBs are also finding applications in high resolution imaging, optical communications, optical tweezers, and also in entanglement

[11-15]. With a wide spectrum of applications, these beams have drawn the interest of researchers for controlled generation and manipulation of complex light beams.

The generation of these beams is mainly classified into two types, active and passive. In active methods, CVBs are directly generated from laser output by modifying the cavity of laser using intra-cavity optical elements such as axial birefringent material like calcite [16], conical axicon [17], Brewster angle reflector [18,19], and polarization sensitive cavity mirrors [20]. In passive methods, the fundamental Gaussian mode from the laser is modified using special optical devices outside the cavity to generate OVBs and CVBs. Computer generated holograms and astigmatic mode converters are simple and cost effective free-space methods of generating OVBs. In computer generated holograms, a fork like pattern is printed onto a transparent substrate, on passing through which a Gaussian beam gets diffracted and converts into a helically phased LG beam in first order diffraction pattern. Whereas, the astigmatic mode converters (a pair of cylindrical lenses) impart an additional phase to a Hermite Gaussian (HG) beam that pass through them, resulting in generation of an LG beam [21,22]. Nowadays, spiral phase plate (SPP) and liquid crystal on silicon based spatial light modulator (LCoS-SLM) are being used to generate OVBs. SPP is a micro structured optical element with an inscribed step that introduces azimuthal phase dependence to the incoming plane phased beam while SLM is a voltage controlled device onto which the phase of desired mode can be loaded using a computer, which when illuminated with laser, generates a mode of desired phase [23,24]. These methods are useful in generating OVBs only i.e., the scalar vortex beams with uniform polarization distribution.

Interferometric technique is useful in generating CVBs by combining two modes of orthogonal polarization [25]. In recent days, micro-structured optical devices such as q-plates serves the needs of generating various vector modes including some novel vector fields [26,27]. Alternatively, the methods that involve optical fibers can directly generate CVBs by selective excitation of inherent waveguide modes [28,29]. The flexibility in generation of nearly degenerate guiding modes with a precise control over coupling conditions makes optical fibers one of the widely used method to generate and study the characteristics of CVBs. Moreover, optical fibers provide an opportunity to explore mode mixing phenomenon, which is quite common and interesting that helps in understanding the evolution of modes with scalar and vector singularities. Optical fiber is an inhomogeneous cylindrical dielectric waveguide in which the eigen modes are the

solutions of vector wave equation. These modes have inhomogeneous spatial polarization and are generally referred to as zeroth order vector modes which include radially polarized TM_{01}, azimuthally polarized $TE_{01}$and hybridly polarized $HE_{21}^{odd,even}$ [29]. All these modes can be excited in optical fiber by precise control over coupling conditions.

1.1.1 Review on fiber based vortex beam generation

Exploiting the selective mode excitation in optical fibers, many methods were proposed to generate radial, azimuthal and hybrid vector beams. Volpe and Petrov demonstrated a method to generate all possible vector modes by launching first order LG beam into the optical fiber and efficiently converted the arbitrary vector beams to pure CVBs using true polarization rotator [30]. Later, T. Grosjean et al. using a pi-phase discontinuity element designed a stable system to generate vector beams in few mode fiber (FMF) with remarkable purity of polarization state [31]. They have also demonstrated an all-fiber method to generate radial and other polarized beams using a combination of mono-mode and bi-mode optical fiber [32]. Wei Gao et al. used multimode liquid core optical fiber for the same and also verified the existence of phase vortices in the generated fields [33]. Recently, a group led by S. Ramachandran designed and fabricated a ring core optical fiber which supports the generation and propagation of donut shaped vector beams for long distances without much distortion, which can find applications in creating a new degrees of freedom for fiber optic communication [34]. The group also demonstrated the generation of modes that carry OAM by exciting the combination of hybrid modes in specially fabricated fiber [35] as well as a method for generating Bessel like beams in higher order linearly polarized modes of optical fiber [36]. A new variety of hybridly polarized beams that have different state of polarization (SOP) on the beam cross section have been recently reported to be generated from a spun fiber, which are named Hybrid-Azimuthal-Radially Polarized modes, HARP in short [37]. The generation and switching between various vector modes has been demonstrated by N.K. Vishwanathan and his co-workers using an optical fiber that supports two modes [38,39]. They have also demonstrated the generation of propagation invariant Bessel beams and dark hollow beams using a micro axicon etched on tip of a fiber [40,41]. Special fibers such as Polarization maintaining optical fibers and photonic crystal fibers are also being used to generate OAM beams, which find applications in sensing and imaging [42-44]. Recently, a micro sized SPP was fabricated onto the fiber tip by focused ion beam which can

efficiently generate the vortex beam [45]. Fused fiber couplers, which are based on mode selective coupling are becoming popular in recent years as the CVBs can be generated using them with good modal purity and stability [46,47].

In this thesis, we demonstrate fiber based method for controlled generation of various vector modes in addition to well-known zeroth order vector modes. The generation of these vector modes is shown to be the inherent combination of first order linearly polarized modes (LP_{11}) with orthogonal polarizations. Stokes polarimetry is used as key characterization tool for the analysis of generated modes by obtaining their spatial polarization distribution and ellipse orientation maps [48]. We have also made a representation of these modes on higher order Poincare sphere which is analogous to that proposed by Milione [49] and justify their positions based on the position of LP_{11} modes on standard Poincare sphere, that combine to generate respective vector modes. Finally, we have experimentally demonstrated controlled generation of C-point polarization singularities in fibers and studied the role of half wave plate and a cylindrical lens in switching C-points from lemon to star and vice-versa.

1.2 Motivation

In view of flexibility in operation and having CVBs as inherent waveguide modes, optical fibers are preferable over bulk optical setups that include devices with complex structural design. Moreover, the capability of these modes to provide additional degrees of freedom for optical communication in fiber networks made them most prominent and impelled the scientific community in the direction of controllable generation and manipulation of these beams in optical fibers. Recently, all-fiber methods, and fused fiber couplers for generating CVBs are becoming very popular as they can be directly deployed in optical communication networks [46,47,50]. Additionally, an optical fiber can exhibit a rich variety of polarization singularities as a result of inherent combination of modes with plane (Gaussian mode) and helical (vortex mode) wave fronts with orthogonal polarizations, which is useful in understanding fundamental aspects of polarization singular structures. There has been a limited research which has investigated the complex polarization topologies such as lemon, star and monstar in optical fiber by exploiting mode combinations and controlled excitations [51,52].

Keeping all these facts in mind, we aimed at controlled generation of various vector modes by taking advantage of the inherent combination of a new set of LP_{11} modes with

diagonal and anti-diagonal polarizations. We have also demonstrated the generation of isolated C-points, dipoles in optical fibers and studied the effect of half wave plate and cylindrical lens in conversion of C-points.

1.3 Objectives

Keeping in view the challenges of polarization and spatial mode instability, we framed the objectives of our research work as follows

- To generate and study the modal behavior of various possible spatial modes of few mode optical fiber and investigate the phase singularities using two-beam interferometry.
- To generate and characterize possible vector modes and to investigate a convenient way of switching between them by controlling input SOP and/or coupling conditions.
- To generate complex beam fields such as isolated C-points and dipoles in few mode fibers and investigate their behavior with respect to input SOP and a convenient method of switching between them.

1.4 Organization of thesis

A schematic representation of organization of the thesis is shown in Fig. 1.1. Chapter 1 and chapter 2 are not included in the figure as they cover the introduction and theory related to the chosen problem. The key results and studies carried out in each chapter are clearly portrayed in Fig. 1.1 for quick understanding of content of the thesis. The thesis has been organized in seven chapters as follows.

CHAPTER 1

This chapter covers the introduction to scalar and vector vortex modes and their generation methods including few mode optical fiber. A brief review of generating such beams in fibers is presented including literature survey, motivation and objectives of the current research followed by organization of the thesis.

CHAPTER 2

In this chapter, we present theoretical aspects of wave propagation in optical fiber by deriving vector wave equation using Maxwell's equations and hence discuss the vector modes of optical fibers. We also discuss the formation of scalar modes by considering

weakly guiding approximation and hence establish a relation between scalar and vector modes.

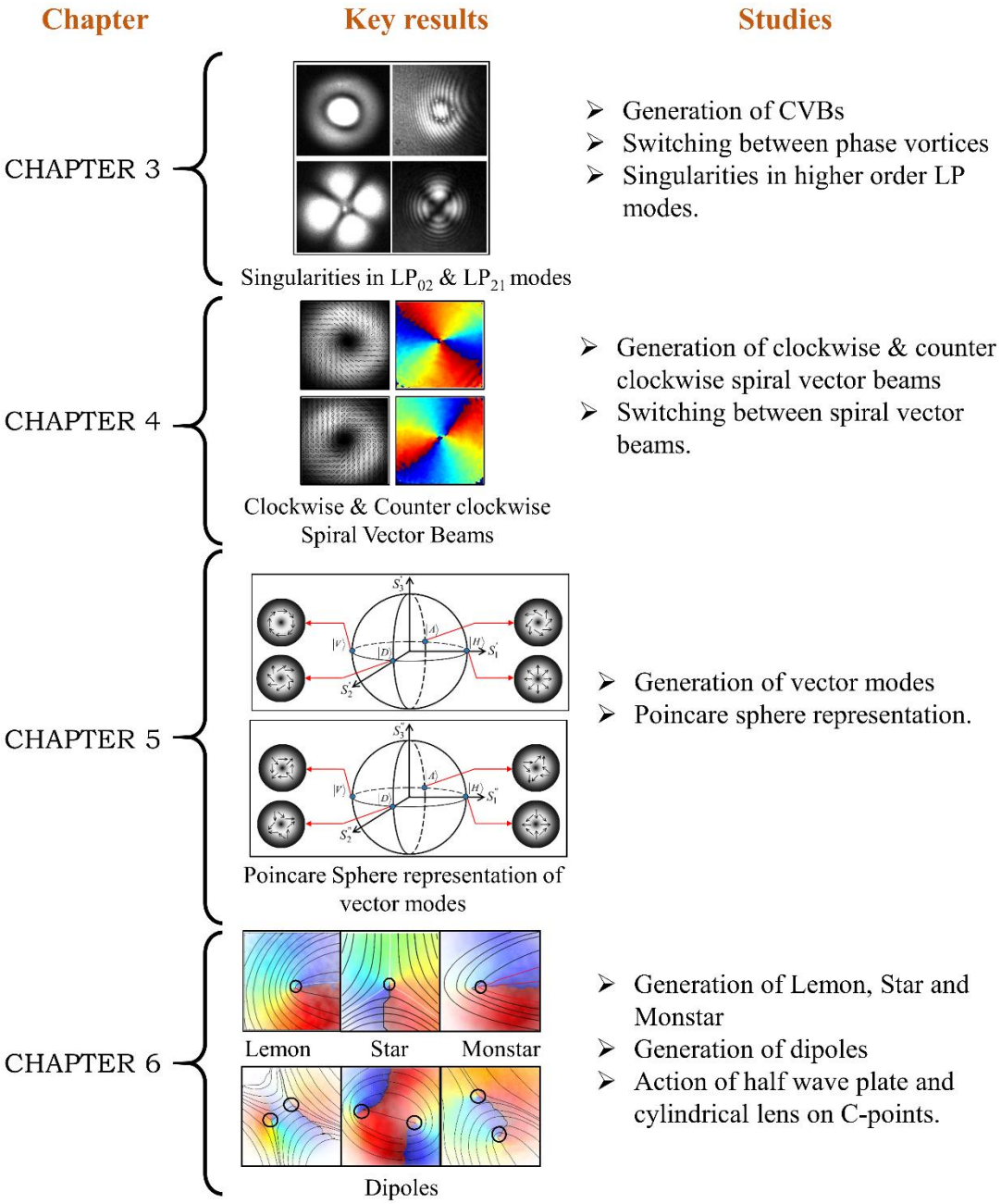

Fig.1.1. Schematic representation of organization of thesis.

CHAPTER 3

This chapter includes the preliminary experimental results of excitation of various modes and their characterization using two beam interferometry. In this chapter, we focus on the phase singular aspects of fiber modal fields. Using two fibers of different V-numbers, we generated vector modes and first four linearly polarized modes by changing the coupling

of input Gaussian beam with optical fiber and the generated modes are examined for the presence of singularities by forming interferograms with a reference Gaussian beam.

CHAPTER 4

In this chapter, the generation of spiral vector beams is demonstrated in a step-index few mode optical fiber by controlling the input SOP and coupling conditions. The spiral vector beams with clockwise and counter clockwise spiral polarization are generated and switching between them is demonstrated. Formation of these beams in the fiber is shown to be a combination of orthogonal linearly polarized modes with diagonal and anti-diagonal polarization vectors. The orthogonal LP_{11} modes are generated for orthogonal input linear polarization and their resultant spiral vector beam is generated for an intermediate input SOP of the orthogonal states, controlled by a half wave plate. The generated beams are analyzed by obtaining spatial polarization and ellipse orientation maps using Stokes polarimetry.

CHAPTER 5

In this chapter, by extending the basis of diagonal and anti-diagonal linearly polarized modes, a class of four vector vortex modes are generated in a similar manner to that of spiral vector beams of the previous chapter. The generation of these vector modes is demonstrated experimentally with a supporting theory, which relies on inherent combination of orthogonal LP_{11} modes. The possible combinations of LP_{11} modes are governed by certain necessary criteria i.e., the combining modes must be orthogonal in polarization and in spatial profile. The necessity of representing vector vortex modes on Poincare sphere is discussed. All the linearly polarized modes are located onto a standard Poincare sphere. Whereas, the inhomogeneously polarized modes, resulted from the combination of orthogonal LP_{11} modes, are accommodated on a pair of higher order Poincare sphere (HOPS). This pair of HOPS serves the need for representation of all possible vector vortex modes of few mode optical fiber. The location of these vector modes on HOPS is justified with the location of LP_{11} modes on standard Poincare sphere that combine to generate respective vector modes.

CHAPTER 6

With a brief introduction to polarization singularities, this chapter discusses the experimental generation of C-points (star, lemon, and monstar) in a step-index few mode

optical fiber. Isolated C-points, and dipoles are generated by controlled launching of light into the fiber. The action of a half wave plate and cylindrical lens on conversion of C-points is studied. 2π- symmetric topologies such as radial, circulation, and saddle are experimentally realized in the Stokes fields, derived from lemon and star topologies and also in the ellipse orientation fields of vector vortex modes.

CHAPTER 7

This chapter summarizes the experimental results presented in previous chapters and discusses the achievements as well as conclusions. We also present the scope of future research with the achievements of current research work.

References

1. I. I. Mokhun, *Introduction to linear singular optics* in "*Optical correlation techniques and applications,"* SPIE Press, Bellingham, USA, 1-132 (2007).
2. Enrique J. Galvej, *Singular optics and phase properties* in *"Structured Light and Its Applications,"* Academic Press, Elsevier, 63-77 (2008).
3. Mark R. Dennis, Kevin O'Holleran, and Miles J. Padgett, "Singular optics: Optical vortices and polarization singularities," *Progress in Optics*, **53**, 293-363 (2009).
4. J. F. Nye and M.V. Berry, "Dislocations in wave trains," *Proc. R. Soc. Lond. A.*, **336**, 165-190 (1974).
5. L. Allen, M. W. Beijersbergen, R. J. C. Spreeuw, et.al., "Orbital angular momentum of light and the transformation of Laguerre-Gaussian laser modes," *Phys. Rev. A*, **45**, 8185–8189 (1992).
6. A.M. Yao, and M.J. Padgett, "Orbital angular momentum : origins, behavior and applications," *Adv. Opt. Phot.*, **3**, 161–204 (2011).
7. Q. Zhan, "Cylindrical vector beams: from mathematical concepts to applications," *Adv. Opt. Photon.*, **1**, 1–57 (2009).
8. R. Dorn, S. Quabis, and G. Leuchs, "Sharper focus for a radially polarized light beam," *Phys. Rev. Lett.*, **91**, 233901 (2003).
9. M. Meier, V. Romano, and T. Feurer, "Material processing with pulsed radially and azimuthally polarized laser radiation," *Appl. Phys. A.*, **86**, 329–334 (2007).
10. H. Wang, L. Shi, B. Lukyanchuk, et.al., "Creation of a needle of longitudinally polarized light in vacuum using binary optics," *Nat. Photonics*, **2**, 501 –505 (2008).

11. M. Kreysing, D. Ott, M. J. Schmidberger, et.al., "Dynamic operation of optical fibres beyond the single-mode regime facilitates the orientation of biological cells," *Nat. Commun.*, **5**, 5481(2014).
12. M. G. Donato, S. Vasi, R. Sayed, et.al., "Optical trapping of nanotubes with Cylindrical vector beams," *Opt. Lett.,* **37**, 3381-3383 (2012).
13. Rui Chen, Krishna Agarwal, Colin J. R. Sheppard, et.al., "Imaging using cylindrical vector beams in a high numerical-aperture microscopy system," *Opt. Lett.*, **38**, 3111-3114 (2013).
14. Jian Wang, "Advances in communications using optical vortices," *Photon. Res.*, **4**, B14-B28 (2016).
15. X. Li, T. H. Lan, C. H. Tien, et.al., "Three-dimensional orientation-unlimited polarization encryption by a single optically configured vectorial beam," *Nat. Commun.,* **3**, 998 (2012).
16. D. Pohl, "Operation of a Ruby laser in the purely transverse electric mode TE01," *Appl. Phys. Lett.,* **20**, 266–267 (1972).
17. J. F. Bisson, J. Li, K. Ueda, et.al., "Radially polarized ring and arc beams of a neodymium laser with an intra-cavity axicon," *Opt. Exp.,* **14**, 3304–3311 (2006).
18. C.C. Shih, "Radial polarization laser resonator," *U.S. patent,* **5**,359,622 (Oct. 25, 1994).
19. Y. Kozawa and S. Sato, "Generation of a radially polarized laser beam by use of a conical Brewster prism," *Opt. Lett.*, **30**, 3063–3065 (2005).
20. M. A. Ahmed, A. Voss, M. M. Vogel, et.al., "Multilayer polarizing grating mirror used for the generation of radial polarization in Yb:YAG thin-disk lasers," *Opt. Lett.,* **32**, 3272 -3274 (2007).
21. N. R. Heckenberg, R. McDuff, C. P. Smith, et.al., "Generation of optical phase singularities by computer-generated holograms," *Opt. Lett.,* **17**, 221-223 (1992).
22. M. W. Beijersbergen, L. Allen, H. E. L. O. van der Veen, et.al., "Astigmatic laser mode converters and transfer of orbital angular momentum," *Opt. Commun.,* **96**, 123-132 (1993).
23. Jingtao Xin, Kunjian Dai, Lei Zhong, et.al., "Generation of optical vortices by using spiral phase plates made of polarization dependent devices," *Opt. Lett.,* **39**, 1984-1987 (2014).
24. Jennifer E. Curtis and David G. Grier, "Structure of Optical Vortices," *Phys. Rev. Lett.,* **90**, 133901 (2003).

25. Steve C. Tidwell, Dennis H. Ford, and Wayne D. Kimura, "Generating radially polarized beams interferometrically", *Appl. Opt*., **29**, 2234-2239 (1990).
26. Lorenzo Marrucci, "The q-plate and its future," J. NANOPHOTONICS., **7**, 078598 (2013).
27. Zhenxing Liu et. al., "Generation of arbitrary vector vortex beams on hybrid-order Poincaré sphere," *Phot. Res.,* **5**, 15-21 (2017).
28. Allan W. Snyder, and William R. Young, "Modes of optical waveguides," *J. Opt. Soc. Am.,* **68**, 297-309 (1978).
29. Allan W. Snyder, and John D. Love, "*Optical Waveguide Theory,"* Chapman and Hall, (1983).
30. G. Volpe, and D. Petrov, "Generation of cylindrical vector beams with few-mode fibers excited by Laguerre–Gaussian beams," *Opt. Commun.*, **237**, 89–95 (2004).
31. T. Grosjean, A. Sabac, and D. Courjon "A versatile and stable device allowing the efficient generation of beams with radial, azimuthal or hybrid polarizations," *Opt. Commun*., **252**, 12-21 (2005).
32. T. Grosjean, D. Courjon, and M. Spajer, "An all-fiber device for generating radially and other polarized light beams," *Opt. Commun.***, 203**, 1–5 (2002).
33. Wei Gao et. al., "Generation of vector vortex beams with a small core multimode liquid core optical fiber," *Opt. Exp.,* **22,** 11325-11330 (2014).
34. Siddharth Ramachandran et al., "Generation and propagation of radially polarized beams in optical fibers," *Opt. Lett.,* **34,** 2525-2527 (2009).
35. P. Gregg, P. Kristensen, and S. Ramachandran, "Conservation of orbital angular momentum in air-core optical fibers," *Optica*, **2**, 267-270 (2015).
36. Paul Steinvurzel et al., "Fiber-based Bessel beams with controllable diffraction resistance distance," *Opt. Lett.,* **36,** 4671-4673 (2011).
37. Henry I. Sztul et al., "Cylindrical vector beam generation from spun fiber", *Proc. of SPIE*, **7227**, 722704-1 (2009).
38. Nirmal K. Viswanathan and V. V. G. Krishna Inavalli, "Generation of optical vector beams using a two-mode fiber," *Opt. Lett.,* **34**, 1189-1191 (2009).
39. V. V. G. Krishna Inavalli and Nirmal K. Viswanathan, "Switchable vector vortex beam generation using an optical fiber," *Opt. Commun.,* **283**, 861-864 (2010).
40. Geo M. Philip and Nirmal K. Viswanathan, "Generation of spirally polarized propagation-invariant beam using fiber microaxicon," *Opt. Lett*., **36**, 3906-3908 (2011).

41. Nirmal K. Viswanathan, Geo M. Philip and Y.V. Jayasurya, "Generic Dark Hollow Beams using Negative Cones Chemically Etched in Fiber Tips," *Proc. of SPIE,* **7613**, 761307 (2010).
42. Robert D. Niederriter, Mark E. Siemens, and Juliet T. Gopinath "Continuously tunable orbital angular momentum generation using a polarization-maintaining fiber," *Opt. Lett.,* **41**, 3213-3216 (2016).
43. Robert D. Niederriter, Mark E. Siemens, and Juliet T. Gopinath "Simultaneous control of orbital angular momentum and beam profile in two-mode polarization-maintaining fiber," *Opt. Lett.,* **41**, 5736-5739 (2016).
44. J. Demas, M. D. W. Grogan, T. Alkeskjold, et.al., "Sensing with optical vortices in photonic-crystal fibers," *Opt. Lett.,* **37**, 3768-3770 (2012).
45. Rita S. Rodrigues Ribeiro, Pabitra Dahal, Ariel Guerreiro, et.al., "Optical fibers as beam shapers: from Gaussian beams to optical vortices," *Opt. Lett*., **41**, 2137-2140 (2016).
46. S. Pidishety et.al., "All-Fiber Fused Coupler for Stable Generation of Radially and Azimuthally Polarized Beams," *IEEE Phot. Tech. Lett.,* **29**, 31-34 (2016).
47. S. Pidishety et.al., "Orbital angular momentum beam excitation using an all-fiber weakly fused mode selective coupler," *Opt. Lett.,* **42**, 4347-4350 (2017).
48. Dennis H. Goldstein, "*Polarized light*," CRC Press, London (2011).
49. G. Milione et al., "Higher-order poincaré sphere, stokes parameters, and the angular momentum of light," *Phys. Rev. Lett.,* **107,** 1–4 (2011).
50. Shuhui Li, Qi Mo, Xiao Hu, et.al., "Controllable all-fiber orbital angular momentum mode converter," *Opt. Lett.,* **40**, 4376-4379 (2015).
51. Enrique J. Galvez, Brett L. Rojec, Vijay Kumar, et.al., "Generation of isolated asymmetric umbilics in light's polarization," *Phys. Rev. A.*, **89**, 031801 (2014).
52. Y. V. Jayasurya, V. V. G. Krishna Inavalli, and Nirmal K. Viswanathan, "Polarization singularities in the two-mode optical fiber output," *Appl. Opt.,* **50,** E131-E137 (2011).

CHAPTER

2

Modes of optical fiber

Contents

CHAPTER 2

Modes of Optical Fiber

In this chapter, we discuss the fundamental aspects of modes of optical fiber beginning from the Maxwell's equations for an optical waveguide. The basic electromagnetic vector wave equation that corresponds to light propagation in optical fiber is derived and general solutions are discussed. The structural conditions of the optical fiber that are responsible for the formation of vector modes of complex spatial polarization are discussed. The vector wave equation is reduced to scalar wave equation by introducing the weakly guiding approximation which is the practical case and accounts for an understanding of the modal behavior of optical fiber in terms of scalar modes. The linearly polarized modal solutions under this approximation are discussed and the relation between vector modes and scalar modes is established.

2.1 Introduction

Optical fiber is a cylindrical dielectric optical wave guide with a uniform refractive index core (n_{co}) surrounded by a cladding of slightly lower uniform refractive index (n_{cl}) which is assumed to be unbounded [1-3]. Thus, the variation in the refractive index at the core-clad interface is a step or jump discontinuity. Optical fibers are translationally invariant optical waveguides where the refractive index does not change along the axis of propagation (z) and only transverse profile of the refractive index ($n(r) = n(x, y)$) describes the characteristic properties of the optical fiber. For an optical fiber, the arbitrary refractive index profile is defined as [1]

$$n(r) = n_{co}[1 - 2\Delta f(r)]^{1/2} \tag{1}$$

Where r is the radial coordinate, $f(r)$ describe the shape of the refractive index profile and Δ is the profile height or the relative refractive index of core and cladding is defined as

$$\Delta = \frac{1}{2}\left\{1 - \frac{n_{cl}^2}{n_{co}^2}\right\} \cong \frac{n_{co} - n_{cl}}{n_{co}} \tag{2}$$

For step profile of refractive index, $f(r) = 0$ in the core and $f(r) = 1$ in the cladding. Hence, from eq. (1), the step profile of refractive index for an optical fiber with core radius ρ is

$$\begin{aligned} n(r) &= n_{co} \qquad for \qquad 0 \le r < \rho \\ n(r) &= n_{cl} \qquad for \qquad \rho < r \le \infty \end{aligned} \tag{3}$$

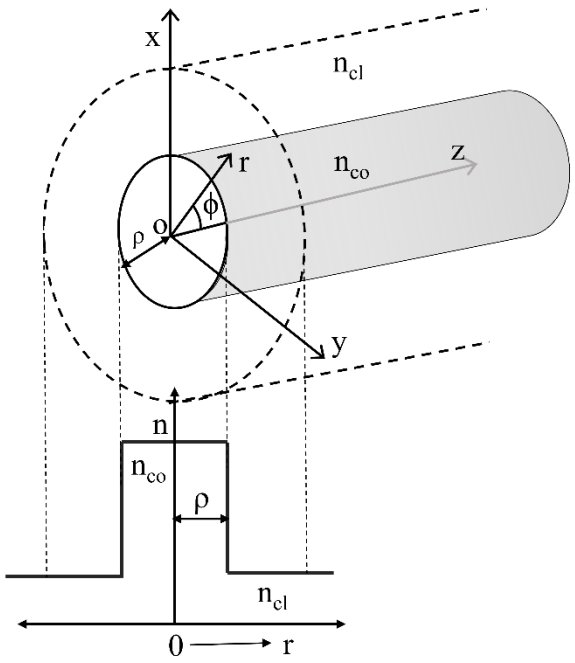

Fig. 2.1 Step profile of refractive index with n_{co}>n_{cl}, and schematic diagram of optical fiber with Cartesian (x,y,z) and polar (r,ϕ,z) coordinates, ρ is the radius of core and n_{co}, n_{cl} are the refractive indices of core and cladding, the axis of fiber is along the z-axis.

The schematic of step profile and an optical fiber is shown in Fig. 2.1. The guided modes of step-index optical fiber have exact analytical solutions for circularly symmetric and elliptical fibers which can be derived from source-free Maxwell's equations [1].

2.2 Vector wave equation

The spatial dependence of the electric field $\boldsymbol{E}(x, y, z)$ and the magnetic field $\boldsymbol{H}(x, y, z)$ of an optical waveguide is determined by Maxwell's equations. The field vectors are assumed to have an implicit time dependence $exp(-i\omega t)$. The dielectric constant or relative permittivity is related to the refractive index $n(x, y, z)$ by ${\varepsilon}/{\varepsilon_o} = n^2$, where ε and ε_o are the electric permittivities of the medium and free-space respectively. For dielectrics (non-magnetic materials) the magnetic permeability μ is close to free space

permeability i.e., μ =μ₀. Under these conditions, the source-free Maxwell's equations with current density **J**=0 and charge density ρ=0 are expressible in the form [4]

$$\nabla \times \boldsymbol{E} = i\left(\frac{\mu_o}{\varepsilon_o}\right)^{1/2} k\boldsymbol{H} \qquad \textbf{(}4(a)\textbf{)}$$

$$\nabla \times \boldsymbol{H} = -i\left(\frac{\varepsilon_o}{\mu_o}\right)^{1/2} kn^2\boldsymbol{E} \qquad \textbf{(}4(b)\textbf{)}$$

$$\nabla.(n^2\boldsymbol{E}) = 0 \qquad (4(c))$$

$$\nabla.\boldsymbol{H} = 0 \qquad (4(d))$$

Where the symbols in bold letters represents vector quantities, $k = \frac{2\pi}{\lambda}$ is the free-space wavenumber, and λ is the wavelength of light in free space. $\nabla \times$ and $\nabla.$ are the curl and divergence operators. The electric and magnetic fields of translationally invariant optical fiber are expressible as a superposition of fields with the separable form [5]

$$\boldsymbol{E}(x,y,z) = \boldsymbol{e}(x,y)\exp(i\beta z); \qquad \boldsymbol{H}(x,y,z) = \boldsymbol{h}(x,y)\exp(i\beta z) \qquad (5)$$

where β is the propagation constant. The corresponding forms for the cylindrical polar coordinates are

$$\boldsymbol{E}(r,\phi,z) = \boldsymbol{e}(r,\phi)\exp(i\beta z); \qquad \boldsymbol{H}(r,\phi,z) = \boldsymbol{h}(r,\phi)\exp(i\beta z) \qquad (6)$$

Decomposing these fields into longitudinal and transverse components, parallel to and orthogonal to the waveguide axis, respectively and denoting by subscripts z and t, we get

$$\boldsymbol{E} = (\boldsymbol{e}_t + e_z\hat{\boldsymbol{z}})\exp(i\beta z); \qquad \boldsymbol{H} = (\boldsymbol{h}_t + h_z\hat{\boldsymbol{z}})\exp(i\beta z) \qquad (7)$$

Where $\hat{z}$ is the unit vector parallel to the waveguide axis. On substituting the field representations of Equ. (7) into source-free Maxwell's equations i.e., Equ. (4), and compare longitudinal and transverse components, we get

$$\boldsymbol{e}_t = -\left(\frac{\mu_o}{\varepsilon_o}\right)^{1/2}\frac{1}{kn^2}\hat{\boldsymbol{z}} \times \{\beta\boldsymbol{h}_t + i\boldsymbol{\nabla}_t h_z\} \qquad (8(a))$$

$$\boldsymbol{h}_t = \left(\frac{\varepsilon_o}{\mu_o}\right)^{1/2}\frac{1}{k}\hat{\boldsymbol{z}} \times \{\beta\boldsymbol{e}_t + i\boldsymbol{\nabla}_t e_z\} \qquad (8(b))$$

$$e_z = i\left(\frac{\mu_o}{\varepsilon_o}\right)^{1/2}\frac{1}{kn^2}\hat{\boldsymbol{z}}.\boldsymbol{\nabla}_t \times \boldsymbol{h}_t \qquad (8(c))$$

$$h_z = -i\left(\frac{\varepsilon_o}{\mu_o}\right)^{1/2}\frac{1}{k}\hat{\boldsymbol{z}}.\boldsymbol{\nabla}_t \times \boldsymbol{e}_t \qquad (8(d))$$

If we eliminate $\boldsymbol{e}_t$ or $\boldsymbol{h}_t$ from eqs. 8(a) and 8(b), the transverse fields in terms of longitudinal fields can be expressed as [5]

$$\boldsymbol{e}_t = \frac{i}{k^2n^2 - \beta^2}\left\{\beta\boldsymbol{\nabla}_t e_z - \left(\frac{\mu_o}{\varepsilon_o}\right)^{1/2} k\hat{\boldsymbol{z}} \times \boldsymbol{\nabla}_t h_z\right\} \qquad (9(a))$$

$$\boldsymbol{h}_t = \frac{i}{k^2n^2 - \beta^2}\left\{\beta\boldsymbol{\nabla}_t h_z + \left(\frac{\varepsilon_o}{\mu_o}\right)^{1/2} kn^2\hat{\boldsymbol{z}} \times \boldsymbol{\nabla}_t e_z\right\} \qquad (9(b))$$

From the above equation it is clear that by knowing longitudinal components, we can determine the transverse components that simplifies the complexity in solving the vector wave equation. Eliminating either the electric or magnetic fields from Maxwell's equations (4(a)) and (4(b)), we obtain the homogeneous vector wave equation [1].

$$\{\boldsymbol{\nabla}^2 + n^2k^2\}\boldsymbol{E} = -\boldsymbol{\nabla}(\boldsymbol{E}_t.\boldsymbol{\nabla}_t \ln n^2) \qquad (10(a))$$

$$\{\boldsymbol{\nabla}^2 + n^2k^2\}\boldsymbol{H} = (\boldsymbol{\nabla} \times \mathbf{H}) \times \boldsymbol{\nabla}_t \ln n^2 \qquad (10(b))$$

From Equ. (7), based on the fields with separable form, Equ. (10) becomes

$$\left\{\boldsymbol{\nabla}_t{}^2 + n^2k^2 - \beta^2\right\}(\boldsymbol{e}_t + e_z\hat{\boldsymbol{z}}) = -(\boldsymbol{\nabla}_t + i\beta\hat{\boldsymbol{z}})\boldsymbol{e}_t.\boldsymbol{\nabla}_t \ln n^2 \qquad (11(a))$$

$$\left\{\boldsymbol{\nabla}_t{}^2 + n^2k^2 - \beta^2\right\}(\boldsymbol{h}_t + h_z\hat{\boldsymbol{z}}) = \{(\boldsymbol{\nabla}_t + i\beta\hat{\boldsymbol{z}}) \times \boldsymbol{h}_t\} \times \boldsymbol{\nabla}_t \ln n^2 \qquad (11(b))$$

Further, if we consider Cartesian field components, the longitudinal and transverse components of above equation are given by

$$\left\{\boldsymbol{\nabla}_t{}^2 + n^2k^2 - \beta^2\right\}\boldsymbol{e}_t = -\boldsymbol{\nabla}_t(\boldsymbol{e}_t.\boldsymbol{\nabla}_t \ln n^2) \qquad (12(a))$$

$$\left\{\boldsymbol{\nabla}_t{}^2 + n^2k^2 - \beta^2\right\}e_z = -i\beta\boldsymbol{e}_t.\boldsymbol{\nabla}_t \ln n^2 \qquad (12(b))$$

$$\left\{\boldsymbol{\nabla}_t{}^2 + n^2k^2 - \beta^2\right\}\boldsymbol{h}_t = (\boldsymbol{\nabla}_t \times \boldsymbol{h}_t) \times \boldsymbol{\nabla}_t \ln n^2 \qquad (12(c))$$

$$\left\{\boldsymbol{\nabla}_t{}^2 + n^2k^2 - \beta^2\right\}h_z = (\boldsymbol{\nabla}_t h_z - i\beta\boldsymbol{h}_t).\boldsymbol{\nabla}_t \ln n^2 \qquad (12(d))$$

Where $\boldsymbol{e}_t = e_x\hat{x} + e_y\hat{y}$ and $\boldsymbol{h}_t = h_x\hat{x} + h_y\hat{y}$.

The vector wave equation is the reformulation of Maxwell's equations for an arbitrary profile shape. These equations contain all the necessary information to determine the spatial dependence of the fields everywhere in the waveguide. The term involving $\boldsymbol{\nabla}_t \ln n^2$ in Equ. (11) and Equ. (12) couple various field components. The polarization phenomena due to the structure of the waveguide are determined by these terms on account of which the modes acquire unique complex polarization behavior [1].

Generally, for finding the solutions of step-profile waveguides, Equ. (11) is solved in regions of core and cladding, where $\boldsymbol{\nabla}_t \ln n^2$ vanishes and then by using the boundary conditions of Maxwell's equations, the field amplitudes can be determined in the core-clad interface region where $\boldsymbol{\nabla}_t \ln n^2 \neq 0$. As $\boldsymbol{\nabla}_t \ln n^2 = 0$ in the homogeneous core and clad regions, the vector wave equation, Equ. (11) reduces to scalar wave equation of the form

$$\{\boldsymbol{\nabla}_t{}^2 + n^2 k^2 - \beta^2\}\Psi = 0 \tag{13}$$

Where Ψ represents either e_z or h_z, as it is sufficient to solve the equation for longitudinal components from which the transverse components can be calculated using Equ. (9). The step profile can be regarded as a special case of graded profile where all the grading occurs at a single interface. Thus, the step profile has the greatest influence on the polarization behavior of the fields.

To facilitate the description of the modal fields, dimensionless modal parameters U and W for the core and cladding can be introduced and are given by

$$U = \rho(k^2 n_{co}^2 - \beta^2)^{1/2}\,; \qquad W = \rho(\beta^2 - k^2 n_{cl}^2)^{1/2} \tag{14(a)}$$

and these parameters are related to the normalized frequency V as

$$V^2 = U^2 + W^2 \tag{14(b)}$$

For core and cladding regions of step-profile optical fiber, Equ. (13) can be written as [1]

$$\left\{\frac{\partial^2}{\partial R^2} + \frac{1}{R}\frac{\partial}{\partial R} + \frac{1}{R^2}\frac{\partial^2}{\partial \phi^2} + U^2\right\}\Psi = 0 \qquad for \quad 0 \leq R < 1 \tag{15(a)}$$

$$\left\{\frac{\partial^2}{\partial R^2} + \frac{1}{R}\frac{\partial}{\partial R} + \frac{1}{R^2}\frac{\partial^2}{\partial \phi^2} - W^2\right\}\Psi = 0 \qquad for \quad 1 < R < \infty \tag{15(b)}$$

Where $R = r/\rho$ is the normalized radius. The separable solutions for the above equation that are bounded everywhere are given by

$$\Psi(r,\phi) = \Psi(r)\begin{Bmatrix}\cos(\upsilon\phi)\\ \sin(\upsilon\phi)\end{Bmatrix} \tag{16}$$

$\Psi(r)$ is the solution in terms of Bessel's functions of first and second kind in core and cladding respectively. Thus, the solutions are $J_\upsilon(UR)\cos(\upsilon\phi)$ or $J_\upsilon(UR)\sin(\upsilon\phi)$ in the core and $K_\upsilon(WR)\cos(\upsilon\phi)$ or $K_\upsilon(WR)\sin(\upsilon\phi)$ in the cladding respectively.

To construct the fields, we first choose the longitudinal components which are continuous across the interface

$$e_z = A\frac{J_\upsilon(UR)}{J_\upsilon(U)}f_\upsilon(\phi);\;\; h_z = B\frac{J_\upsilon(UR)}{J_\upsilon(U)}g_\upsilon(\phi) \quad for \quad 0 \le R < 1 \tag{17(a)}$$

$$e_z = A\frac{K_\upsilon(WR)}{K_\upsilon(W)}f_\upsilon(\phi);\;\; h_z = B\frac{K_\upsilon(WR)}{K_\upsilon(W)}g_\upsilon(\phi) \quad for \quad 1 < R < \infty \tag{17(b)}$$

Where A and B are constants and $f_\upsilon(\phi)$ and $g_\upsilon(\phi)$ are either $\sin(\upsilon\phi)$ or $\cos(\upsilon\phi)$. The dependence can be derived from the transverse components because each transverse component can depend on either $f_\upsilon(\phi)$ or $g_\upsilon(\phi)$ but not both. The transverse components can be written from Equ. (9) as

$$\begin{aligned}
e_r &= \frac{i}{k^2n^2-\beta^2}\left\{\beta\frac{\partial e_z}{\partial r} + \left(\frac{\mu_o}{\varepsilon_o}\right)^{1/2}\frac{k}{r}\frac{\partial h_z}{\partial\phi}\right\}\\
e_\phi &= \frac{i}{k^2n^2-\beta^2}\left\{\frac{\beta}{r}\frac{\partial e_z}{\partial\phi} - \left(\frac{\mu_o}{\varepsilon_o}\right)^{1/2}k\frac{\partial h_z}{\partial r}\right\}\\
h_r &= \frac{i}{k^2n^2-\beta^2}\left\{\beta\frac{\partial h_z}{\partial r} - \left(\frac{\varepsilon_o}{\mu_o}\right)^{1/2}\frac{kn^2}{r}\frac{\partial e_z}{\partial\phi}\right\}\\
h_\phi &= \frac{i}{k^2n^2-\beta^2}\left\{\frac{\beta}{r}\frac{\partial h_z}{\partial\phi} + \left(\frac{\varepsilon_o}{\mu_o}\right)^{1/2}kn^2\frac{\partial e_z}{\partial r}\right\}
\end{aligned} \tag{18}$$

From the above equations it is clear that the derivative of f_υ or $g_\upsilon$appear in the term $\frac{\partial}{\partial\phi}$. If we define$f_\upsilon = \sin(\upsilon\phi)$, we should have$g_\upsilon = \cos(\upsilon\phi)$, so that $e_r$is a function of $\sin(\upsilon\phi)$ but not a combination of $\sin(\upsilon\phi)$ and $\cos(\upsilon\phi)$. Similarly, the other combination can be $f_\upsilon = \cos(\upsilon\phi)$ and $g_\upsilon = -\sin(\upsilon\phi)$. Hence, there are only two possible combinations given below. The first combination results in even modes, symmetric with

respect to x-axis and the second combination results in odd modes, symmetric with respect to y-axis.

$$f_\upsilon(\phi) = \begin{Bmatrix}\cos(\upsilon\phi)\\ \sin(\upsilon\phi)\end{Bmatrix} \; and \; g_\upsilon(\phi) = \begin{Bmatrix}-\sin(\upsilon\phi)\\ \cos(\upsilon\phi)\end{Bmatrix} \qquad \begin{matrix} even\ modes \\ odd\ modes \end{matrix} \qquad (19)$$

The eigen value equation can be obtained by imposing the boundary conditions that the tangential fields are continuous at interfaces. The eigen value equation for the step-index fiber is

$$\left\{\frac{J_\upsilon'(U)}{UJ_\upsilon(U)} + \frac{K_\upsilon'(W)}{WK_\upsilon(W)}\right\}\left\{\frac{J_\upsilon'(U)}{UJ_\upsilon(U)} + \frac{n_{cl}^2}{n_{co}^2}\frac{K_\upsilon'(W)}{WK_\upsilon(W)}\right\} = \left(\frac{\upsilon\beta}{kn_{co}}\right)^2\left(\frac{V}{UW}\right)^4 \qquad (20)$$

This equation has discrete solutions giving the values of U or equivalently the discrete values of β as they are related. These solutions depend on υ, the core-clad refractive indices and the V-parameter.

2.3 Vector modes

The modes which are the solutions of the eigen value equation (20) are strongly dependent on υ. Here, we discuss two cases $\upsilon = 0$ and $\upsilon \neq 0$ that leads to generation of various vector modes.

2.3.1 Transverse electric (*TE*) and Transverse magnetic (*TM*) modes

If we consider $\upsilon = 0$, equation (19) have two sets of values i.e., $f_0(\phi) = 1$, $g_0(\phi) = 0$ and $f_0(\phi) = 0$ and $g_0(\phi) = 1$. On substituting $f_0(\phi) = 1$, $g_0(\phi) = 0$ in Equ. (17) and Equ. (18), the components $h_z = 0$, $h_r = 0$ and $e_\phi = 0$ which represent a transverse magnetic (*TM*) mode as the longitudinal component of magnetic field is absent in the propagation direction. Similarly, if we substitute $f_0(\phi) = 0$, $g_0(\phi) = 1$ in Equ. (17) and Equ. (18), the components $e_z = 0$, $e_r = 0$ and $h_\phi = 0$ which represent a transverse electric (*TE*) mode as the longitudinal component of electric field is absent in the propagation direction [6]. For $\upsilon = 0$, Equ. (20) reduces to two equations corresponding to TE_{0m} and TM_{0m} modes given by

$$\left\{\frac{J_1(U)}{UJ_0(U)} + \frac{K_1(W)}{WK_0(W)}\right\} = 0 \qquad (21)$$

$$\left\{n_{co}^2\frac{J_1(U)}{UJ_0(U)} + n_{cl}^2\frac{K_1(W)}{WK_0(W)}\right\} = 0 \qquad (22)$$

The electric and magnetic fields of *TE* and *TM* modes propagate parallel to the interface in an optical waveguide respectively. Hence, only meridional rays, passing through the waveguide axis can preserve $e_z = 0$ or $h_z = 0$ at every reflection. Thus, only meridional rays can make up *TE* and *TM* modes on circular waveguides.

These *TE* and *TM* modes are ideal or rare case in optical waveguides as we consider $\boldsymbol{\nabla}_t \ln n^2 = 0$ in vector wave equation. In general, the non-zero $\boldsymbol{\nabla}_t \ln n^2$ term mix e_z and $h_z$fields resulting in *EH* and *HE* hybrid modes for which neither $e_z = 0$ nor $h_z = 0$ and both components are present simultaneously. Moreover, the modal fields can never be transverse electromagnetic (*TEM*) i.e., $e_z = h_z = 0$.

2.3.2 Hybrid (*EH* and *HE*) modes

For $\upsilon \neq 0$, none of the field components are zero and the eigen value equation, Equ. (20) remains the same. The solutions are even and odd $HE_{\upsilon m}$ and $EH_{\upsilon m}$ modes [7]. Each mode is given two subscripts of which the first subscript υ is order and the second subscript m denotes the mth root of the eigen value equation.

In general, a ray follows the helical or skew trajectory on step or graded index profiles. If we follow the direction of the electric vector along a skew ray path, it is impossible to maintain either $e_z = 0$ or $h_z = 0$ because the direction of propagation rotates along the ray trajectory. Consequently, a skew ray mixes *TE* and *TM* polarizations at each reflections, so that the corresponding fields couple both e_z and h_z field components, consistent with the definition of hybrid modes. Hence, all *EH* and *HE* modes are composed of skew rays. The fundamental HE_{11} mode has Gaussian distribution and two orthogonal polarizations which can be assumed as x- and y-polarized modes.

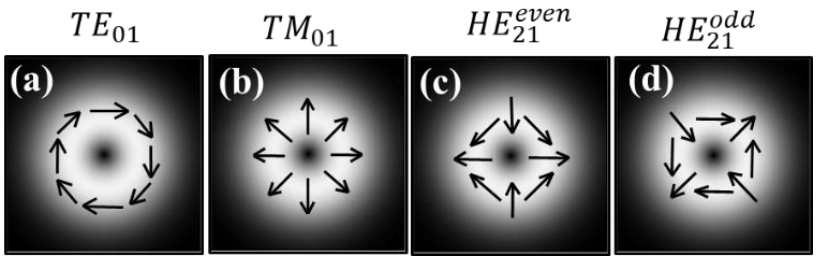

Fig.2.2. Vector modes of a step-index optical fiber. (a) Azimuthally polarized TE_{01} mode, (b) radially polarized TM_{01} mode, (c) and (d) $HE_{21}^{o,e}$ modes with hybrid polarization

Figure 2.2 shows the vector modes of step-index optical fiber with spatial inhomogeneous polarization distribution. These modes are also referred to as zeroth order vector modes

or CVBs due to their cylindrically symmetric spatial intensity and polarization distribution. It is difficult to identify the polarization distribution of vector modes from their spatial intensity pattern as they are all look alike with a donut shaped mode. To identify the spatial polarization, the vector mode has to pass through a rotating analyzer which results in rotating two lobe pattern, based on which the mode can be identified, as shown in Fig. 2.3.

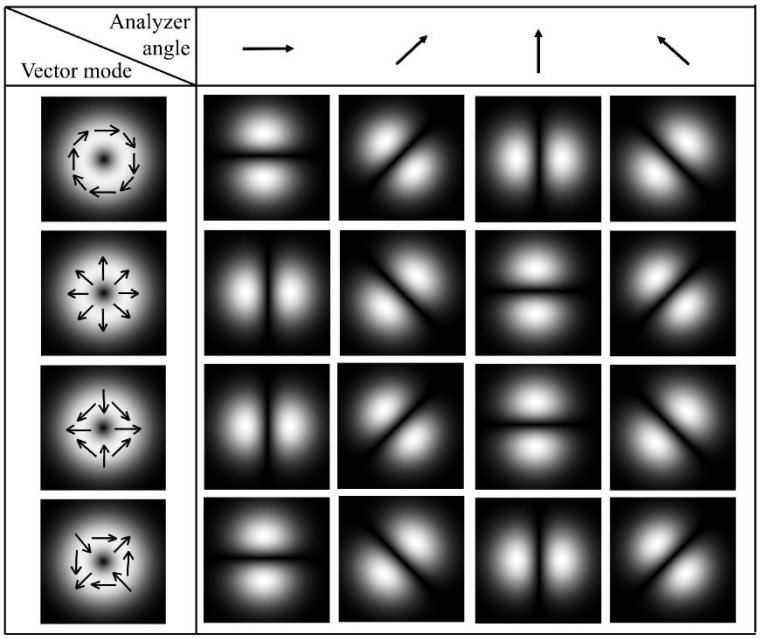

Fig. 2.3. Behavior of vector modes with respect to discrete analyzer orientation angles.

Further, the polarization state of these modes is undefined at the center due to spatial inhomogeneity for which they are known as polarization vortex or vector vortex modes. These modes are analogous to *LG* modes of radial order zero and azimuthal order one i.e., LG_0^1, in spatial intensity but do not have a phase vortex. However, the linear combinations of these modes with π/2 phase difference i.e., $TE_{01} \pm iTM_{01}$ and $HE_{21}^{even} \pm iHE_{21}^{odd}$ result in homogeneous circularly polarized modes with an embedded phase vortex [1].

2.4 Weakly guiding approximation

In the previous section, we discussed that the term $\boldsymbol{\nabla}_t \ln n^2$ is responsible for the polarization effects of modes in step-index optical fiber. If the refractive indices of core and cladding are nearly equal i.e., $n_{co} \cong n_{cl}$ or the step height is so small ($\Delta \ll 1$), then the term $\boldsymbol{\nabla}_t \ln n^2$ becomes negligible and vector wave equation reduces to scalar wave equation. This approximation with $\Delta \ll 1$ is called the weakly guiding approximation [8-

11]. This approximation is useful in practical cases where the fiber is used for long distance communication. In contrast to the name 'weak guiding', this approximation allows strong guidance and total confinement of light within the core. The modes of weakly guiding optical waveguides were first reported for step-index fiber by Snyder [12], and the name 'weak guidance' was coined later by Gloge [13] and additional insights were reported there after [14].

The longitudinal components e_z and h_z of weakly guiding waveguides are so small that they can be neglected. Hence, the modes are nearly transverse in nature with transverse components $\boldsymbol{e}_t$ and $\boldsymbol{h}_t$ related by

$$\boldsymbol{h}_t = n_{co}\left(\frac{\varepsilon_o}{\mu_o}\right)^{1/2} \hat{\boldsymbol{z}} \times \boldsymbol{e}_t \tag{23}$$

When $\Delta \ll 1$, the polarization effect due to the waveguide structure are small and Cartesian components of $\boldsymbol{e}_t$ are approximated by solutions of scalar wave equation. If we write $\boldsymbol{e}_t = e_x\hat{x} + e_y\hat{y}$ and $\boldsymbol{h}_t = h_x\hat{x} + h_y\hat{y}$, and let Ψ denote e_x or e_y, then Ψ satisfies

$$\left\{\nabla_t^2 + k^2 n^2(x,y) - \tilde{\beta}^2\right\}\Psi = 0 \tag{24}$$

$\tilde{\beta}$ is the scalar propagation constant. The solutions of the above equation for both components of $\boldsymbol{e}_t$ and $\boldsymbol{h}_t$ are the same and are related to each other by Equ. (23). Hence, it is sufficient to solve for either e_x or e_y due to which the transverse fields are polarized in one direction and because of this reason, the modes are called linearly polarized (*LP*) modes. Although, the Cartesian components of $\boldsymbol{e}_t$satisfy Equ. (24), we can determine their spatial dependence in cylindrical polar coordinate system also. The solutions for the above equation in the separable forms are $\Psi = F_l(r)\cos(l\phi)$ and $\Psi = F_l(r)\sin(l\phi)$, where $l = 0,1,$ ...., and $F_l(r)$ satisfies the ordinary differential equation

$$\left\{\frac{d^2}{dr^2} + \frac{1}{r}\frac{d}{dr} + k^2 n^2(r) - \frac{l^2}{r^2} - \tilde{\beta}^2\right\} F_l(r) = 0 \tag{25}$$

To make this equation dimensionless, we take the definition of $n(r)$ from Equ. (1) and set $R = r/\rho$ which leads to

$$\left\{\frac{d^2}{dR^2} + \frac{1}{R}\frac{d}{dR} - \frac{l^2}{r^2} + \tilde{U}^2 - V^2 f(R)\right\} F_l(R) = 0 \tag{26}$$

The solutions of the above equation, $F_l(R)$ are the Bessel functions of first and second kind within the core and cladding respectively.

$$F_l = \frac{J_l(\widetilde{U}R)}{J_l(\widetilde{U})}; 0 \le R < 1 \quad and \quad F_l = \frac{K_l(\widetilde{W}R)}{K_l(\widetilde{W})}; 1 \le R < \infty \tag{27}$$

Where $\widetilde{U}$ and $\widetilde{W}$ are scalar dimensionless quantities given by $\widetilde{U} = \rho\left(k^2 n_{co}^2 - \tilde{\beta}^2\right)^{1/2}$and $\widetilde{W} = \rho\left(\tilde{\beta}^2 - k^2 n_{cl}^2\right)^{1/2}$and are connected to V parameter by $V^2 = \widetilde{U}^2 + \widetilde{W}^2$. The complete solution for equation (24) is given by

$$\Psi = \frac{J_l(\widetilde{U}R)}{J_l(\widetilde{U})}\begin{bmatrix}\sin(l\phi)\\ \cos(l\phi)\end{bmatrix}; 0 \le R < 1 \ and \ \ \Psi = \frac{K_l(\widetilde{W}R)}{K_l(\widetilde{W})}\begin{bmatrix}\sin(l\phi)\\ \cos(l\phi)\end{bmatrix}; 1 \le R < \infty \tag{28}$$

Continuity of F_l and dF_l/dR at the interface of fiber leads to eigen value equation for $\tilde{\beta}$ of each mode or equivalently $\widetilde{U}$ and $\widetilde{W}$. The eigen value equation is given by

$$\widetilde{U}\frac{J_{l+1}(\widetilde{U})}{J_l(\widetilde{U})} = \widetilde{W}\frac{K_{l+1}(\widetilde{W})}{K_l(\widetilde{W})} \tag{29}$$

The eigen value equation is the same for both *EH* and *HE* modes in scalar approximation. For $l = 0$, Equ. (28) is the same as that of eigen value equation for *TE* mode given in Equ. (21), which implies that the *TE* mode has the same propagation constants in both scalar and vector wave equations.

2.4.1 Propagation constant and polarization correction

Solving Equ. (28) yields the scalar propagation constant $\tilde{\beta}$.

$$\tilde{\beta} = \frac{V}{\rho(2\Delta)^{1/2}}\left\{1 - 2\Delta\frac{\widetilde{U}^2}{V^2}\right\}^{1/2} \tag{30}$$

From Equ. (29), it is clear that all modes have the same propagation constant. To account for the polarization effects of modes, we need to add a polarization correction term to the scalar propagation constant. This can be done by introducing the polarization term $\boldsymbol{\nabla}_t \ln n^2$ through the perturbation method to the scalar wave equation. This is equivalent to assuming that the fiber has slightly deformed core which introduces birefringence effect to the modes. Hence, the sum of scalar propagation constant and the polarization correction term gives the exact or vector propagation constant i.e., $\beta_i = \tilde{\beta} + \delta\beta_i$, where β_i is the vector propagation constant, $\tilde{\beta}$ is the scalar propagation constant and $\delta\beta_i$ is the

polarization correction term to the i[th] mode. The polarization correction terms for fundamental ($\delta\beta$), odd and even HE_{21} modes ($\delta\beta_1, \delta\beta_3$), TM_{01} ($\delta\beta_2$) and TE_{01} ($\delta\beta_4$) are given by [1]

$$\delta\beta = -\frac{(2\Delta)^{3/2}}{2\rho}\frac{\widetilde{U}^2\widetilde{W}}{V^3}\frac{K_0(\widetilde{W})}{K_1(\widetilde{W})}$$

$$\delta\beta_1 = \delta\beta_3 = -\frac{(2\Delta)^{3/2}}{2\rho}\frac{\widetilde{U}^2\widetilde{W}}{V^3}\frac{K_1(\widetilde{W})}{K_0(\widetilde{W})} \tag{31}$$

$$\delta\beta_2 = -\frac{(2\Delta)^{3/2}}{2\rho}\frac{\widetilde{U}^2\widetilde{W}}{V^3}\frac{K_1(\widetilde{W})}{K_2(\widetilde{W})}$$

$$\delta\beta_4 = 0$$

From the above equation, the polarization correction term for TE_{01} mode is $\delta\beta_4 = 0$, which implies that the TE_{01} mode formed due to the combination of linearly polarized modes under weakly guiding approximation has the same propagation constant as that of the TE_{01} mode, which is a direct solution of vector wave equation.

2.5 Linearly polarized modes

The modes of weakly guiding fiber are referred to as linearly polarized (LP_{lm}) modes, where l and m denote azimuthal and radial dependence of the mode. For $l = 0$, the Equ. (28) has only one solution that has no azimuthal variation i.e., $\Psi = F_0(R)$. As there is no preferred axis of symmetry in circular fibers, the transverse electric field can be treated to be parallel to one of an arbitrary pair of orthogonal axes, which may be assumed as x- and y-axis [8]. Hence, there are two fundamental modes, one with transverse electric field parallel to x-axis ($LP_{01(\hat{x})}$ or $HE_{11(\hat{x})}$) and the other to y-axis ($LP_{01(\hat{y})}$ or $HE_{11(\hat{y})}$). This is applicable for all HE_{1m} modes. HE_{1m} modes are exceptional cases because their modal equation does not have any polarization information while all other modes retain some polarization information.

For $l \geq 1$, Equ. (28) has two solutions and with azimuthal dependency i.e., $\Psi = F_l(R)\sin(l\phi)$ and $\Psi = F_l(R)\cos(l\phi)$. As discussed above, each solution can be further assumed to have x- and y-polarizations. The transverse electric field $\boldsymbol{e}_t$ depends on the particular combinations of these solutions with orthogonal polarizations. Hence, there are four possible modes. These four modes have the same scalar propagation constant $\tilde{\beta}$ but

their exact propagation constants are different. The four vector solutions constructed from solutions of scalar wave equation are given by

$$\begin{aligned} e_{xe} &= F_l(R)\cos(l\phi)\,\hat{x}; \qquad e_{xo} = F_l(R)\sin(l\phi)\,\hat{x} \\ e_{ye} &= F_l(R)\cos(l\phi)\,\hat{y}; \qquad e_{yo} = F_l(R)\sin(l\phi)\,\hat{y} \end{aligned} \tag{32}$$

These four modes e_{xe}, e_{xo}, e_{ye}, and e_{yo} are represented as $LP^{a}_{11(\hat{x})}$, $LP^{b}_{11(\hat{x})}$, $LP^{a}_{11(\hat{y})}$, and $LP^{b}_{11(\hat{y})}$ respectively under LP mode designation and the same notation is used throughout this thesis. Due to circular symmetry, a fiber is unchanged by rotation about its axis. Hence, if a mode is rotated arbitrarily then it must remain a mode with the same propagation constant, although not necessarily the same mode. The new mode can be represented as the linear combinations of all other four modes with the same propagation constants. But, these four modes have different exact propagation constants (β) although they have the same scalar propagation constant ($\tilde{\beta}$). Hence, none of these four modes are the modes of a fiber. The correct linear combination can be formed by combining those modes which have same properties under rotation by 90° and under reflections in x- and y-axes [8, 15].

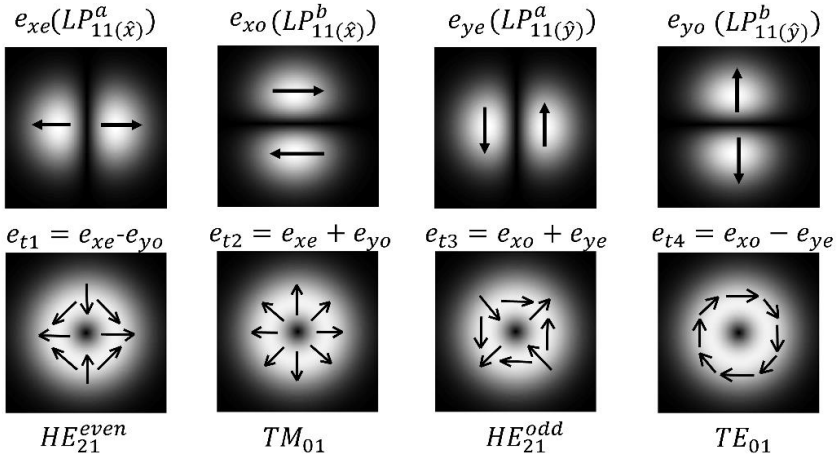

Fig. 2.4. Linearly polarized modes and the vector modes generated from their linear combination.

Figure 2.4 shows four LP_{11} modes and their possible linear combinations that generate vector modes. Following the symmetry operations, e_{xe} can be combined with e_{yo} and e_{xo} can be combined with e_{ye} as they are same under rotation. By considering the symmetric and anti-symmetric combinations, the transverse fields of four modes can be constructed. These combinations are consistent with the symmetry properties of fiber. The transverse fields $\boldsymbol{e}_{t2}$ and $\boldsymbol{e}_{t4}$ remain unchanged under rotation by arbitrary angle and under reflection. However, $\boldsymbol{e}_{t1}$ changes into a pattern which is a linear combination of

$\boldsymbol{e}_{t1} + \boldsymbol{e}_{t3}$ under arbitrary rotation. But, these two modes have the same correction term ($\delta\beta_1 = \delta\beta_3$) and hence the same exact propagation constant for which their combination is allowed under symmetry. The representation of vector modes in terms of LP_{11} modes is given by

$$\begin{aligned} e_{HE^{e}_{21}} &= F_l(R)\{cos\phi\hat{x} - sin\phi\hat{y}\} \\ e_{TM_{01}} &= F_l(R)\{cos\phi\hat{x} + sin\phi\hat{y}\} \\ e_{HE^{o}_{21}} &= F_l(R)\{sin\phi\hat{x} + cos\phi\hat{y}\} \\ e_{TE_{01}} &= F_l(R)\{sin\phi\hat{x} - cos\phi\hat{y}\} \end{aligned} \tag{33}$$

We use these relations in chapter 4 and chapter 5 to construct a new set of vector vortex modes. A few mode optical fiber that can support upto two *LP* modes is used in the experiments so as to generate all vector vortex modes. The theory presented in this chapter helps in better understanding of further chapters.

References

1. Allan W. Snyder, and John D. Love, "*Optical Waveguide Theory,"* Chapman and Hall, (1983).
2. Ajoy Ghatak and K. Thyagarajan, "*Introduction to fiber optics,"* Cambridge University Press, (1997).
3. M. S. Sodha and A. K. Ghatak, "*Inhomogeneous Optical Waveguides,"* Plenum Press, New York and London (1977).
4. J.A. Stratton, "*Electromagnetic Theory,"* McGraw-Hill, New York (1941).
5. R.B. Adler, "Waves on inhomogeneous cylindrical structures," *Proc. I.R.E.*, **40,** 339-48 (1952).
6. C. C. Johnson, "*Fields and Wave Electrodynamics,"* McGraw-Hill, New York (1965).
7. E. Snitzer, "Cylindrical dielectric waveguide modes," *J. Opt. Soc. Am.*, **51**, 491-498 (1961).
8. Allan W. Snyder and William R. Young, "Modes of optical waveguides," *J. Opt. Soc. Am.,* **68**, 297-309 (1978).
9. K. Thyagarajan, Ajoy K. Ghatak, and Anurag Sharma, "Vector modes of an optical fiber in the weakly guiding approximation," *J. Light. Tech.,* **7**, 51-53 (1989).

10. R.A. Sammut, C.D. Hussey, J.D. Love, et al. "Modal analysis of polarization effects in weakly-guiding fibres," *IEEE Proc.*, **128**, 173-187 (1981).
11. A. Sharma, "On constructing linear combinations of LP-modes to obtain zeroth order vector modes of optical fibers," *Appl. Opt.*, **27**, 2647-2649 (1998).
12. A. W. Snyder, "Asymptotic expressions for eigen functions and eigenvalues of dielectric or optical waveguides," *IEEE. Trans. Microwave Theory Tech.*, **17**, 1130-1138 (1969).
13. D. Gloge, "Weakly guiding fibers," *Appl. Opt.*, **10**, 2252-2258 (1971).
14. J.A. Arnaud, "*Beam and Fiber Optics*," Academic Press, New York (1976).
15. D. L. A. Tjaden, "First-Order Correction to 'Weak-Guidance' Approximation in Fiber Optics Theory," *Philips J. Res.* **33**, 103 (1978).

CHAPTER

3

Singularities in Fiber Modal Fields

Contents

CHAPTER 3

Singularities in Fiber Modal Fields

In this chapter, we experimentally demonstrate the excitation of various vector modes and linearly polarized modes using few mode optical fiber. Two fibers of different V-numbers, 3.57 and 4.46 are chosen for this purpose. The modal excitation is achieved with on-axis and off-axis skew launching of linearly polarized Gaussian beam onto the core of optical fiber. The vector modes discussed in previous chapter are generated and their spatial polarization distribution is estimated with the help of a rotating analyzer. Higher order linearly polarized modes LP_{02}, LP_{21} and some arbitrary modal fields are generated. Further, we investigate all the generated modal fields for the presence of singularities in their intensity null regions. A first order phase vortex is generated from a donut shaped mode and switching between oppositely charged vortices is demonstrated by changing input state of polarization. Singularities are also observed in LP_{02}, LP_{21} modes and also a few arbitrary modal fields and these are observed to increase with V number of the fiber.

3.1 Introduction

Singularities are points or lines where a physical quantity representing the system is undefined [1,2]. Generally these singularities are mainly classified into two types in optics i.e., scalar and vector, of which the former corresponds to the undetermined phase and the latter for undetermined polarization [2-4]. Nye and Berry were the first to discover the presence of dislocations in electromagnetic waves which are analogous to crystals [5,6]. Later, it was reported that optical fields contain phase singularities in null intensity regions, where the phase changes by a multiple of 2π around the singular point [7-9]. These singularities were first identified in the donut shaped higher order *LG* mode fields and then in speckle fields, where each speckle spot is shown to have one phase singular point [10]. The presence of phase singular region can be identified using simple interferometric technique, in which the interferograms of singular beams with a Gaussian beam show a signature of fork or spiral pattern as a result of the helicity of the wave front [7]. The order of phase singularity is measured with the number of forks that appear in the interferogram and is often referred as topological charge, which is positive for right

helical waves and negative for left helical waves [2,3]. The presence of singularities in fiber modal fields was first reported by Bazhenov [11]. Later, Lim et. al. studied the nature of singularities in fiber modal fields using few mode and multimode fibers [12]. The study of modal behavior in few mode fiber (FMF) is of great interest due to their applications in various fields such as long distance communications [13], fiber lasers [14], optical sensors [15-17], and singular optics [18,19]. Recently, nonlinear effects and ultra violet four wave mixing are reported to be observed in higher order LP_{02} mode of FMF [20,21]. The FMFs are also found to be useful in quantum cryptography [22], and STED microscopy [23] by specially designing the fiber geometry, called vortex fibers, which can preserve vortex modes for longer distances.

In this chapter, we discuss the scalar or phase singularities present in the higher order linearly polarized fiber modal fields. We use two optical fibers with different V-numbers to excite various vector and scalar modes. The zeroth order vector modes such as radial, azimuthal and hybrid spatial polarization are excited by controlling coupling conditions. A first order phase singularity is generated from a donut shaped vortex mode and switching between the vortices of opposite helicity is demonstrated by changing the input SOP. The singularities present in higher order linearly polarized fiber modes such as LP_{11}, LP_{02} and LP_{21} are discussed along with some arbitrary modal fields. The presence of singularity in respective modes is verified by forming interferograms of the modes with a reference Gaussian mode.

3.2 Experimental details

A 5 mW He-Ne laser of wavelength 632.8 nm operating in TEM_{00} vertically polarized Gaussian mode is first made to pass through a step neutral density (ND) filter to control the intensity of light, which then passes through a half wave plate (HWP). Light emerging from the HWP is focused using a high numerical aperture (40X, 0.65 NA) and short focal length microscope objective lens (L1) which is mounted on a precise rotational stage that enables the light to launch at an angle with respect to fiber axis.

To study the singularities in the linearly polarized modes of FMF, we first choose a fiber that supports only 2 LP modes, LP_{01} and LP_{11}. The optical fiber chosen for the experiment has an approximate length of 23 cm, core radius of 1.8 μm, 0.2 NA and V-number of 3.57 when operated at a wavelength of 632.8 nm. This indicates the fiber can support 6 wave guide modes of which the fundamental LP_{01} (HE_{11}) mode is a two-fold

degenerate and first order LP_{11} mode is a four-fold degenerate whose combinations result in four vector modes TE_{01}, TM_{01} and $HE_{21}^{o,e}$ [24-26]. The focused spot from L1 is adjusted to fall on the tip of the cleaved end of optical fiber, mounted using a 3-axis micro translational stage, enabling an offset launching of light with respect to fiber axis. The output from the fiber is then collimated using L2 on to a charge coupled device (CCD) camera (Thorlabs DCU223C with 2x2 mm capture area and 4.65µm pixel size) to scan tip of the fiber and image the modal field, placed at a distance of 20 cm from the fiber tip. An analyzer is inserted between L2 and CCD to study the polarization content of output beams. An interferometer is constructed in parallel to the fiber, where a Gaussian beam from the Laser is guided directly in free space with the help of two beam splitters (BS1, BS2) and two mirrors (M1, M2) and made to interfere with the fiber output modal field to investigate the singularities present in them. The phase singularities in fiber modal fields can be identified with the presence of fork like structures in the interferograms. The schematic diagram of the experimental setup is shown in Fig. 3.1 and the photograph is shown in Fig. 3.2.

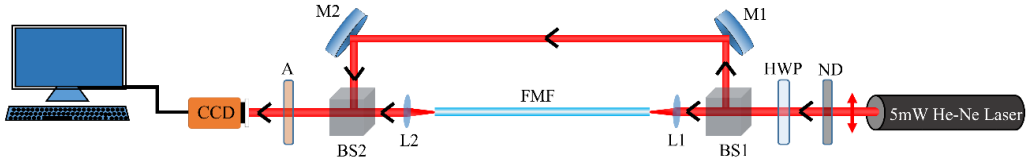

Fig. 3.1. Schematic diagram of the experimental setup for generating LP modes.

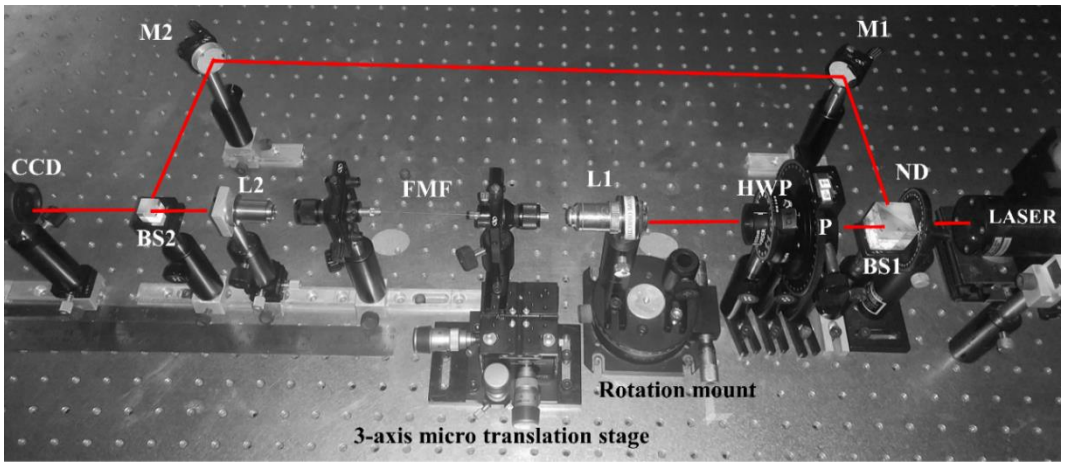

Fig. 3.2. Photograph of experimental setup for generating LP modes.

3.3 Results and discussion

At first, the tip of the fiber is adjusted such that the focused spot from MO falls on the center of the core which excites the fundamental Gaussian mode LP_{01} (HE_{11}), shown in Fig. 3.3 (a1). As the LP_{01} mode does not have intensity null regions within the modal field, the interferograms contain only concentric circular fringes but no singularities as shown in Fig. 3.3 (a2). Next, the tip of the fiber is adjusted for an offset illumination to excite LP_{11} mode that has two lobes separated by a null intensity line where the presence of singularity is expected. The LP_{11} mode generated at the fiber output is shown in Fig. 3.3 (b1). As the two adjacent lobes are π phase shifted, there appears a fringe jump along the null line of the LP_{11} mode as shown in Fig. 3.3 (b2).

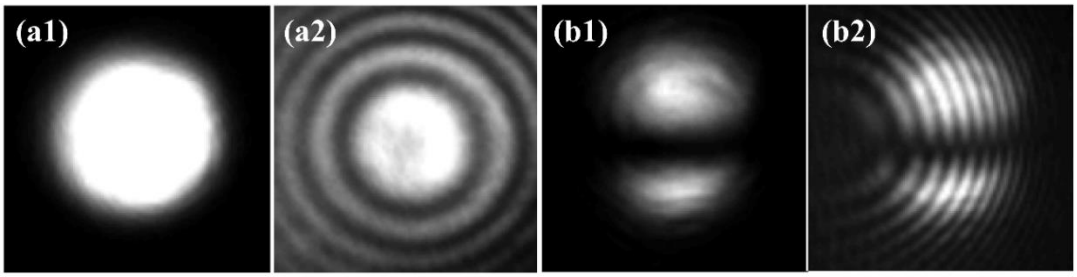

Fig. 3.3. Modes at fiber output (a1) fundamental LP_{01} mode, (b1) LP_{11} mode, (a2) and (b2) are the interferograms of (a1) and (b1) respectively.

3.3.1 Generation of Vector modes

As discussed in Chapter 2, LP_{11} modes are four-fold degenerate and their selective combinations will result in vector modes. These vector modes can be generated by precisely controlling the coupling conditions of fiber with respect to incident light. Various modes can be excited by launching tilted and/or offset Gaussian beam into the optical fiber [27-29]. By launching skew and offset rays into the fiber core, one can realize four possible vector modes i.e., TE_{01}, TM_{01} and $HE_{21}^{o,e}$ at the fiber output [30,31]. The theoretical background of these modes is discussed in Sec. 2.3.2 of chapter 2.

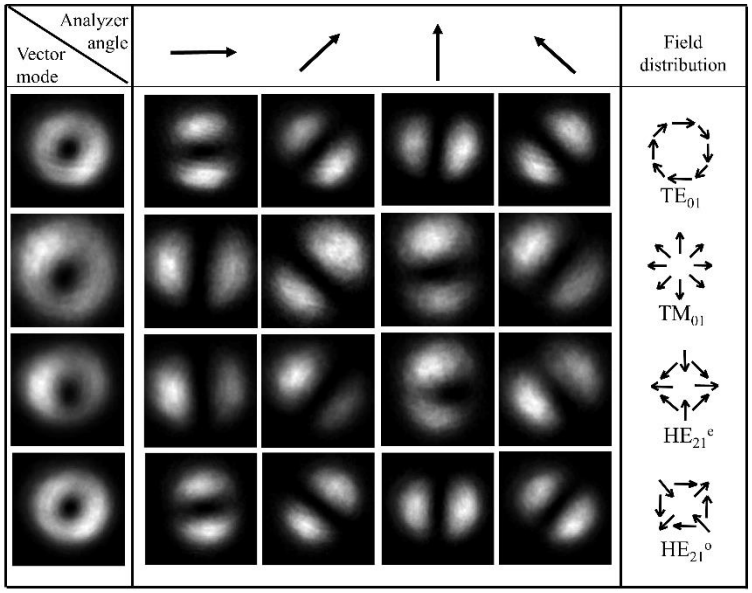

Fig. 3.4. Cylindrical vector beams excited for different coupling conditions.

Figure 3.4 shows the experimentally generated vector modes and their behavior when passed through an analyzer at discrete orientation angles 0° (→), 45° (↗), 90° (↑), and 135° (↖) respectively. As all the vector modes look alike in their intensity distribution, an analyzer is essential to distinguish them. By observing the rotation of two lobe pattern with respect to rotation of analyzer, the field distribution across the mode can be estimated. Though these vector modes have null intensity at the core region, due to the polarization inhomogeneity across the mode, the phase cannot be defined. But, the donut modes with homogenous polarization and dark core region have a phase vortex at their center and are often referred to as scalar vortex modes or simply vortex modes. These modes are equivalent to *LG* modes of radial order zero and azimuthal order one (LG_0^1). In fibers, these modes can be generated as linear combinations of vector modes i.e., $TE_{01} \pm iTM_{01}$ or $HE_{21}^o \pm iHE_{21}^e$ [26].

3.3.2 Switching of first order phase vortices

Figure 3.5(a) shows a near homogenously polarized donut shaped vortex mode generated at fiber output. In fiber, the most commonly observed modes are the inhomogeneously polarized vector vortex modes for arbitrary coupling. To excite a homogeneously polarized vortex mode, precise control over the coupling conditions is needed so as to selectively excite a combination of TE_{01}, TM_{01} modes or HE_{21}^o, HE_{21}^e modes with $\pi/2$ phase difference. Hence, the generated mode appears to be slightly distorted as it is a homogeneously polarized vortex mode. This mode is interfered with reference Gaussian

beam to observe the presence of vortex or phase singularity on the beam axis, which results in a downward fork in non-coaxial interference and a left handed spiral in coaxial interference of vortex mode with reference Gaussian beam, as shown in Fig. 3.5 (b) and Fig. 3.5 (c) respectively. These fork and spiral like structures in the interferograms point to the significance of the dislocation in wave front. This indicates that the generated mode has left helical wave front with topological charge -1.

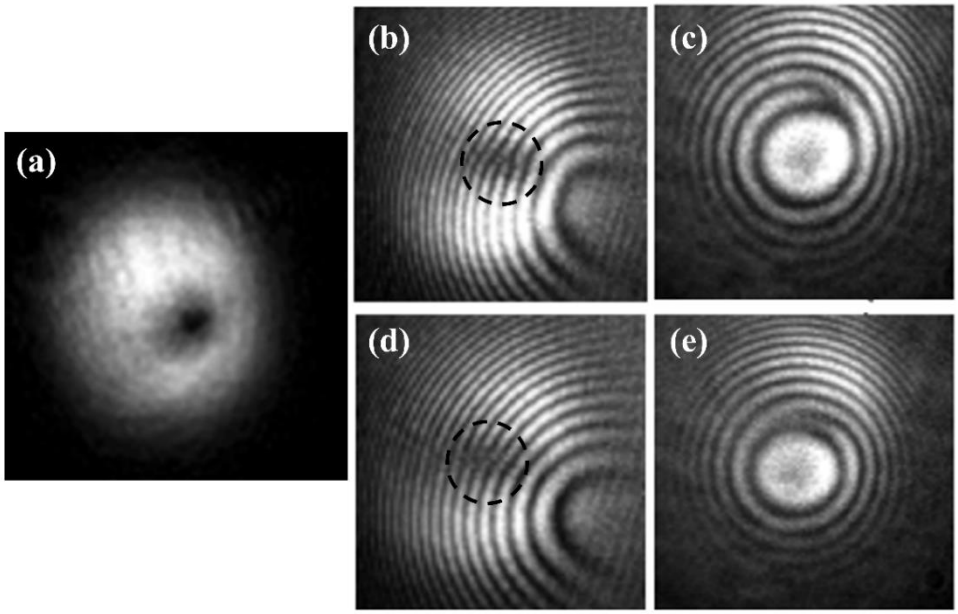

Fig. 3.5. Switching of fork and spiral interferograms of vortex mode; (a) generated vortex mode, (b) a downward fork, (c) left handed spiral, (d) an upward fork and (e) right handed spiral.

The charge of this vortex mode is observed to change under the action of change in input polarization. Keeping the coupling conditions unaltered, the input SOP is changed using a HWP at launching end. It is observed that for 90^{o} change in input SOP, the downward fork flipped and became an upward fork as shown in Fig. 3.5 (d). Further, Fig. 3.5 (e) shows the right handed spiral, which is formed due to coaxial interference, indicating that the vortex mode has right helical wave front with topological charge +1. Hence, just by changing the input SOP between orthogonal states, one can switch between the vortex modes of opposite charge.

3.3.3 Singularities in higher order modes

Then, to observe the singularities in higher order *LP* modes, a fiber that supports more than 2 *LP* modes is required. In this case, we chose an optical fiber with a core radius of 4.5 μm, 0.1 NA and with V-number 4.46 when operated at 632.8 nm and of

approximately the same length as the previous case (23 cm) for exciting higher order *LP* modes by launching linearly polarized Gaussian beam. A linearly polarized LP_{lm} mode has 2 degenerate modes for l=0 and 4 degenerate modes for l≥1. The fiber used for our experiment can support 4 LP_{lm} modes i.e., LP_{01}, LP_{11}, LP_{02}, and LP_{21}. Calculating the degenerate modes for each *LP* mode, the fiber can support 12 distinct vector modes [25,26]. These modes can be regarded as true wave guide modes as they are independent of each other and can be realized at fiber output by altering the coupling conditions and input SOP.

At first, the laser beam is focused using L1 on to the center of core of cleaved fiber tip held on a 3-axis precision translation stage, for which the fundamental LP_{01} mode is excited. As LP_{0m} modes are circularly symmetric modes and can be excited by launching light along the fiber axis, a slight offset in the position of fiber core with respect to focused spot will excite LP_{02} mode. The excited LP_{02} mode, when observed under rotating analyzer, shows linearly polarized behavior i.e., the intensity becomes minimum when the axis of analyzer is perpendicular to the plane of polarization of the excited mode. We assume that most of the power in the excited mode is coupled to LP_{02} mode and the amount of power coupled to LP_{01} may be neglected. Furthermore, LP_{01} mode doesn't have singular behaviour. So the observed singularities in the modal field can be completely attributed to LP_{02} mode alone.

The LP_{02} mode generated from fiber output is shown in Fig. 3.6 (a1), which resembles the intensity profile of an *LG* mode of radial order one and azimuthal order zero (LG_1^0). The central bright spot and the outer ring of LP_{02} mode are π phase shifted and are separated by a ring like null intensity region [32]. This change in phase leads to a phase distortion in the null intensity region where the phase is undetermined or singular at certain points and the nature of singularity can be identified from interferograms. The reference Gaussian beam is allowed to interfere with LP_{02} mode from fiber output and the interferograms are captured using CCD camera. The interferogram contains fork like structures in the dark region of LP_{02} mode, which symbolizes the presence of phase singularities in the modal field. As the inner and outer rings are π phase shifted, a fringe jump at the boundary can be observed in Fig. 3.6 (a2). Careful observation reveals that the interferogram consists of a pair of upward and downward forks indicating phase singular regions with opposite sign. The two upward and downward forks are shown with '*' and '+' respectively in Fig. 3.6 (a2). Considering the topological charge of individual

forks, +2 charge can be assigned for a pair of upward forks and -2 charge for a pair of downward forks. Hence the resultant topological charge of the LP_{02} modal field is observed to be zero.

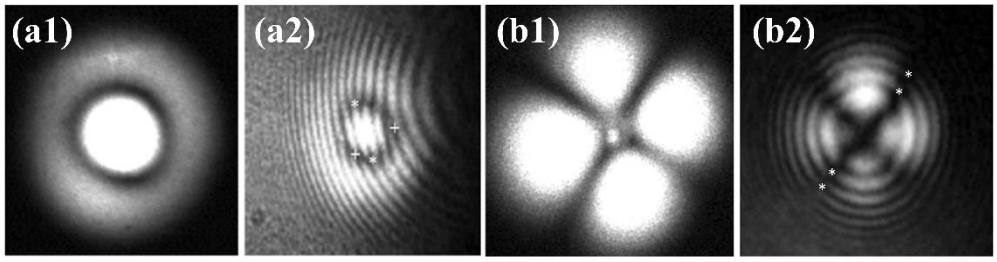

*Fig. 3.6. (a1) LP_{02} mode, (a2) Interferogram showing the upward (denoted with *) and downward (denoted with +) forks in the LP_{02} mode, (b1) LP_{21} mode, (b2) interferogram of LP_{21} mode (fringe jumps are shown with *).*

Further, to generate LP_{21} mode we adjusted the coupling condition for offset and skew launching of light into the fiber that resulted in a four lobe intensity pattern as shown in Fig. 3.6 (b1). This mode has intensity nulls between adjacent lobes and also resembles the spatial profile of HG_{11} mode where adjacent lobes are π phase shifted. The excited mode is interfered with reference Gaussian mode to observe the presence of singularities. As expected, the interferogram contains fringe jumps between adjacent lobes which confirms that adjacent lobes are π phase shifted as shown in Fig. 3.6 (b2). The intensity of the generated modes is lowered using an additional ND filter while recording the interferograms to obtain good contrast fringes.

Apart from LP_{lm} modes, which can be excited by precise control over coupling conditions, some arbitrary modes also get generated in the fiber which are linear combinations of certain vector modes. One such complex modal field is encountered while adjusting the coupling conditions to excite LP_{21} mode, which is the linear combination of $2HE_{12} - EH_{11} + HE_{31}$ [32]. The intensity patterns of the mode with respect to rotating analyzer are captured using CCD camera and shown in Fig. 3.7. From Fig. 3.7, it can be observed that the modal patterns at 45^0 and 135^0 resemble the intensity profile of tilted HG_{02} mode and the pattern at 90^0 resembles HG_{11} mode respectively.

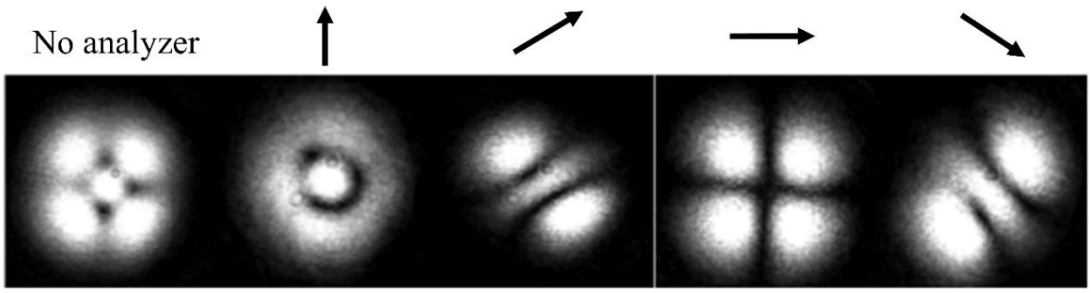

Fig. 3.7. A mode excited by the linear combination of $2HE_{12} - EH_{11} + HE_{31}$*; and their intensity patterns with respect to analyzer rotation.*

3.3.4 Singularities in arbitrary modal fields

Further, some random modal fields are generated for arbitrary coupling conditions. Figure 3.8 (a1) shows a donut shaped mode, which is expected to be second order vortex mode. When this mode is interfered with the reference beam, the interferogram reveals that this mode is a combination of two vortex modes of opposite charge (+1 and -1) separated by a small distance. From this it is evident that higher order vortices are unstable and they decompose into single charged vortices under small perturbations. Hence, it is difficult to generate modal fields with second order phase vortex in fibers [12]. It can be clearly observed from Fig. 3.8 (a2) that two forks i.e., an upward fork and a downward fork are closely spaced at the center dark region of the modal field. Figure 3.8 (b1) shows another arbitrary modal field that embeds two null intensity regions within. The interferogram of this mode is shown in Fig. 3.8 (b2) in which three fork patterns (2 upward and 1 downward) can be observed. These singularities are observed to be stable and sustain small perturbations. It can be observed from the experimental results that as V number increases, the number of modes supported by the fiber increases as well as the number of singularities present in the modal fields also increases. It is reported that the total charge of the singularities is not preserved in fibers where the modal fields are strongly dependent on the boundary [33]. This can be rectified by using fibers of large core diameters, where the generation of individual modes is difficult and the modal fields are often referred to as speckle fields. The number of singularities present in the modal field is very high for scattered fields or speckle fields of multimode fiber where each speckle point can consist of one singularity and the number of positive and negative charged phase singularities is equal and hence the total charge is preserved.

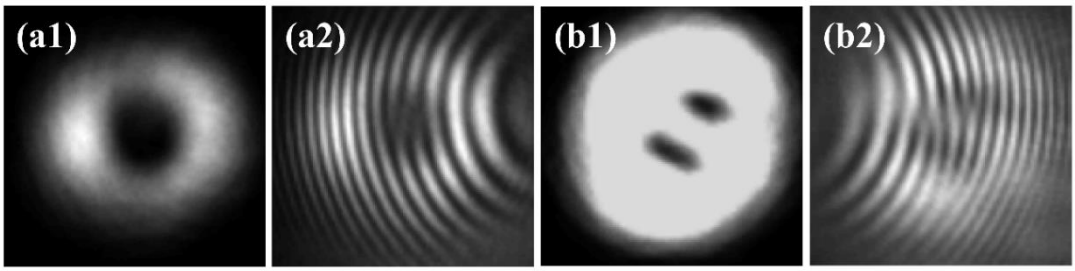

Fig. 3.8. (a1), (b1) arbitrary modal fields, (a2), (b2) their corresponding interferograms showing fork like structures.

3.4 Conclusion

In summary, we have presented the singular aspects of linear polarized modes of few mode optical fiber. The vector modes are experimentally generated by precisely controlling the coupling conditions. First order phase vortex is generated from donut shaped vortex mode and switching between positive and negative charged vortices is demonstrated by changing input SOP. The presence of singularities in higher order *LP* modes is examined and analyzed. Apart from *LP* modes, some arbitrary modal fields are generated and the presence of phase singularities is identified. The generation of phase singularities of second order in fiber is found to be difficult as they are highly unstable and decompose into single charged vortices for small ambient perturbations. It is also observed that the number of singularities present in the modal field is directly proportional to the V-number of the fiber and is maximum in case of multimode fibers of large core diameters. This investigation helps us to understand the fiber modal fields in terms of phase singularities present in them. As the phase of the modal fields is highly sensitive to external perturbations on the fiber, the results may find applications in interferometric sensors.

References

1. J.F. Nye, *'Natural Focusing and Fine Structure of Light,'* IOP Publishing, London, (1999).
2. I. I. Mokhun, *Introduction to linear singular optics* in '*Optical correlation techniques and applications'*, SPIE Press, Bellingham, USA, 1-132 (2007).
3. Enrique J. Galvej, *Singular optics and phase properties* in *'Structured Light and Its Applications'*, Academic Press, Elsevier, 63-77 (2008).

4. Mark R. Dennis, Kevin O'Holleran, and Miles J. Padgett, "Singular optics: Optical vortices and polarization singularities," *Progress in Optics,* **53**, 293-363 (2009).
5. M.V. Berry and M.R. Dennis, "Phase Singularities in Isotropic Random Waves," *Proc. R. Soc. Lond. A.,* **456**, 2059-2079 (2000).
6. J. F. Nye and M. V. Berry, "Dislocations in wave trains," *Proc. R. Soc. Lond. A.,* **336**, 165-190 (1974).
7. M. Harris, C.A. Hill and J. M. Vaughan, "Optical helices and spiral interference fringes," *Opt. Commun.,* **106**, 161-166 (1994).
8. N. R. Heckenberg, R. McDuff, C. P. Smith, et.al., "Generation of optical phase singularities by computer-generated holograms," *Opt. Lett.,* **17**, 221-223 (1992).
9. J. Courtial and M.J. Padgett, "Performance of a cylindrical lens mode converter for producing Laguerre–Gaussian laser modes," *Opt. Commun.,* **159**, 13–18 (1999).
10. B. Ya. Zel'dovich, N. F. Pilipetskil and V. V. Shkunov, *"Principles of Phase conjugation,"* Nauka, Moscow (1986).
11. V. Yu. Bazhenov, M. V. Vasnetsov, and M. S. Soskin, "Laser beams with screw dislocations in their wave fronts," *JETP Lett.,* **52**, 429-431 (1990).
12. Dong Sung Lim, and El-Hang Lee, "Structural characteristics and properties of phase singularities in optical fibers," *J. Opt. Soc. Korea*., **1**, 81-89 (1997).
13. Fatih Yaman, Neng Bai, Benyuan Zhu, et.al., "Long distance transmission in few-mode fibers," *Opt. Express.,* **18**, 13250-13257 (2010).
14. M. Faucher, and Y. K. Lizé, "Mode field adaptation for high power fiber lasers," *2007 Conference on Lasers and Electro-Optics (CLEO), IEEE Proc.,* CF17, 1-2 (2007).
15. An Li, Yifei Wang, Qian Hu, et.al., "Few-mode fiber based optical sensors," *Opt. Express.,* **23**, 1139-1150 (2015).
16. Yuqiang Fan, George Wu, Wanting Wei, et.al., "Fiber-optic bend sensor using LP_{21} mode operation," *Opt. Express.,* **20**, 26127-26134 (2012).
17. Yufeng Yuan, George Wu, Xian Li, et al., "Effect of twisting and bending on LP_{21} mode propagation in optical fiber," *Opt. Express.,* **36**, 4248-4250 (2011).
18. A. V. Volyar and T. A. Fadeeva, "Optics of singularities of a low mode fiber: optical vortices," *Opt. Spectros.,* **85**, 272–280 (1998)
19. A. V. Volyar, V. Z. Zhilaitis, and T. A. Fadeeva, "Optical vortices in low-mode fibers: III. Dislocation reactions, phase transitions, and topological birefringence," *Opt. Spectrosc.,* **88**, 397–405 (2000)

20. Y. Chen, Z. Chen, W. J. Wadsworth, et.al., "Nonlinear optics in the LP_{02} higher-order mode of a fiber," *Opt. Express.*, **21**, 17786-17799 (2013).
21. Y. Chen, W. J. Wadsworth, and T. A. Birks, "Ultra violet four-wave mixing in the LP_{02} fiber mode," *Opt. Lett.*, **38**, 3747-3750 (2013).
22. Alicia Sit, Robert Fickler, Fatimah Alsaiari, et. al., "Quantum cryptography with structured photons through a vortex fiber," *Opt. Lett.,* **43**, 4108-4111 (2018).
23. Lu Yan, Poul Kristensen, and Siddharth Ramachandran, "Vortex fibers for STED microscopy," *APL Photonics.,* **4**, 022903 (1-7) (2019).
24. Allan W. Snyder and William R. Young, "Modes of optical waveguides," *J. Opt. Soc. Am.,* **68**, 297-309, (1978).
25. Ajoy Ghatak and K. Thyagarajan, *"Introduction to fiber optics,"* Cambridge University Press, (1997).
26. Allan W. Snyder, and John D. Love, "*Optical Waveguide Theory,"* Chapman and Hall, (1983).
27. M. Mostafavi, T. Itoh, and R. Mittra, "Excitation of an optical fiber by a Gaussian beam," *Appl. Opt.*, **14**, 2190-2193 (1975)
28. Masaaki Imai and Elmer H. Hara, "Excitation of the Fundamental and Low-Order Modes of Optical Fiber Waveguides with Gaussian Beams.2: Offset Beams," *Appl. Opt.*, **14,** 169-173 (1975).
29. Masaaki Imai and Elmer H. Hara, "Excitation of the Fundamental and Low-Order Modes of Optical Fiber Waveguides by Gaussian Beams.1: Tilted Beams," *Appl. Opt.*, **13**, 1893-1899 (1974).
30. V.V.G. Krishna Inavalli and Nirmal K. Viswanathan, "Switchable vector vortex beam generation using an optical fiber," *Opt. Commun.,* **283**, 861–864 (2009).
31. Nirmal K. Viswanathan and V. V. G. Inavalli, "Generation of optical vector beams using a two-mode fiber," *Opt. Lett.* **34**, 1189-1191 (2009).
32. E. Snitzer and H. Osterberg, "Observed Dielectric Waveguide Modes in the Visible Spectrum," *J. Opt. Soc. Am.*, **51**, 499-505. (1961).
33. F. T. Arecchi, *Pattern formation and space-time organization in nonlinear optics* in "*Nonlinear dynamics and spatial complexity in optical systems*," IOP Publishing, Bristol, 65-113 (1993).

CHAPTER

4

Generation and Characterization of Spiral Vector Beams

Contents

CHAPTER 4

Generation and Characterization of Spiral Vector Beams

A simple method for generating spiral vector beams using few mode optical fiber is demonstrated. These beams are generated due to a combination of orthogonal linearly polarized modes with diagonal and anti-diagonal polarization vector in the few mode optical fiber. The excitation of these modes is controlled by the incident state of polarization and coupling conditions at the fiber input end. Vector beams with spiral distribution (clockwise and counter clockwise) of polarization axis in transverse direction are generated and switching between them is demonstrated. The experimental results obtained emphasize strong dependency of polarization of generated spiral vector beams and other orthogonal modes on input state of polarization. Experimental results are found to be in good agreement with simulated results.

4.1 Introduction

Spiral vector beams (SVB) are optical vector fields wherein the linear polarization vector makes a constant azimuthal angle in radial direction across the beam and the electric field lines form a logarithmic spiral, first theoretically proposed by Gori [1]. Later, Borghi et al., predicted that these beams can be generated from coherent superposition of orthogonal *HG* modes and they studied the focusing and propagation characteristics of these beams in both paraxial and non-paraxial regime [2,3]. The focusing properties of these beams make them useful in fields such as optical trapping, lithography and high resolution microscopy [2,4]. Few characteristic quality parameters of spirally polarized fields in paraxial limit are theoretically investigated by Ramirez et al., and experimentally realized by generating such beams using polarization conversion devices [5,6]. Generation of these beams is also reported by using special optical devices such as stress birefringent wave plates and subwavelength gratings [7,8]. Apart from theoretical predictions and bulk optical experimental methods, SVBs were also generated in an optical fiber by chemically etching a micro-axicon on the tip of a fiber that converts the excited vortex beam into a spirally polarized beam [9]. All these methods involve special optical components with complex fabrication techniques which increases cost and

complexity of the experiment. Nevertheless, fiber based methods are preferable over bulk optics methods in many applications due to flexibility and ease of operation [10-12].

Keeping this in view, in this chapter, we presented a simple approach for generating SVBs using few mode fiber (FMF). It is well known that vector beams in optical fiber are linear combinations of orthogonally polarized LP_{11} modes. By exploiting this mode mixing phenomenon, we propose that SVBs can be generated by the inherent combination of orthogonally polarized LP_{11} modes with diagonal and anti-diagonal polarization vector using FMF. Here, we performed a proof-of-concept experiment to achieve the same. The excitation of these modes is controlled by the incident SOP and coupling conditions at the input fiber end. The spiral polarization nature of the generated SVBs is characterized by analyzing the Stokes field. The SVBs with polarization vector oriented in clockwise (CW) and counter clockwise (CCW) direction across the beam are generated and switching between them is demonstrated.

4.2 Formation of Spiral Vector Beams from LP_{11} modes

The field distribution of degenerate LP_{11} mode group is given by [13]

$$LP^{a}_{11(\hat{x})} = \hat{x} f(r) cos\varphi \qquad LP^{b}_{11(\hat{x})} = \hat{x} f(r) sin\varphi$$

$$LP^{a}_{11(\hat{y})} = \hat{y} f(r) cos\varphi \qquad LP^{b}_{11(\hat{y})} = \hat{y} f(r) sin\varphi \tag{1}$$

In Equ. (1), $\hat{x}$ and $\hat{y}$ denote the polarization vector orientation along X and Y axes respectively and $f(r)$ represents the radial field distribution described by a Bessel function while sine and cosine terms represent the azimuthal field distribution of LP_{11} mode. Depending on the polarization vector orientation in the respective modes, $LP^{a}_{11(\hat{x})}$ and $LP^{b}_{11(\hat{y})}$ are called even modes, $LP^{b}_{11(\hat{x})}$and $LP^{a}_{11(\hat{y})}$ as odd modes. A suitable combination of orthogonal LP_{11} modes form zeroth order vector modes or CVBs i.e., radial, azimuthal and hybrid polarized beams with cylindrical symmetry of polarization as shown in Fig. 4.1.

The field distributions of radially polarized TM_{01} and azimuthally polarized TE_{01} modes are given by [13]

$$E_{TM_{01}} = f(r)(\hat{x} cos\varphi + \hat{y} sin\varphi) \tag{2}$$

$$E_{TE_{01}} = f(r)(\hat{x} sin\varphi - \hat{y} cos\varphi) \tag{3}$$

From Equ. (2) and Equ. (3), it is clear that the combination of $\hat{x}$ ($\hat{y}$)-polarized and $\hat{y}$ ($\hat{x}$)-polarized even (odd) modes generate radially (azimuthally) polarized vector beam [14,15]. However, other combination result in hybridly polarized HE_{21}^{odd} and HE_{21}^{even} modes which are not of much scientific interest individually, while their combination with ±π/2 phase difference can generate a circularly polarized optical vortex beam that has both spin and orbital angular momenta [16].

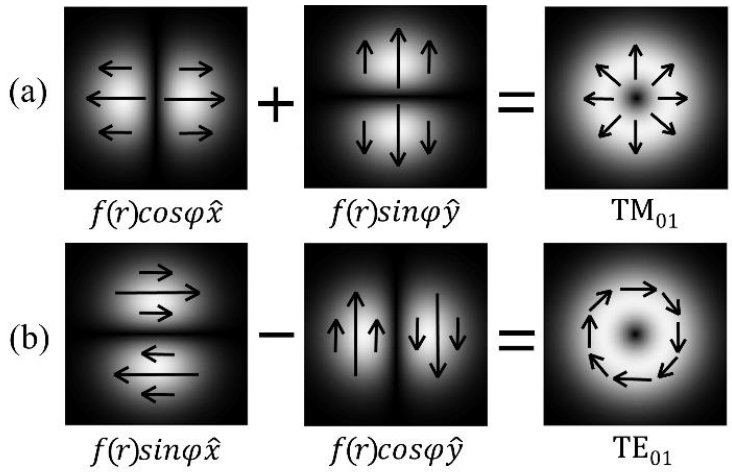

Fig. 4.1.Vectorial representation of orthogonal LP_{11} modes and their combinations; (a) radial vector beam (b) azimuthal vector beam.

From Fig. 4.1, it is clear that the radial and azimuthal CVB have orthogonal polarization and can be transformed into one another by rotating the local polarization vector. During such transformation, the SVBs can be generated at any specific orientation of polarization vector across the beam with varying degrees of spiral nature. Precisely, in our case, the polarization vector in SVBs makes a constant azimuthal angle of π/4 across the beam. However, the generation of SVBs in optical fiber was reported to be due to in-phase and out-of-phase combination of TM_{01} and TE_{01} modes [17, 18]. Another simplest and efficient way to generate the SVBs is similar to that of CVBs i.e., by a combination of orthogonal LP_{11} modes with diagonal and anti-diagonal polarization vector.

The out-of-phase combination of TM_{01} and TE_{01} is given by $E_{TM_{01}} + (e^{i(\pi)})E_{TE_{01}}$ i.e.,

$$E_{(TM_{01}-TE_{01})} = f(r)(\hat{x}cos\varphi + \hat{y}sin\varphi) - f(r)(\hat{x}sin\varphi - \hat{y}cos\varphi) \quad (4)$$

Which can be simplified to obtain the following

$$E_{(TM_{01}-TE_{01})} = f(r)\{(\hat{x} + \hat{y})cos\varphi - (\hat{x} - \hat{y})sin\varphi\} \quad (5)$$

Equation (5) represents a combination of orthogonal LP_{11} modes and this combination generates an SVB with polarization vector oriented in CCW sense.

Further, the in-phase combination of TM_{01} and $TE_{01}$is given by $E_{TM_{01}} + (e^{i(0)})E_{TE_{01}}$ i.e.

$$E_{(TM_{01}+TE_{01})} = f(r)(\hat{x}cos\varphi + \hat{y}sin\varphi) + f(r)(\hat{x}sin\varphi - \hat{y}cos\varphi) \tag{6}$$

Which can be simplified to obtain the following

$$E_{(TM_{01}+TE_{01})} = f(r)\{(\hat{x} - \hat{y})cos\varphi + (\hat{x} + \hat{y})sin\varphi\} \tag{7}$$

Equation (7) also represents a similar field distribution as that of Equ. (5) but the generated SVB has CW oriented polarization vector. By denoting the resultant direction of polarization of $\hat{x} + \hat{y}$ as $\hat{u}$ and $\hat{x} - \hat{y}$ as $\hat{v}$, Equ. (5) and Equ. (7) can be rewritten as

$$E_1 = f(r)(\hat{u}cos\varphi - \hat{v}sin\varphi) \tag{8}$$

$$E_2 = f(r)(\hat{u}sin\varphi + \hat{v}cos\varphi) \tag{9}$$

Where E_1 and E_2 represent the resultant field distribution of CCW and CW-SVBs. Equations (8) and (9) represent a combination of a set of four LP_{11} modes,$LP^{a}_{11(\hat{u},\hat{v})}$ and$LP^{b}_{11(\hat{u},\hat{v})}$, which can be excited in an optical fiber by manipulating input SOP and launching conditions. Therefore, it can be stated that SVBs can be generated from a combination of LP_{11} modes with polarization vector oriented along $\hat{u}$ and $\hat{v}$ respectively, which meets the prediction made by Borghi et. al., for orthogonal Hermite-Gaussian modes [2]. The vectorial representation of Equ. (8) and Equ.(9) is shown in Fig. 4.2.

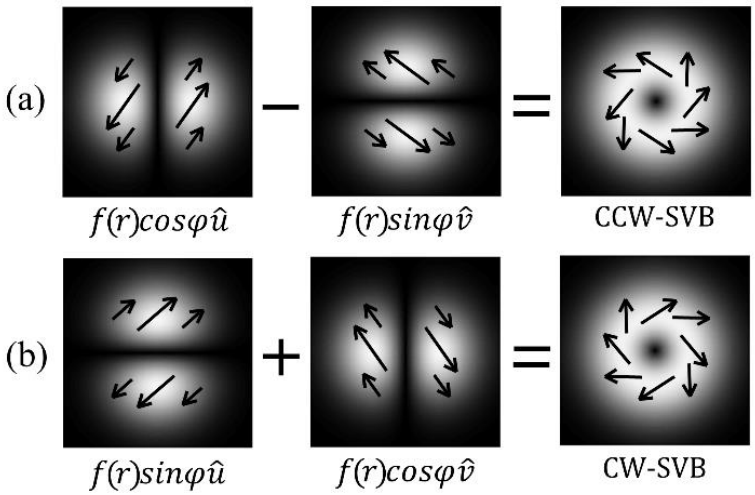

Fig.4.2.Combination of orthogonal LP_{11} modes, formation of (a) CCW-SVB (b) CW-SVB

4.3 Experimental details

The schematic diagram of the experimental setup used for the generation of SVBs is shown in Fig. 4.3. Vertically polarized fundamental Gaussian mode from a 5 mW He-Ne laser with 632.8 nm wavelength is made to pass through an ND filter and a HWP for controlling the optical power and the state of polarization respectively. A 45X microscope objective lens (L1), placed after HWP, focuses the laser beam on to the cleaved end of FMF. The microscope objective is situated on a micro-rotational stage for tilted launching of light into the fiber. The calculated V-number of FMF (980HP of Thorlabs; 0.2 NA, 3.6/125 µm) is 3.57 which means the fiber supports only two modes i.e., LP_{01} and LP_{11} at the chosen wavelength. Additionally, these two LP modes have a polarization degeneracy of 2 and 4 respectively, which result in a total of 6 modes i.e., $LP_{01(\hat{x},\hat{y})}$ and $LP^{a}_{11(\hat{x},\hat{y})}, LP^{b}_{11(\hat{x},\hat{y})}$. The selective combination of orthogonal LP_{11} modes generates various vector modes as explained in previous section. The fiber is held straight with the help of fiber holders at both launching and output ends to avoid bends and twists. At the launching end, the fiber is held with a 3-axis micro translational stage for precise movement of the optical fiber along and transverse to its axis. Gentle stress (S) applied on the optical fiber at the middle over a length of 1 cm reduces the noise in modal output and also helps in controlling the excitation of modes [19]. Here, the applied stress is just sufficient enough to suppress the noise in modal output and has not been varied throughout the experiment. Varying applied stress alone may lead to the generation of vector modes [20], whereas in our work only the input SOP and coupling conditions play a key role in the excitation of modes. A 20X microscope objective lens (L2) decouples and collimates the light beam from the fiber output end. A combination of quarter wave plate (QWP) and analyzer (A) is kept in the path of the collimated beam between L2 and CCD for analyzing the SOP of the excited mode and to carry out Stokes polarimetry [21].

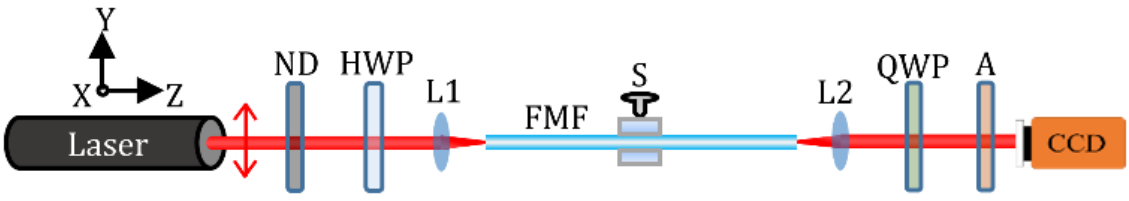

Fig. 4.3. Schematic representation of the experimental setup. ND, neutral density filter; HWP, half wave plate; L1 and L2, microscope objective lens; FMF, few-mode fiber; S, stress unit; QWP, quarter wave plate; A, analyzer; CCD, charge coupled device camera.

A brief description of Stokes polarimetry is presented here. The images of excited modes are captured and intensity is recorded using CCD camera at four discrete orientation angles of the analyzer i.e., horizontal (I_0), diagonal (I_{45}), vertical (I_{90}) and anti-diagonal (I_{135}) with respect to X-axis. A QWP is then inserted before the analyzer at an angle of 90^o and two more images are captured for diagonal ($I_{(45,\ 90)}$) and anti-diagonal ($I_{(135,\ 90)}$) orientation of the analyzer. These six images are processed further using MATLAB program [22] for polarization mapping of the beam. The four normalized Stokes parameters S_0, S_1, S_2 and S_3 are numerically calculated for regular intervals of pixels on the cross section of the excited mode along X and Y directions and polarization ellipses are plotted on the gray scale image of the corresponding mode captured without any filter. The Stokes parameters in terms of intensity of captured images are $S_0 = I_0 + I_{90}$, $S_1 = I_0 - I_{90}$, $S_2 = I_{45} - I_{135}$, $S_3 = I_{(45,\ 90)} - I_{(135,\ 90)}$.

And the polarization ellipse parameters, ellipticity χ and ellipse orientation ψ in terms of Stokes parameters are given by

$$\chi = \frac{1}{2} sin^{-1}\left(\frac{S_3}{S_0}\right) \tag{10}$$

$$\psi = \frac{1}{2} tan^{-1}\left(\frac{S_2}{S_1}\right) \tag{11}$$

4.4 Results & Discussion

The generation of modes in an optical fiber depends mainly on input SOP and the skew and offset launching of Gaussian beam onto the tip of fiber [23,24]. In this experiment, we consider an FMF of fixed length of around 30 cm and just by changing the coupling parameters and input SOP we generate the desired modes. The spatial polarization content of these modes is analyzed with Stokes analysis.

4.4.1 Counter-clockwise spiral vector beam

Vertically polarized Gaussian beam from the laser is focused using L1 while keeping HWP at 0^o initially. The focused spot, incident on the center of core of the FMF, excites the fundamental Gaussian mode LP_{01} as a result of on-axis launching. Now, the tip of FMF is slightly adjusted using micro translation stage for off-axis launching of input Gaussian beam. At a fixed coupling condition, a two lobe LP_{11} mode with a horizontal dark line is observed directly from the fiber output end without analyzer. Keeping the

coupling conditions unaltered, the HWP is slowly rotated up to 26^o where a cylindrically symmetric donut mode is observed.

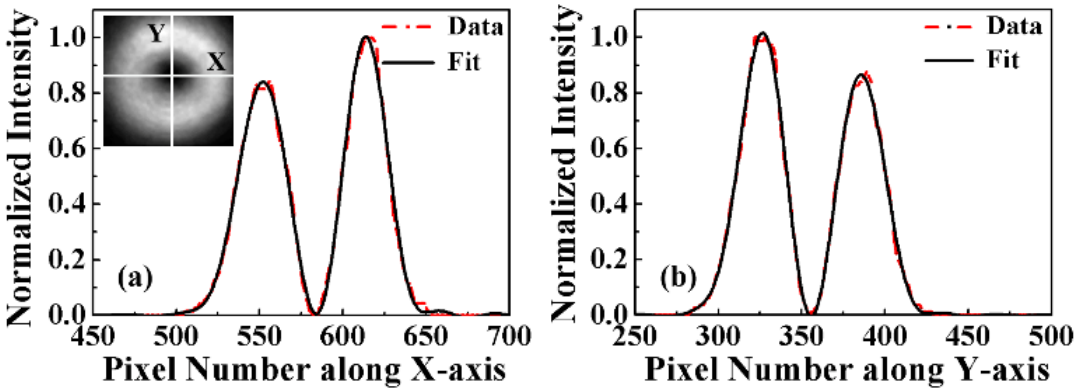

Fig. 4.4. Normalized intensity profiles of the donut mode through its center along (a) X-axis (b) Y-axis

Figures 4.4 (a) and 4.4 (b) show the normalized intensity profiles along X and Y axes of the generated mode through the center respectively. The zero intensity at the center of both plots indicates that the launched Gaussian beam is entirely coupled to the generated donut mode while the coupling to the fundamental Gaussian mode is minimal. In order to investigate the spatial polarization, intensities of the donut mode are recorded using CCD camera at 6 discrete orientations of analyzer and QWP. Further, the captured images are processed to obtain Stokes parameters and hence the polarization ellipse parameters. Subsequently, the transverse spatial polarization is mapped by plotting polarization ellipses across the generated mode.

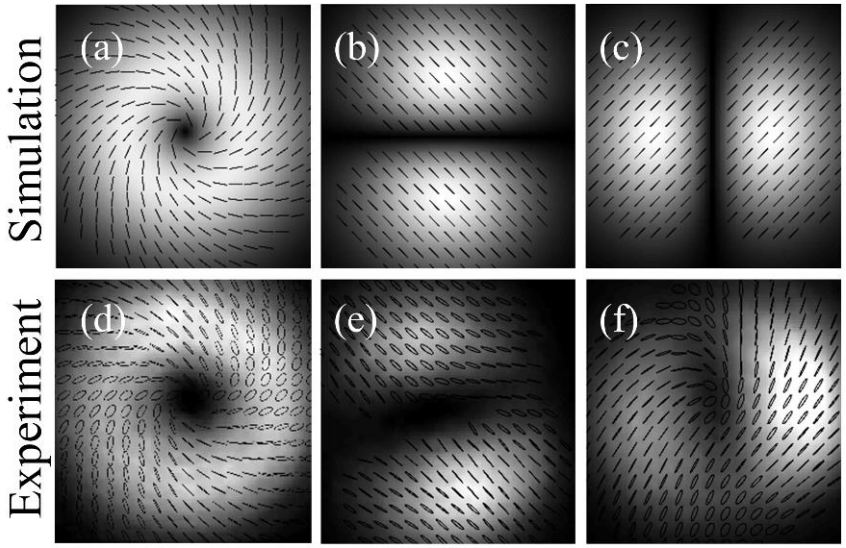

Fig. 4.5. Polarization mapping, first row are the simulation results for Equ. (8) and second row are the corresponding experimental results for HWP orientation angles (d) 26^o (e) 6^o and (f) 45^o.

Figures 4.5 (a) – 4.5 (c) are the simulation results corresponding to Equ. (8) which illustrates the formation of CCW-SVB from a combination of orthogonal LP_{11} modes. It is evident from Fig. 4.5 (d) that the mode has spiral polarization with counter clockwise oriented polarization vector. The spatial polarization across this CCW-SVB is observed to be elliptical at certain regions rather than linear as predicted by theory. The beam has slight variation in ellipticityχ, while moving across in azimuthal direction. The possible reason for such variation is believed to be the inhomogeneity and linear birefringence of the optical fiber [25].

Now, without disturbing the coupling conditions, HWP is rotated back from 26^o to 6^o where a two lobe LP_{11} mode with horizontal null intensity line is observed. This LP_{11} mode is expected to be one of the orthogonal modes that contributes to the generation of CCW-SVB. The spatial polarization of the generated LP_{11} mode is mapped with Stokes polarimetry and is found to be linearly polarized in the direction of $\hat{v}$ (making 45^o with –ve X-axis) as shown in Fig. 4.5 (e). Further, in order to generate the other orthogonal LP_{11} mode, we launched orthogonal SOP into the optical fiber by rotating the HWP to 45^o. As expected, a two lobe LP_{11} mode is observed with spatial intensity as well as polarization which is orthogonal to that of previously excited LP_{11} mode. This mode is observed to be linearly polarized in the direction of $\hat{u}$ (making 45^o with +ve X-axis) as shown in Fig. 4.5 (f). These two orthogonal LP_{11} modes can be excited simultaneously by launching an intermediate SOP to that of the SOP launched to excite them individually, which results in the generation of CCW-SVB.

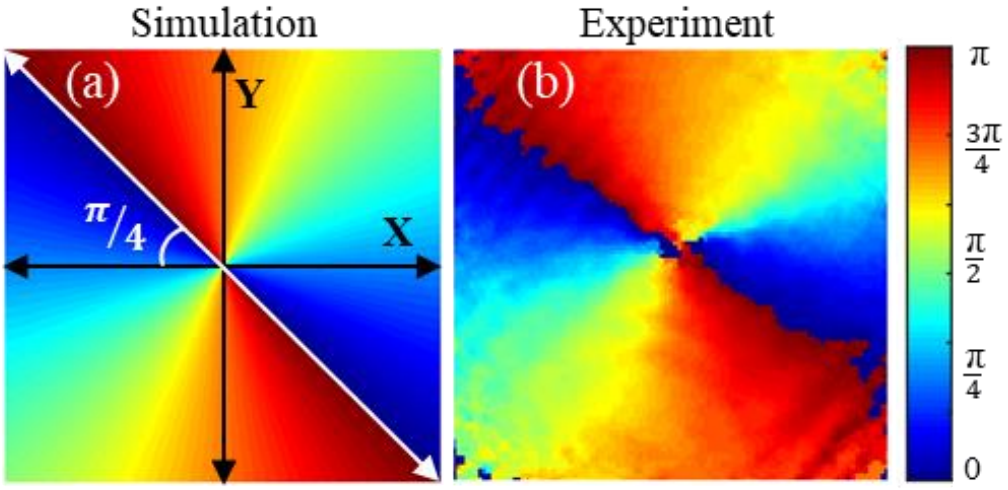

Fig. 4.6. Ellipse Orientation map of CCW-SVB (a) Simulation (b) Experimental.

Figures 4.6 (a) and 4.6 (b) show the ellipse orientation map corresponding to Fig. 4.5 (a) and 4.5 (d) respectively. The color bar, towards right side of Fig. 4.6 (b), emphasizes the orientation of polarization ellipses from 0 to π twice across the beam at a fixed radial distance from the core, in azimuthal direction. In Fig. 4.6 (a), the line of separation of 0 and π ellipse orientations makes an angle π/4 with –ve X-axis in CCW direction and the angle of ellipse orientation is increasing in the same sense which implies the CCW nature of spiral polarization.

As the CCW-SVB has local linear polarization, the Stokes parameter S_3=0 and hence from Equ. (10) the ellipticity χ =0 ideally. The ellipticity of the experimentally generated CCW-SVB is calculated by averaging the χ value over 30x30 pixel matrix around the core of the beam which is found to be -0.25. The –ve sign indicates left handedness of the polarization ellipses across the beam. The slight deviation of the experimental value from theoretical value may be attributed to the linear birefringence of optical fiber [25].

4.4.2 Clockwise spiral vector beam

The HWP is then set back to 26^o where the CCW-SVB was observed and we then changed the coupling condition for the fiber by moving its tip along X-axis to a diametrically opposite position on the core with respect to incident light beam. The HWP is then slowly rotated to excite another donut-shaped vortex mode which is observed at 30^o. The normalized intensity profiles of this mode along X and Y axes respectively are shown in Fig. 4.7 (a) and 4.7 (b). Akin to the previously generated donut mode, this mode also have a dark core intimating the coupling to fundamental Gaussian mode is negligible.

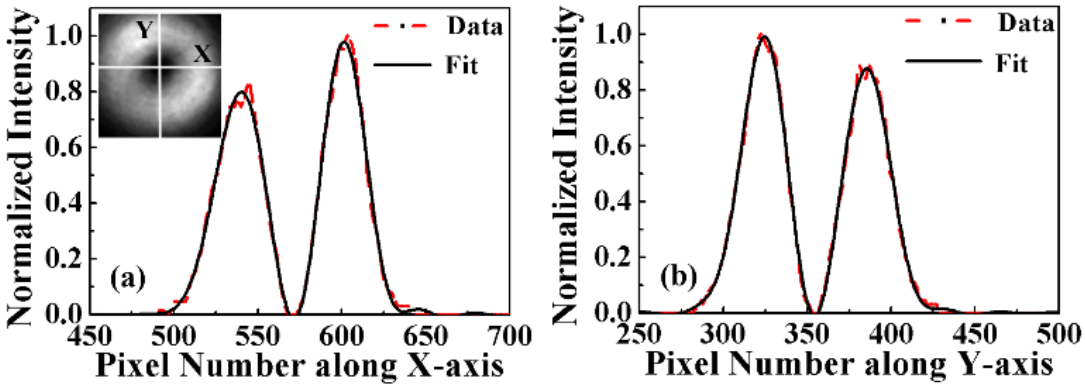

Fig. 4.7. Normalized intensity profiles of the donut mode through its center along (a) X-axis (b) Y-axis.

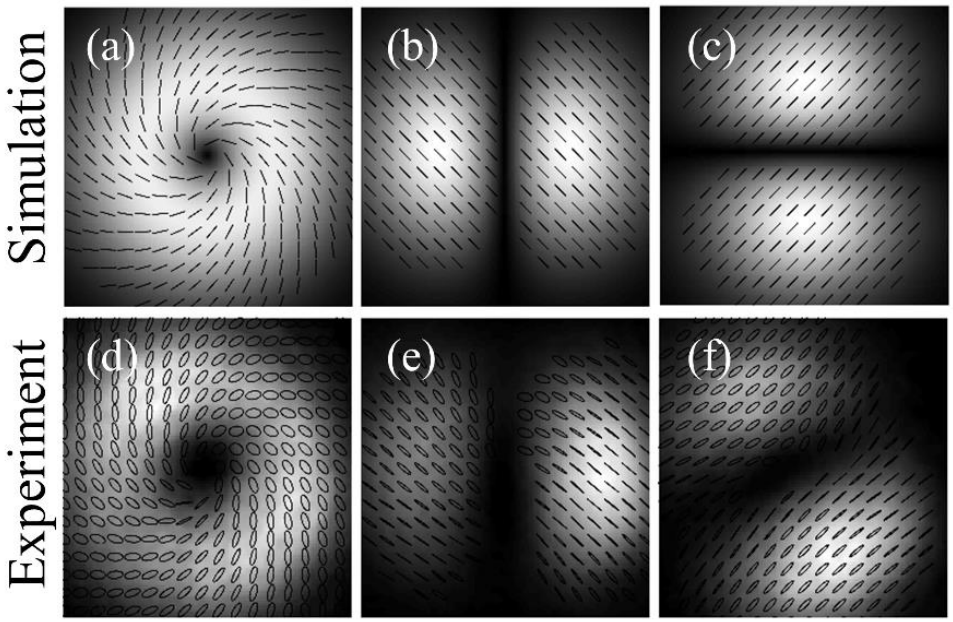

Fig. 4.8. Polarization mapping, first row are the simulation results for Equ. (9) and second row are the corresponding experimental results for HWP orientation angles (d) 30^o (e) 0^o and (f) 45^o.

Figures 4.8 (a) – 4.8 (c) are simulation results corresponding to the formation of CW-SVB from orthogonal LP_{11} modes as mentioned in Equ. (9), while experimental results for the same are shown in Fig. 4.8 (d) – 4.8 (f). Slight variation in ellipticity is observed across the generated donut mode, yet maintaining uniformity in ellipse orientation in clockwise direction as shown in Fig. 4.8 (d). Similar to the previous case, Fig. 4.8 (e) and 4.8 (f) show the orthogonal LP_{11} modes with linear polarization vector oriented in the direction of $\hat{v}$ and $\hat{u}$, generated by launching orthogonal SOP at fiber input end for 0^o and 45^o of HWP orientation angles respectively. It is observed from both cases that for orthogonal SOP launched at the fiber input end, the output polarization remains the same ($\hat{v}$ for 0^o and $\hat{u}$ for 45^o) while the spatial patterns are orthogonal.

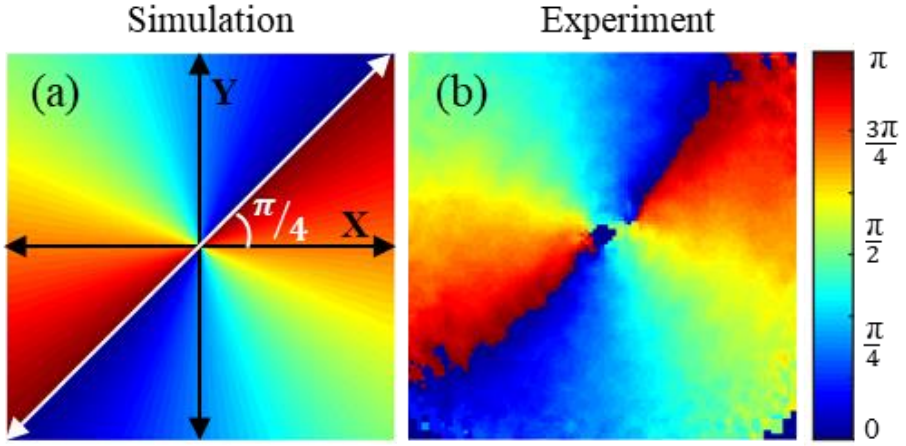

Fig. 4.9. Ellipse Orientation map of CW-SVB (a) Simulation (b) Experimental.

Fig. 4.9 (a) and 4.9 (b) are the simulated and experimentally generated ellipse orientation maps of the CW-SVB corresponding to Fig. 4.8 (a) and 4.8 (d) respectively. In this case also polarization ellipses are oriented twice across the beam but the line of separation of 0 and π makes an angle of π/4 with +ve X-axis in CW direction and the angle of ellipse orientation increases in opposite sense as shown in Fig. 4.9 (a). The average value of χ for CW-SVB is calculated in a similar manner to the previous case and is found to be 0.359. Here, the +ve sign of χ indicates right handedness of the polarization ellipses across the beam.

The phenomenon of degenerate LP mode mixing for the generation of CW & CCW-SVBs best suits LP_{11} modes alone. As we move to higher order LP_{lm} (l >1, m >1) modes, the combination may result in an arbitrary mode due to the difference in topology of phase and polarization from LP_{11} modes. Moreover, the polarization behavior of LP modes in FMF that support more than 2 LP modes (LP_{01} and LP_{11}) is highly unstable which increases the complexity in generation of higher order vector modes.

It is worth noting that just by controlling coupling conditions and input SOP, we have generated the beams with opposite spiral nature. Though the local SOP of the experimentally generated beams is not as linear as predicted by theory, the same approach may be implemented using high quality optics and a custom designed optical fiber which may result in pure spiral vector vortex beams. The slight deviation in experimental results from theoretical predictions may be attributed to the quality of the optics, inhomogeneity and linear birefringence of optical fiber and the ambient conditions of the experimental setup. By precise control over all these conditions, modes of desired polarization can be generated.

4.5 Conclusions

A new approach for the generation of CW & CCW SVBs via combination of orthogonal LP_{11} modes with diagonal and anti-diagonal polarization vector has been demonstrated. The generation of SVBs with polarization vector oriented in CW and CCW direction has been verified experimentally using a few mode optical fiber by controlling the coupling conditions and input SOP. The experimental results obtained are found to be in good agreement with theoretical predictions. The slight deviation in the ellipticity of the generated SVBs may be attributed to the fiber birefringence and quality of optics. The

obtained results are expected to find potential applications in particle trapping and manipulation.

The work presented in this chapter is published in *Applied Optics.*

C. Hari Krishna and Sourabh Roy, "Analyzing characteristics of spiral vector beams generated by mixing of orthogonal LP_{11} modes in few-mode optical fiber", *Appl. Opt.*, 57, 3853-3858 (2018).

References

1. Franco Gori, "Polarization basis for vortex beams," *J. Opt. Soc. Am. A.,* **18**, 1612-1617 (2001).
2. Riccardo Borghi, Massimo Santarsiero, and Miguel A. Alonso, "Highly focused spirally polarized beams," *J. Opt. Soc. Am. A.*, **22**, 1420-1431 (2005).
3. Riccardo Borghi and Massimo Santarsiero, "Nonparaxial propagation of spirally polarized optical beams," *J. Opt. Soc. Am. A.,* **21**, 2029-2037 (2004).
4. Bing Hao and James Leger, "Numerical aperture invariant focus shaping using spirally polarized beams," *Opt. Commun.,* **281**, 1924–1928 (2008).
5. V Ramırez-Sanchez and G Piquero, "The beam quality parameter of spirally polarized beams," *J. Opt. A: Pure Appl. Opt.,* **10**, 125004 (1-6) (2008).
6. V. Ramirez-Sanchez, G. Piquero and M. Santarsiero, "Generation and characterization of spirally polarized fields," *J. Opt. A: Pure Appl. Opt.,* **11**, 085708 (2009).
7. Alexis K. Spilman and Thomas G. Brown, "Stress birefringent, space-variant wave plates for vortex illumination," *Appl. Opt.,* **46**, 61-66 (2007).
8. Avi Niv, Gabriel Biener, Vladimir Kleiner, et.al., "Rotating vectorial vortices produced by space-variant subwavelength gratings," *Opt. Lett.,* **30**, 2933-2935 (2005).
9. Geo M. Philip and Nirmal K. Viswanathan, "Generation of spirally polarized propagation-invariant beam using fiber microaxicon," *Opt. Lett.,* **36**, 3906-3908 (2011).
10. Rita S. Rodrigues Ribeiro, Pabitra Dahal, Ariel Guerreiro, et.al., "Optical fibers as beam shapers: from Gaussian beams to optical vortices," *Opt. Lett*., **41**, 2137-2140 (2016).

11. S. Pidishety et. al., "Orbital angular momentum beam excitation using an all-fiber weakly fused mode selective coupler," *Opt. Lett.,* **42**, 4347-4350 (2017)
12. Zeinab Sanjabi Eznaveh et al., "Photonic lantern broadband orbital angular momentum mode multiplexer," *Opt. Exp.,* **26**, 30042-30051 (2018)
13. Allan W. Snyder and John D. Love, "*Optical Waveguide Theory,"* Chapman and Hall, (1983).
14. Allan W. Snyder and William R. Young, "Modes of optical waveguides," *J. Opt. Soc. Am.* **68**, 297-309 (1978).
15. Anurag Sharma, "Constructing linear combination of LP modes to obtain zeroth order vector modes of optical fibers," *Appl. Opt.,* **27**, 2647-2649 (1998).
16. Nenad Bozinovic, Steven Golowich, Poul Kristensen, et.al., "Control of orbital angular momentum of light with optical fibers," *Opt. Lett.,* **37**, 2451-2453 (2012).
17. V.V.G. Krishna Inavalli and Nirmal K. Viswanathan, "Switchable vector vortex beam generation using an optical fiber," *Opt. Commun.,* **283**, 861–864 (2010).
18. G. Volpe and D. Petrov, "Generation of cylindrical vector beams with few-mode fibers excited by Laguerre–Gaussian beams," *Opt. Commun.,* **237**, 89–95 (2004).
19. David McGloin, Neil B. Simpson and Miles J. Padgett, "Transfer of orbital angular momentum from a stressed fiber-optic waveguide to a light beam," *Appl. Opt.* **37**, 469-472 (1998).
20. Yu Zhang, Fufei Pang, Huanhuan Liu et.al., "Generation of the First-Order OAM Modes in Ring Fibers by Exerting Pressure Technology," *IEEE Photon. J.,* **9**, 1-9 (2017).
21. Dennis H. Goldstein, "*Polarized light,"* CRC Press (2011).
22. Joshua A. Jones, Anthony J. D'Addario, Brett L. Rojec, et.al., "The Poincare-sphere approach to polarization: Formalism and new labs with Poincare beams," *Am. J. Phys.,* **84**, 822-835 (2016).
23. Masaaki Imai and Elmer H. Hara, "Excitation of the Fundamental and Low-Order Modes of Optical Fiber Waveguides by Gaussian Beams.1: Tilted Beams," *Appl. Opt.,* **13**, 1893-1899 (1974).
24. Masaaki Imai and Elmer H. Hara, "Excitation of the Fundamental and Low-Order Modes of Optical Fiber Waveguides with Gaussian Beams.2: Offset Beams," *Appl. Opt.,* **14,** 169-173 (1975).
25. A. M. Smith, "Birefringence induced by bends and twists in single-mode optical fiber," *Appl. Opt.,* **19**, 2606-2611 (1980).

CHAPTER

5

Generation of Vector Vortex Modes and Poincare Sphere Representation

Contents

CHAPTER 5

Generation of Vector Vortex Modes and Poincare Sphere Representation

In this chapter, we have demonstrated the generation of inhomogeneously polarized vector vortex modes in a step-index few mode optical fiber. These vector modes are other than well-known zeroth order vector modes such as modes with radial, azimuthal and hybrid polarization distribution in transverse direction. Extending the basis of linearly polarized modes with diagonal and anti-diagonal polarization that are proposed and experimentally generated in the previous chapter, a set of four vector vortex modes are generated by controlling the coupling conditions and input state of polarization. Further, Poincare sphere representation for all possible first order linearly polarized modes and the vector vortex modes generated from their combinations of few mode optical fiber are presented. All homogeneously polarized fiber modes are accommodated on standard Poincare sphere and inhomogeneously polarized vector vortex modes are accommodated on a pair of higher order Poincare sphere. The location of vector vortex modes on higher order Poincare sphere is justified by the positions of orthogonal linearly polarized modes on standard Poincare sphere.

5.1 Introduction

In this chapter, we present the experimental generation of vector vortex modes (VVMs) in FMF and analyse their polarization content with Stokes polarimetry. These VVMs are then located on a pair of higher order Poincare sphere (HOPS) depending on their spatial polarization distribution and also according to the position of orthogonal LP_{11} modes on standard Poincare sphere that combine to generate respective VVMs.

5.1.1 Vector Vortex Modes

VVMs are complex light beams with inhomogeneous spatial linear polarization vector. The orientation angle of the polarization vector across the beam in azimuthal direction at any fixed radial distance makes a full cycle of 2π (or 0 to π twice). As a result of this polarization inhomogeneity, there exist a polarization singular point at the center of the

mode where the state of polarization is undefined, known as V-type polarization singularity as it is present in a vector field. In next chapter, we discuss another type of polarization singularity i.e., C-point present in ellipse fields. Whereas, this chapter is dedicated to the experimental generation of VVMs and their Poincare sphere representation.

CVBs such as radial and azimuthal vector beams exhibit a rich variety of applications in scientific and industrial fields due to which numerous ways have been proposed to generate them [1,2]. Recently, the generation of novel vector fields with hybrid and arbitrarily varying spin angular momentum are reported which are expected to find potential applications in polarization multiplexing and imaging [3-6]. The underlying fundamental scientific interest and the promising applications of such vector fields creates a path for exploring various generation schemes.

In this chapter, we discuss the experimental generation of a class of four VVMs using FMF by exploiting the degenerate mode mixing phenomenon of first order orthogonal linearly polarized LP_{11} modes with diagonal ($\hat{u}$) and anti-diagonal ($\hat{v}$) polarization vectors. These VVMs are briefly discussed by Milione et. al., in describing the HOPS [7,8]. The generation of radial and azimuthal vector modes has been paid much attention in fibers while these VVMs are relatively unexplored and no experimental demonstration is presented for their efficient generation till date, to the best of our knowledge.

5.1.2 Poincare Sphere and Stokes parameters

Poincare sphere, proposed by H. Poincare, is an imaginary sphere with Stokes parameters as coordinate axes (S_1, S_2, S_3 with S_0 being origin). Poincare sphere is the most convenient and efficient tool for representing homogeneously polarized states of light beams which are plane wave solutions of Maxwell's equations. A standard Poincare sphere contains all possible states of polarization on its surface with circular polarizations at the poles, linear polarizations along the equator and elliptical polarization elsewhere as shown in Fig. 5.1. An arbitrary polarization state can be located on the surface of Poincare sphere using spatial spherical coordinates (2ψ, 2χ) where 2ψ and 2χ are the latitude and longitude of the point 'p' and are related to Stokes parameters as [9]

$$\begin{bmatrix} S_1 \\ S_2 \\ S_3 \end{bmatrix} = \begin{bmatrix} cos(2\chi)cos(2\psi) \\ cos(2\chi)sin(2\psi) \\ sin(2\chi) \end{bmatrix} \quad (1)$$

The latitude and longitude have their own physical significance in the sense that they represent ellipse orientation angle (ψ) and ellipticity (χ) of the polarization ellipse respectively. The points (0,0), (π/2,0), (π,0) and (3π/2,0) along the equator of the Poincare sphere represent the horizontal (H), diagonal (D), vertical (V) and anti-diagonal (A) linear polarizations, while the points (0,π/2) and (0,-π/2) at the north and south poles represents right (R) and left (L) circular polarizations respectively.

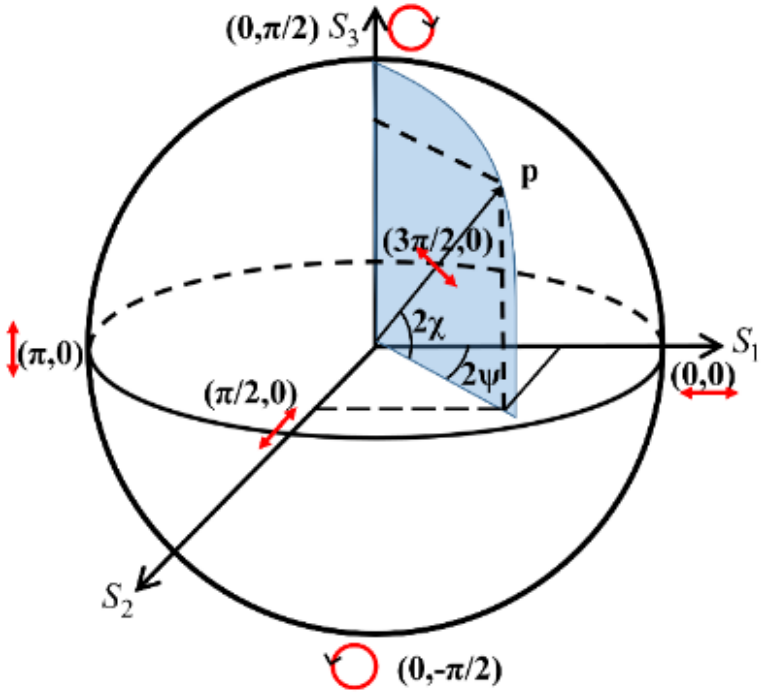

Fig. 5.1. Standard Poincare sphere, p: arbitrary point on the surface of sphere, (2ψ, 2χ): latitude and longitude of the point p.

5.1.3 Necessity of higher order Poincare sphere

As discussed above, based on the SOP of modes, their position is justified on the Poincare sphere. This method is valid only for modes with homogeneously polarized states which are fundamental plane wave solutions of Maxwell's vector wave equation. The linear combinations of orthogonal LP_{11} modes generate VVMs with inhomogeneously polarized states, which are higher-order solutions for Maxwell's vector wave equation [7]. Moreover, these modes have spatially varying linear polarization vector that can span over the equator of standard Poincare sphere. Hence, it is difficult to represent these modes at a particular position on the standard Poincare sphere. As a consequence, another efficient geometric representation for such inhomogeneous vector fields is essential by extending the standard Poincare sphere to higher order Poincare sphere that can

accommodate various VVMs. Additionally, the geometrical representation of these inhomogeneously polarized VVMs is of fundamental scientific interest which is essential in understanding the geometric phase of light beams [8].

Some representations were proposed in the literature that deal with light beams having definite orbital and spin angular momenta (OAM and SAM). Of them, the sphere of first order modes, proposed by M. J. Padgett, deals with the OAM of optical beams by accommodating *HG* modes on equator and *LG* modes at the poles, irrespective of their spatial polarization [10]. Recently, Milione et al. proposed a pair of HOPS that accommodates all kinds of inhomogeneously polarized modes that have both SAM and OAM simultaneously and they also discussed higher-order Pancharatnam-Berry phase associated with them [7,8]. A generalized Poincare sphere is proposed recently by exploiting an additional parameter (the radial distance of the surface from center of Poincare sphere) to represent the degree of polarization which elucidated the higher order mode representation by unifying all inhomogeneous states onto a single sphere [11]. All these representations of HOPS describe vector fields that could be generated in free-space using bulk optical setups. Though, some modes that are analogous to optical fiber modes have been discussed briefly by Milione et al., minimal attention has been focused towards their generation while most of the attention is given to other inhomogeneous states.

Keeping this in view, in this chapter, we have presented a Poincare sphere approach exclusively for modes of FMF. All possible LP_{11} modes of few-mode fiber are located onto a standard Poincare sphere according to their spatial polarization distribution. The orthogonal combinations of LP_{11} modes, which results in the generation of various possible VVMs, are mapped onto a pair of HOPS. As all LP_{11} modes and VVMs have local linear polarization, the equator of Poincare sphere and HOPS is sufficient to accommodate them.

5.2 Formation of vector vortex modes from LP_{11} modes

In the previous chapter, we proposed a set of orthogonal LP_{11} modes with diagonal and anti-diagonal polarization vectors. Here, extending the possible combinations of these LP_{11} modes, we generate a set of four VVMs. For a suitable and allowed combination of the LP_{11} modes, some typical criteria are mentioned in the literature, such as field invariance of the modes under plane rotations, modes that follow rotational and reflection symmetries and solving the set of equations of LP modes [12-15]. Though these modes

are not exact solutions of the scalar wave equation, there is a possibility of generating such modes in optical fiber by controlling the incident SOP experimentally. These modes may be considered as the superposition of $LP_{11(\hat{x},\hat{y})}$ modes with the same parity but orthogonal polarization i.e., $LP^{a,b}_{11(\hat{u})} = LP^{a,b}_{11(\hat{x})} + LP^{a,b}_{11(\hat{y})}$ and $LP^{a,b}_{11(\hat{v})} = LP^{a,b}_{11(\hat{x})} - LP^{a,b}_{11(\hat{y})}$, similar to CP_{11} mode formalism in which $LP_{11(\hat{x},\hat{y})}$ modes of orthogonal polarization and same parity combine with π/2 phase difference in order to form circularly polarized modes [16]. The four possible LP_{11} modes with diagonal and anti-diagonal polarization vector are given by

$$LP^{a}_{11(\hat{u})} = \hat{u}f(r)cos\varphi \qquad LP^{b}_{11(\hat{u})} = \hat{u}f(r)sin\varphi$$

$$LP^{a}_{11(\hat{v})} = \hat{v}f(r)cos\varphi \qquad LP^{b}_{11(\hat{v})} = \hat{v}f(r)sin\varphi \tag{2}$$

Where $\hat{u}$ and $\hat{v}$ are the diagonal and anti-diagonal polarization vectors. The study of these modes is helpful in understanding the generation of VVMs other than zeroth order vector modes. The possible linear combinations of Equ. (2) are as follows

$$E(r,\varphi) = f(r)\begin{Bmatrix} \hat{v}cos\varphi + \hat{u}sin\varphi \\ \hat{v}cos\varphi - \hat{u}sin\varphi \\ \hat{u}cos\varphi - \hat{v}sin\varphi \\ \hat{u}cos\varphi + \hat{v}sin\varphi \end{Bmatrix} \tag{3}$$

Equation (3) represents higher order VVMs of FMF which include spiral and hybrid vector modes where $E(r,\varphi)$ is the field distribution. The generalized equation that concerns all possible linear combination of LP_{11} modes and the generation of VVMs is given by

$$E(r,\varphi) = f(r)(\hat{p}cos\varphi \pm \hat{q}sin\varphi) \tag{4}$$

Where $\hat{p}$ and $\hat{q}$ are orthogonally oriented polarization vectors. These VVMs may also be written as linear combinations of zeroth order vector modes ($TE_{01} \pm TM_{01}$ and $HE^{o}_{21} \pm HE^{e}_{21}$), but we have chosen LP_{11} mode basis in our study as the difference of refractive indices of core and cladding of the FMF chosen for the experiment of the order 10^{-2} ($n_{co} \cong n_{cl}$ and $\Delta n << 1$) i.e., weakly guiding. Moreover, LP_{11} modes are the simplest solutions for weakly guiding approximation and are the building blocks for the vector modes in step index fiber. Hence LP_{11} mode approach is still valid [13,14].

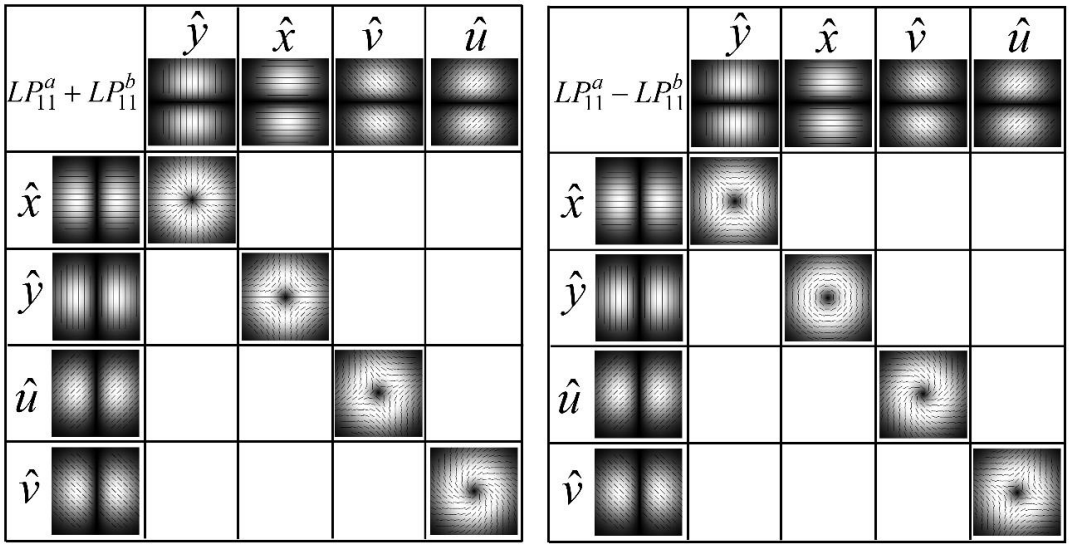

Fig. 5.2. Orthogonal LP_{11} mode mixing and formation of VVMs.

Figure 5.2 illustrates the LP_{11} modes and their possible linear combinations to form various VVMs. All the cosine modes (LP_{11}^{a}) are shown along the column whereas sine modes (LP_{11}^{b}) are shown along the row. The VVMs are present only along the diagonal of Fig. 5.2 as other combinations do not satisfy polarization orthogonality though they are orthogonal in their spatial mode pattern. The +ve and –ve signs in the modal Equ. (4) may be treated as in-phase ($e^{i(0)}$=1) and out-of-phase ($e^{i(\pi)}$= -1) combination of the respective LP_{11} modes.

5.3 Experimental details

The experimental setup used for the generation of VVMs in a FMF is similar to that described in the previous chapter and shown in Fig. 5.3. A 5 mW He-Ne laser operating at 632.8 nm wavelength is used as source for the excitation of fiber modes. A step ND filter and a polarizer are placed in the path of a laser beam to control the intensity and allow a vertically polarized Gaussian beam respectively. In order to alter the SOP of the input Gaussian beam, a HWP is inserted after the polarizer. The Gaussian beam with well-defined SOP is then focused using a microscope objective (L1) and the focused spot is made incident on the tip of the cleaved end of around 30 cm long FMF. The output mode from the rear end of the FMF is collimated with another microscope objective (L2) and captured using a CCD camera. A quarter wave plate (QWP) and an analyser (A) are inserted between L2 and the CCD to analyse the spatial polarization of the generated mode.

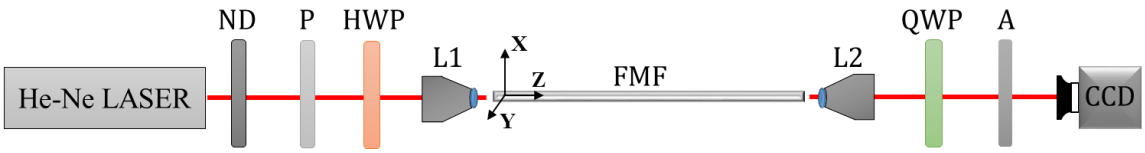

Fig. 5.3. Schematic diagram of the experimental setup.

5.4 Results and Discussion

Initially, a vertically polarized Gaussian beam is focused onto the tip of the cleaved end of FMF. The fiber is held straight to avoid bends and twists which may affect the generation of desired modes. The tip of the fiber is adjusted carefully using 3-axis micro positioner so that the input focused Gaussian beam from the laser is entirely coupled to fundamental Gaussian fiber mode LP_{01}.

5.4.1 Generation of Vector vortex modes

From our previous experimental results, we learnt that at an intermediate SOP of orthogonal states, a vector mode is getting excited. For proper input coupling conditions, we repeated the experiment and ascertained the same. Here, our aim is to generate a set of four VVMs in FMF by controlling input SOP and coupling conditions. First, the HWP is slowly rotated 22.5° in anti-clockwise direction which is intermediate SOP of the two orthogonal states. By slight adjustment of HWP to an angle of 26°, a donut shaped mode is observed. By observing the orientation of two lobe pattern after the rotating analyser, this mode is confirmed to have spiral polarization in anti-clockwise direction which is out-of-phase combination of $LP^{a}_{11(\hat{u})}\ and\ LP^{b}_{11(\hat{v})}\ i.e., LP^{a}_{11(\hat{u})} - LP^{b}_{11(\hat{v})}$ as shown in Fig. 5.4 (a5). Next, the HWP is slowly rotated 22.5° in clockwise direction where another donut shaped mode is observed with a slight adjustment of HWP to 24°. The rotating analyser test confirms the hybrid spatial polarization of the generated mode which is an in-phase combination of $LP^{a}_{11(\hat{u})}\ and\ LP^{b}_{11(\hat{v})}\ i.e., LP^{a}_{11(\hat{u})} + LP^{b}_{11(\hat{v})}$ as shown in Fig. 5.4 (b5).

The coupling conditions are then altered by moving the tip of the fiber along the core to a diametrically opposite position to that of previous launching conditions using 3-axis micro positioner stage. Akin to previous case, the HWP is rotated in anti-clockwise and clockwise directions for which two vector vortex modes are excited for 30° and 26° orientation of HWP in respective cases. These modes are examined under rotating

analyser to know the spatial polarization. Observation of two lobe orientation patterns after the analyser reveals that these modes have clockwise spiral and hybrid polarizations which are in-phase $(LP^{a}_{11(\hat{v})} + LP^{b}_{11(\hat{u})})$ and out-of-phase $(LP^{a}_{11(\hat{v})} - LP^{b}_{11(\hat{u})})$ combinations of $LP^{a}_{11(\hat{v})}\ and\ LP^{b}_{11(\hat{u})}$ modes as shown in Fig. 5.4 (c5) and Fig. 5.4 (d5) respectively.

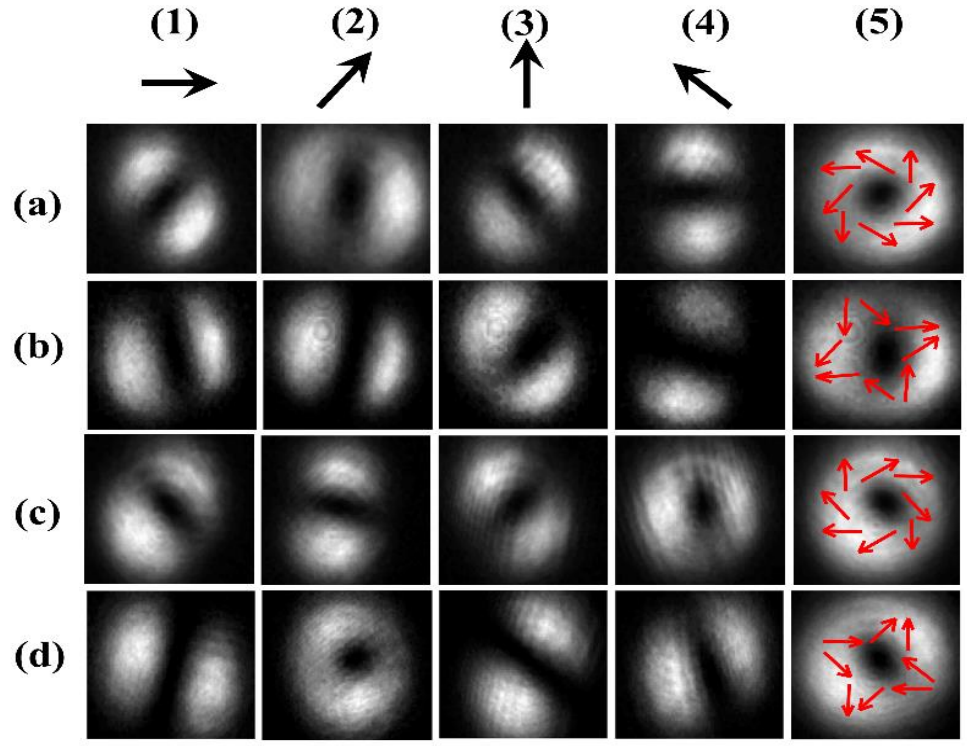

Fig. 5.4. Orientation of two lobe patterns after crossing the analyser for orientation angles (a1) – (d1) 0°, (a2) – (d2) 45°, (a3) – (d3) 90°, (a4) – (d4) 135°, and (a5) – (d5) the polarization distribution in generated VVMs.

Further, Stokes polarimetry is carried out for all VVMs to strictly identify the spatial polarization distribution across the modes. The polarization ellipses are plotted onto the generated mode as shown in Fig. 5.5. The first row of Fig. 5.5 corresponds to the simulated intensity patterns of VVMs with their spatial polarization mapped across the mode. The ellipse orientation map of the corresponding modes is shown in the inset of each mode which is mapped with a colour scale from 0 to π, each colour representing a specific orientation angle of polarization ellipse across the mode. The second row of Fig. 5.5 shows the experimentally generated VVMs in FMF. It is observed that the spatial polarization distribution of the experimentally generated modes closely matches the simulated results while a slight deviation appears in the ellipticity of the polarization

ellipses. Ideally, all VVMs have spatial linear polarization as a result of combination of two orthogonal LP_{11} modes. But, in practice, the generated VVMs are observed to have elliptical polarization at certain regions across the mode. This deviation of experimental results from theoretical prediction may be attributed to the birefringence of the fiber used [17]. Though ellipticity of the modes varies at certain regions, the ellipse orientation across the generated modes exactly matches the simulated results as shown in the inset of second row in Fig. 5.5. The ellipse orientation maps of generated modes emphasizes that each VVM is unique in its spatial polarization content and is different from well-known zeroth order vector modes.

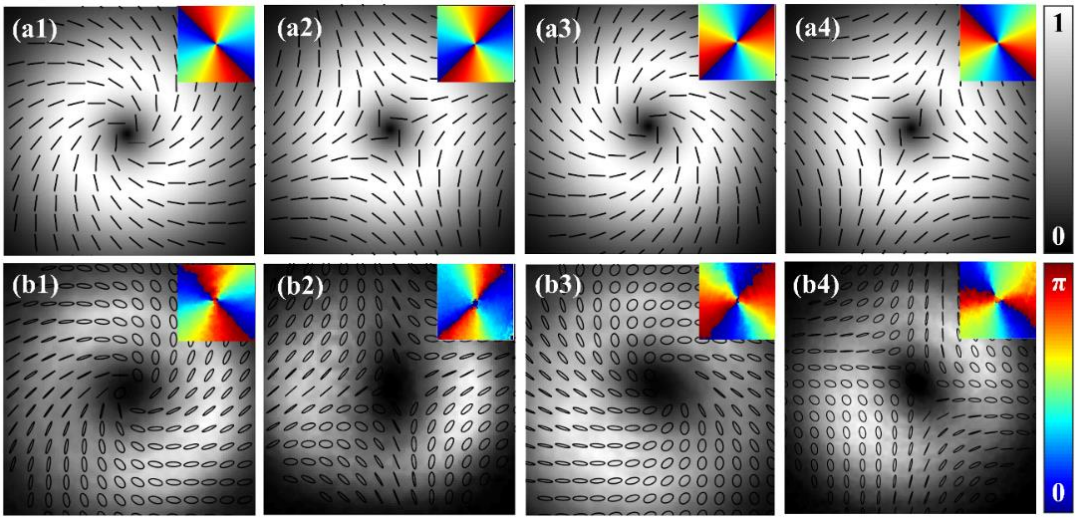

Fig. 5.5. Vector vortex modes and their corresponding ellipse orientation maps shown in inset; (a1) – (a4) simulated, (b1) – (b4) experimental results.

Here, the modes in Fig. 5.5 (b1) & Fig. 5.5 (b2) are generated for anti-clockwise and clockwise orientations of HWP for an orientation angle of 26^o and 24^o respectively before changing the coupling conditions and the modes in Fig. 5.5 (b3) & Fig. 5.5 (b4) are generated for anti-clockwise and clockwise orientations of HWP for an orientation angle of 30^o and 26^o respectively after changing the coupling conditions. Hence, by just altering the coupling conditions and input SOP, all the VVMs can be generated. It is noteworthy that the VVMs generated before and after the changing of coupling conditions, for specific input SOP, are orthogonal in their spatial polarization distribution, which is clearly evident from the ellipse orientation maps shown in the inset of respective modes.

5.4.2 Poincare sphere representation

As described in section 5.1.3, homogeneous polarization states can be accommodated on standard Poincare sphere and inhomogeneous states on HOPS. As the LP_{11}modes are linearly polarized, they can be accommodated on the equator of standard Poincare sphere. The standard Poincare sphere with LP_{11} modes of all possible polarizations situated on the equator is shown in Fig. 5.6.

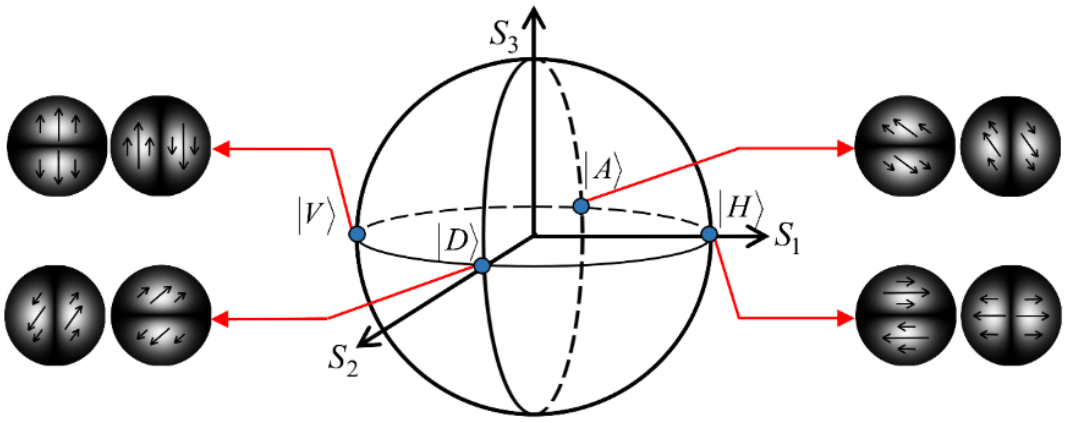

Fig. 5.6. Linearly polarized LP_{11} modes situated on standard Poincare sphere.

It is clear that conventional modes with orthogonal $\hat{x}$ and $\hat{y}$ polarizations occupy $|H\rangle$and $|V\rangle$ positions whereas tilted polarized LP_{11} modes with orthogonal $\hat{u}$ and $\hat{v}$ polarizations occupy $|D\rangle$ and $|A\rangle$ positions respectively.

The linear combination of these orthogonal LP_{11} modes leads to the generation of various VVMs such as radial, azimuthal, spiral and a set of hybrid vector modes as discussed in previous section. All generated VVMs are identical in spatial intensity but are unique in spatial polarization distribution as shown in second row (b1-b8) of Fig. 5.7. The third row (c1-c8) of Fig. 5.7 illustrates the spatial polarization maps of the corresponding VVMs in second row. It is observable from row 2 and row 3 of Fig. 5.7 that the adjacent VVMs (b1 and b2, b3 and b4, b5 and b6, b7 and b8) are orthogonal in spatial polarization distribution and are expected to be situated at diametrically opposite location on the HOPS.

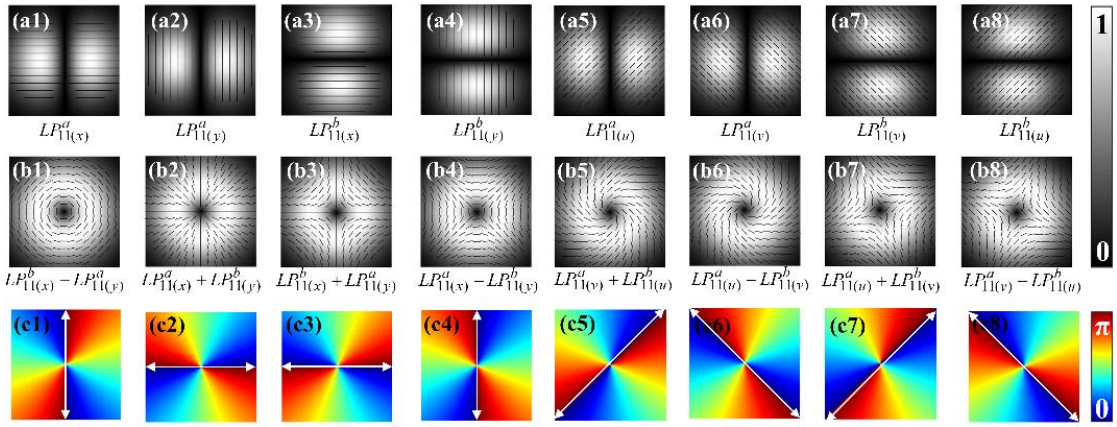

Fig. 5.7. Row 1: linearly polarized LP_{11} modes; Row 2: Various inhomogeneously polarized VVMs, Row 3: Spatial polarization maps of VVMs.

To accommodate inhomogeneously polarized VVMs, a pair of HOPS is considered which is analogous to that proposed by Milione et al. It is to be noted that, in addition to VVMs, a HOPS may also accommodate a wide variety of inhomogeneously polarized vortex modes with spatially varying SAM i.e., modes with circular and elliptical spatial polarization. But, here our discussion is limited to LP_{11} modes and VVMs generated from their combination in a few-mode fiber, both of which have local linear polarization. Hence, the equator of Poincare sphere and HOPS alone suffices the need for accommodating these modes. The VVMs generated from a combination of $|H\rangle \pm |V\rangle$ LP_{11} modes occupy $|H\rangle$ and $|V\rangle$ positions, whereas the VVMs from a combination of $|D\rangle \pm |A\rangle$ LP_{11} modes occupy $|D\rangle$ and $|A\rangle$ positions, respectively, on HOPS with new coordinate axes S_1', S_2' and S_3' as shown in Fig. 5.8. Further, the in-phase combinations of orthogonal LP_{11}modes i.e., $LP_{11}^a + LP_{11}^b$ are located on +ve Stokes axis (radially polarized TM_{01} at $|H\rangle$ and clockwise spiral at$|D\rangle$) while out-of-phase combinations i.e., $LP_{11}^a - LP_{11}^b$ on –ve Stokes axis (azimuthally polarized TE_{01} is at $|V\rangle$ and anti-clockwise spiral at $|A\rangle$). This HOPS contains vector modes with regular spatial polarization distribution such as radial, azimuthal, clockwise and anti-clockwise spiral polarizations.

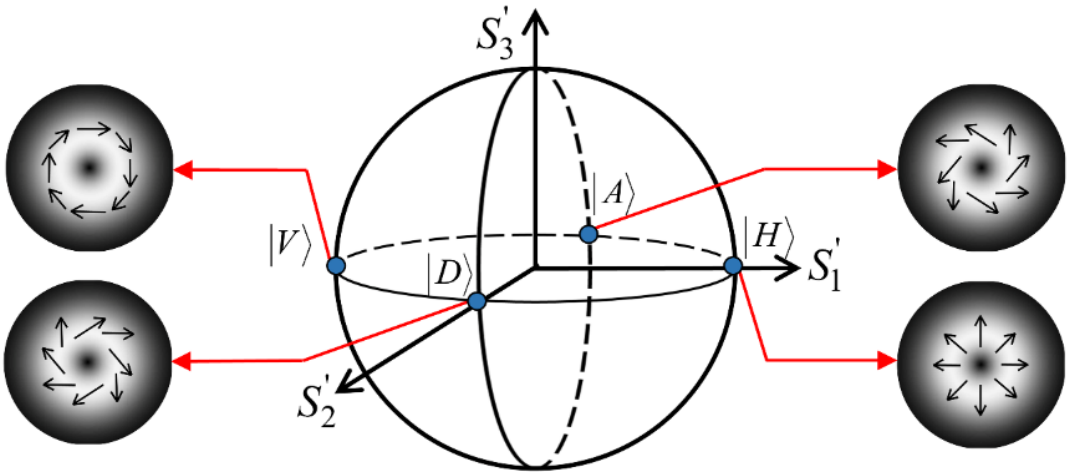

Fig. 5.8. Vector vortex modes of regular states of polarization distribution situated on the equator of higher order Poincare sphere.

The other linear combinations of LP_{11} modes results in the generation of vector modes with irregular or hybrid polarization. These modes cannot be accommodated on the same HOPS due to hybrid spatial polarization. Hence, another HOPS is needed to accommodate these new hybrid VVMs. The accommodation of these hybrid VVMs on the HOPS with a new set of Stokes axes S_1'', S_2'' and S_3'' is akin to the previous case i.e., the VVMs generated from the orthogonal LP_{11} modes on standard Poincare sphere are situated at either of the orthogonal positions on HOPS, shown in Fig. 5.9.

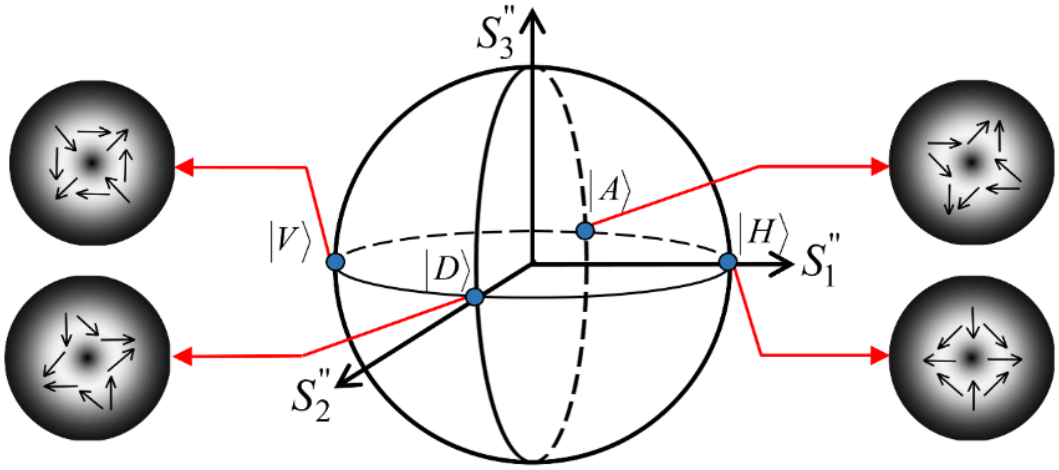

Fig. 5.9. Vector vortex modes of hybrid states of polarization distribution situated on the equator of higher order Poincare sphere.

These two HOPS, as a pair, serve the need for representation of all possible VVMs of a step-index few mode optical fiber. As all the VVMs have local linear polarization, the SAM of the mode is σ = 0. It can be observed that the linear translation along the

equator of HOPS helps to switch across the VVMs which can be achieved using a couple of wave plates.

5.5 Conclusion

In summary, we have presented an experimental demonstration on generating VVMs in a step index few mode optical fiber by exploiting scalar mode combination of orthogonal LP_{11} modes with diagonal and anti-diagonal polarization vector. The VVMs are generated by controlling the coupling conditions of the fiber and input SOP. The clockwise and anti-clockwise orientations of HWP from its mean position, before and after changing the coupling conditions, generated all VVMs of orthogonal polarization distribution, which is evident from the ellipse orientation maps. The slight deviation in ellipticity of experimentally generated VVMs is attributed to fiber inhomogeneity, core ellipticity and fiber birefringence. The obtained results are found to be in good agreement with simulated results. Further, a Poincare sphere approach is presented for LP_{11} modes as well as the VVMs generated from their linear combination. The location of regular and hybrid VVMs on the HOPS is justified by the position of orthogonal LP_{11} modes on standard Poincare sphere, which combine to generate respective VVMs. This approach is efficient and much useful in the representation of vector modes of FMF. The VVMs with clockwise and anti-clockwise spiral spatial polarization which have sharper focusing properties next to radial and azimuthal vector modes are suitable for fields such as particle trapping, optical micro manipulation and lithography. The other VVMs with hybrid polarization may also have considerable contribution towards imaging, microscopy and polarization based data encryption by providing additional degree of freedom.

A part of the work (Generation of VVMs) presented in this chapter is published in *Optical and Quantum Electronics* and other part (Poincare sphere representation) is published in *Optical Engineering.*

1. C. Hari Krishna and Sourabh Roy*, "*Generation of inhomogeneously polarized vector vortex modes in a few mode optical fiber*", Opt Quant Electron*, 51: 41, 1-10 (2019).
2. C. Hari Krishna and Sourabh Roy, "Poincare sphere representation for vector vortex modes of few-mode optical fiber," *Opt. Eng*., 58(1), 016109, 1-6 (2019).

References

1. Qiwen Zhan, "Cylindrical vector beams: from mathematical concepts to applications," *Adv. Opt. Photon.*, **1**, 1-57 (2009).

2. Alison M. Yao and Miles J. Padgett, "Orbital angular momentum: origins, behavior and applications," *Adv. Opt. Photon.,* **3**, 161-204 (2011).
3. Zhi-Cheng Ren, Ling-Jun Kong, Si-Min Li, et.al., "Generalized Poincaré sphere," *Opt. Express*., **23**, 26586-26595 (2015).
4. Xi-Lin Wang, Yongnan Li, Jing Chen, et.al., "A new type of vector fields with hybrid states of polarization," *Opt. Express.,* **18**, 10786-10795 (2010).
5. Shiyao Fu, Chunqing Gao, Tonglu Wang, et.al., "Anisotropic polarization modulation for the production of arbitrary Poincaré beams," *J. Opt. Soc. Am. B.,* **35**, 1-7 (2018).
6. R. Kalita et al., "The generation of arbitrary vector beams using a division of a wavefront-based setup," *J. Opt.,* **18** 1–8 (2016).
7. G. Milione et al., "Higher-order poincaré sphere, stokes parameters, and the angular momentum of light," *Phys. Rev. Lett.,* **107,** 1–4 (2011)
8. Giovanni Milione et al., "Highser Order Pancharatnam-Berry Phase and the Angular Momentum of Light," *Phys. Rev. Lett.,* **108**, 190401 (2012).
9. Dennis H. Goldstein, "*Polarized light,"* CRC Press (2011).
10. M.J. Padgett and J. Courtial, "Poincaré-sphere equivalent for light beams containing orbital angular momentum," *Opt. Lett.,* **24,** 430-432 (1999).
11. Z.C. Ren, et al., "Generalized Poincaré sphere," *Opt. Exp.,* **23**, 26586-26595 (2015)
12. D. L. A. Tjaden, "First-Order Correction to 'Weak-Guidance' Approximation in Fiber Optics Theory," *Philips J. Res.,* **33**, 103 (1978)
13. Allan W. Snyder and William R. Young, "Modes of optical waveguides," *J. Opt. Soc. Am.,* **68**, 297-309 (1978).
14. Allan W. Snyder, and John D. Love, "*Optical Waveguide Theory,"* Chapman and Hall, (1983).
15. Anurag Sharma, "Constructing linear combination of LP modes to obtain zeroth order vector modes of optical fibers," *Appl. Opt*., **27**, 2647-2649 (1998).
16. V.V.G. Krishna Inavalli and Nirmal K. Viswanathan, "Rotational Doppler-effect due to selective excitation of vector-vortex field in optical fiber," *Opt. Exp.,* **19**, 448-457 (2011)
17. Smith A. M., "Birefringence induced by bends and twists in single-mode optical fiber," *Appl. Opt.,* **19**, 2606-2611 (1980)

CHAPTER

6

Polarization Singularities in few-mode optical fiber

Contents

CHAPTER 6

Polarization Singularities in Few Mode Optical Fiber

In this chapter, we demonstrate a fiber based method to generate complex π-symmetric polarization singular topologies such as lemon, star and monstar. These singularities are formed as a result of a combination of orthogonally polarized Gaussian and Laguerre-Gaussian modes excited simultaneously in the few mode optical fiber, controlled by input coupling conditions. Dipoles, the beam fields consisting of two opposite index C-points, are also generated and their topology is analysed with Stokes polarimetry. We have also studied the conversion schemes of lemon to star and vice-versa using a cylindrical lens and a half wave plate.

6.1 Introduction

Polarization singularities which are the vector analogues of phase (scalar) singularities in complex electromagnetic fields arise when one of the parameters defining the polarization of light becomes undefined [1,2]. These are mainly classified as C-points (circularly polarized) and L-lines (linearly polarized) in the polarization ellipse field where the orientation of major axis and the handedness of the polarization ellipse are undefined respectively [3]. C-point is surrounded by polarization ellipses of spatially varying ellipticity in a specific manner. Depending on the geometrical orientation of this ellipse field around C-point, the topologies are classified as lemon, star and monstar. All these topologies are π-symmetric i.e., the ellipses make a full cycle of π around the C-point. The orientation angle of ellipses increases with the angular coordinate (anti-clockwise direction) for lemon and monstar and the orientation angle increases opposite to the angular coordinate (clockwise direction) for stars as shown in first row of Fig. 6.1 [4-7]. Depending on this orientation of polarization ellipses, the topological index $I_c = \frac{1}{2\pi}\oint d\psi$ (ψ is the ellipse orientation angle) is +1/2 for lemon and monstar and -1/2 for star [8,9]. The circle with the dashed line in the first row of Fig. 6.1 is the L-line (line of linear polarizations) where the polarization changes handedness from left circular (green ellipses) to right circular (red ellipses) due to orthogonal field overlapping [3]. The size of this L-line varies with the amplitude of interfering modes. Additionally, a lemon topology has one radial line (where the major axes of ellipses are aligned with angular

coordinate) while star and monstar topologies have three radial lines originating from or terminating on the C-point which can be realized by drawing streamlines as shown in second row of Fig. 6.1. The radial lines are highlighted in red color and the C-point is enclosed in black circle.

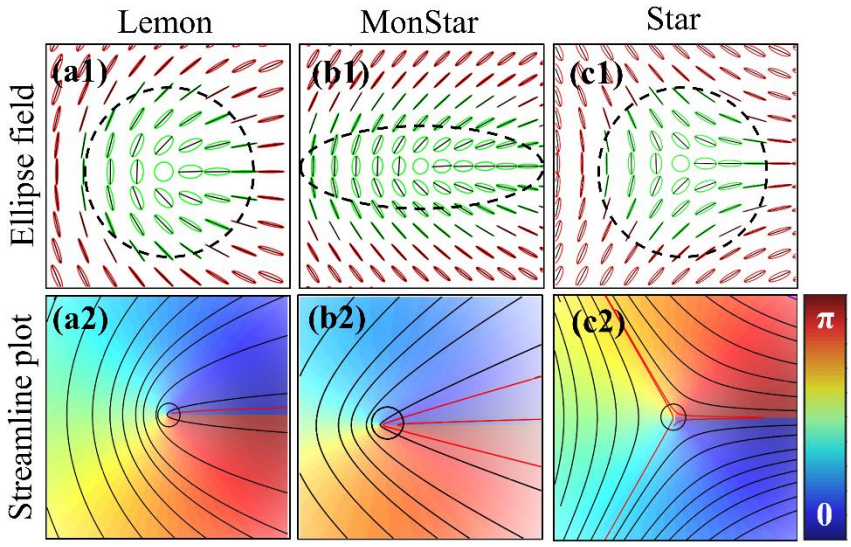

Fig. 6.1. π- Symmetric polarization singularities; (a1) lemon, (b1) monstar, (c1) star, (a2)-(c2) are the corresponding streamline plots.

Stokes polarimetry has evolved as the key characterization tool to study the polarization singularities in free space [3] as well as in media [10-12] there by creating a new characterization technique called *singular polarimetry* [13], which is useful in understanding the propagation dynamics of singularities in anisotropic media. This technique, in recent days, is also being used to study the material properties and to evaluate the modal characteristics of few-mode optical fibers. The production and characterization of C-points is also useful in the study of higher order phase vortices as it is difficult to preserve them in isolated state [3,14,15]. Apart from characteristic studies, the beams with singularities are showing significant applications in various fields such as second harmonic generation [16,17], optical tweezers [18], and multiplexing/ demultiplexing [19]. In view of these applications and also with an interest to explore yet-unknown aspects of polarization singular beams, numerous techniques were reported for their generation based on interferometry that include SLMs [20-22], SPPs [23], and q-plates [24,25]. Recently, polarization singularities are also reported to be generated in plasmonic fields [26], and nematic liquid crystal cells [27]. An alternative method to generate such complex vector fields is by using optical fibers. The inherent combination

of vortex and Gaussian modes within optical fiber can generate rich variety of polarization singularities [21,28-30].

In this chapter, we demonstrated the generation of π-symmetric topologies such as lemon, star and monstar using a few mode optical fiber and studied the effect of relative phase difference of the interfering modes on formation of C-points. The effect of HWP and cylindrical lens (CL) in conversion of C-points is studied. We have also studied the formation of dipoles, two isolated C-points in the fiber modal fields as a result of combination of Gaussian and vortex modes in linear polarization basis and also as a combination of two vortex modes of displaced cores. The 2π-symmetric topologies such as radial, circulation, spiral, and saddle are realized in the Stokes field of lemon and star and also in the ellipse orientation field of vector vortex modes.

6.2 Origin and types

C-points are formed due to the interference of vortex mode of helical wave front (LG_0^l, l being the topological charge) and a Gaussian mode of plane wave front having orthogonal polarizations [3].

Left circularly polarized vortex mode can be represented as

$$E_1 = (\hat{x} + i\hat{y}) r e^{-r^2/w^2} e^{i\varphi} \tag{1}$$

Where $\hat{x}$ and $\hat{y}$ are the unit vectors, $e^{i\varphi}$ is the helical phase, r is the radial coordinate and w is the beam diameter. Further, a right circularly polarized Gaussian mode can be represented as

$$E_2 = (\hat{x} - i\hat{y}) e^{-r^2/w^2} \tag{2}$$

The combination of these two uniformly polarized fields results in a right circular C-point and the modal field is given by

$$E = (\hat{x} + i\hat{y}) r e^{-r^2/w^2} e^{i\varphi} e^{i\delta} + (\hat{x} - i\hat{y}) e^{-r^2/w^2} \tag{3}$$

where δ is the relative phase difference between interfering modes. Equation (3) represents a specific case of C-point formation. Additionally, one can take freedom to change the helicity of vortex mode and the polarization basis to realize a variety of singular modes. A more general case can be given by

$$E = re^{-r^2/w^2}e^{\pm i\varphi}e^{i\delta}\hat{e}_{L(R)} + e^{-r^2/w^2}\hat{e}_{R(L)} \quad (4)$$

Here, $\hat{e}_L = \hat{x} + i\hat{y}$ and $\hat{e}_R = \hat{x} - i\hat{y}$ represent left circular and right circular polarizations respectively. Variety of C-points that can be generated from the above equation are shown in Fig. 6.2. The relative phase difference is considered to be zero ($\delta = 0$) for simplicity.

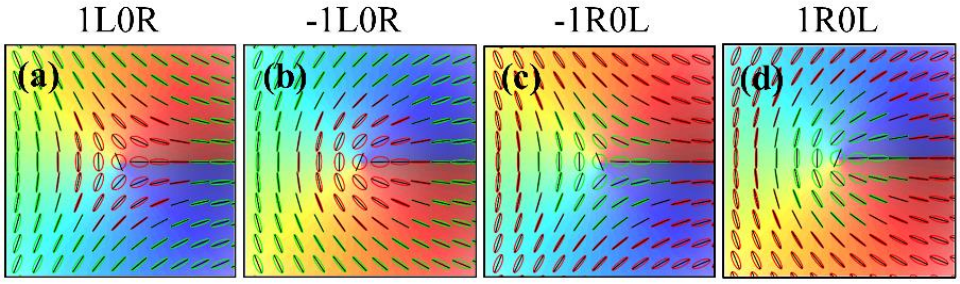

Fig. 6.2. C-points (a) right circular star, (b) right circular lemon, (c) left circular star, (d) left circular lemon.

In the four letter code mentioned in the figure, first and third digits represent the helicity of vortex and Gaussian modes and the second and fourth letters indicate the polarization basis (L-left circular, R-right circular). In coming sections, we show the experimental generation of C-points and characterize them using Stokes polarimetry.

Introducing anisotropy in the vortex mode in Equ. (4) results in the generation of a monstar. The combination of an anisotropic vortex mode and a Gaussian mode of orthogonal polarizations that form a monstar pattern is given by

$$E = re^{-r^2/w^2}(cos\varphi + e^{i\alpha}sin\varphi)e^{i\delta}\hat{e}_{L(R)} + e^{-r^2/w^2}\hat{e}_{R(L)} \quad (5)$$

In Equ. (5), α is the anisotropy parameter. If $\alpha = \frac{\pi}{2} or\ \frac{3\pi}{2}$, the vortex becomes isotropic and the resultant topology will be either star or lemon. The complex monstar topology can also be realized in three beam combinations in which two vortex modes of opposite helicity combine with a Gaussian mode of orthogonal polarization.

The master equation that corresponds to a generalized C-point in polar coordinates (r, φ) is given by [21]

$$E = \left(cos\beta\ re^{i\varphi} + sin\beta\ re^{-i\varphi}\ e^{i\gamma}\right)e^{i\delta}\hat{e}_{R(L)} + \hat{e}_{L(R)} \quad (6)$$

Where β and γ are the parameters that control amplitude and relative phase of the vortex modes. The first term in the brackets corresponds to a vortex mode of right helicity and the second term with left helicity with a relative phase difference γ between these two modes. The first term of Equ. (6) represents anisotropic vortex mode and the second term represents Gaussian mode of orthogonal polarizations which combine with a relative phase difference δ to form a monstar topology. Consider $\beta = 0$ for a simple case. Then, the above equation becomes

$$E = \left(re^{i\varphi}\right)e^{i\delta}\hat{e}_{R(L)} + \hat{e}_{L(R)} \tag{7}$$

Equation (7) is the same as that of Equ. (4), which results in the generation of symmetric lemon and star topologies.

6.3 Experimental details

The schematic diagram of experimental setup used for the generation of polarization singular beams is shown in Fig. 6.3. A focused spot of 5 mW He-Ne laser of 632.8 nm wavelength is launched onto the cleaved tip of FMF. By adjusting the coupling conditions at the fiber input end, the output modes are recorded using CCD camera and simultaneously Stokes polarimetry is carried out to investigate the spatial polarization content of the generated mode. A HWP and CL are inserted in the path of singular modes to study their effect on C-points.

Fig. 6.3. Schematic diagram of the experimental setup.

6.4 Results and discussions

6.4.1 Generation of lemon and star

Lemon and star are orthogonal polarization singular beams that lie at north and south poles on the sphere of Poincare modes [4,5,31]. Generation of these modes in optical fiber needs precise control over the launching conditions. Unlike the vector vortex modes, these modes do not necessarily have a dark core as the contribution from the fundamental Gaussian mode is equally important in the formation of C-points. These modes mostly

appear with a near uniform intensity distribution across the mode as the central dark region of *LG* mode is occupied by orthogonally polarized Gaussian mode. From our experimental observations, we believe that the probability of generating an isolated C-point is high for input linear polarization than elliptical polarization. For input elliptical polarizations, the modes observed are mostly dipoles except for right and left circular polarizations for which orthogonal C-points may be generated. Moreover, the effect of varying input linear/elliptical polarization on the topological behaviour of output mode also depends on the relative amplitudes of combining orthogonal modes and the position of singular region in the modal output. In our experiment we maintain the input SOP to be vertical in lab frame throughout the experiment. The fiber tip is adjusted for offset and skew launching of light unless a donut mode with near uniform intensity is observed. Then, Stokes polarimetry is performed to characterize the mode. In similar manner, for four different coupling conditions, we observed following C-points.

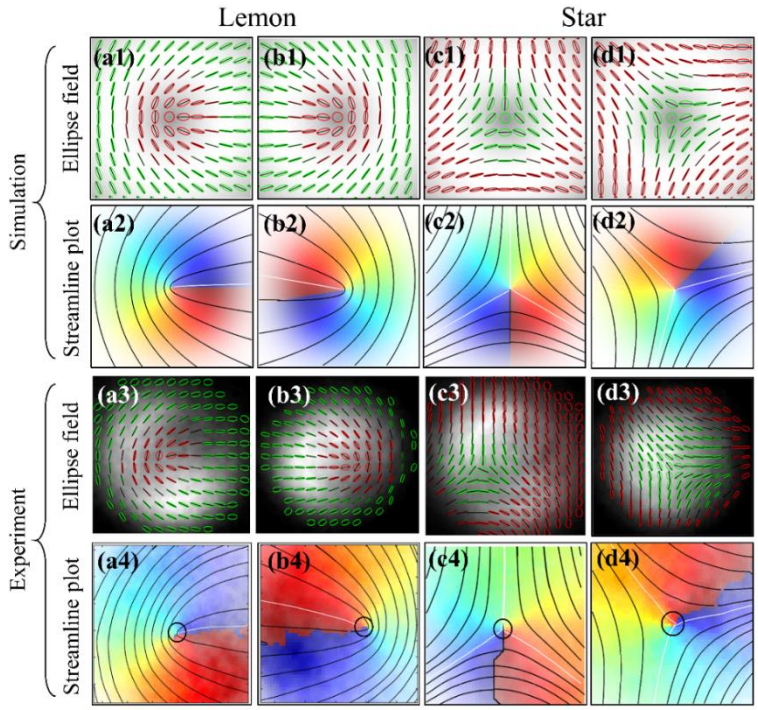

Fig. 6.4. Row 1: Simulation results (a1), (b1) Lemons with right circular C-point, (c1), (d1) Stars with left circular C-point, Row 2: (a2)-(d2) are the corresponding streamline plots, Row 3 and Row 4 are corresponding experimental results for Row 1 and Row 2.

Figure 6.4 shows the numerically and experimentally generated lemon and star patterns for different coupling conditions. First and second rows are simulated results using Equ. (4). From the simulated patterns the relative phase (δ) between the interfering

modes is estimated. Figures 6.4 (a3) and (b3) are lemon topologies with right circular C-points generated from a combination of right circular Gaussian mode and left circular, left helical *LG* mode with 0^o and 170^o relative phase difference between them respectively. Similarly, Fig. 6.4 (c3) and Fig. 6.4 (d3) are the star topologies with left circular C-points generated from the combinations of left circular Gaussian mode and right circular, left helical *LG* mode with -270^o and -45^o relative phase difference between them respectively. These four polarization singular modes are encountered for different input coupling conditions. Interestingly, for all singular patterns, the helicity of vortex mode is -1. From the singular pattern and its polarization content, one can predict the topological charge or helicity of the combining modes and also the relative phase difference between them. Figures 6.4 (a4) - (d4) are the corresponding streamline plots. The white solid line among the curved black lines indicates the radial line and the black circle at the center is the location of C-point.

6.4.2 Generation of Monstars

Monstar is a hybrid polarization singular topology that has the properties of both lemon and star [31]. The geometrical orientation of polarization ellipses around the C-point of a monstar resembles the topology of a lemon but it has three radial lines originating from the C-point that coincide with the characteristics of a star and hence the name 'Mon-Star'. It has been recently reported that monstar is an anisotropic lemon which can be formed either by squeezing or rotating a lemon [32]. For example, let us consider the lemon pattern of Fig. 6.4 (a2) for which the radial line is along +ve X-axis. On squeezing this lemon along Y-axis towards origin, some of the curved lines around C-point come closer resulting in the formation of new radial lines and hence a monstar is generated.

In general, an isolated monstar is rarely realized in experiments [23,33,34], however the probability is more in random speckle fields [35,36]. Here, we have made an attempt to realize the isolated monstar using an FMF by taking advantage of its inherent modal and polarization characteristics. As discussed in the previous section, the combination of plane and helical wave fronts of orthogonal circular polarization results in the formation of lemon and star patterns. But, the formation of monstar takes place when two *LG* modes of opposite helicity combine with a plane wave front Gaussian mode of orthogonal polarization i.e., an anisotropic vortex mode combines with a Gaussian mode as shown in Equ. (5). This can also be explained as the combination of orthogonal HG_{01} and HG_{10}

modes (which are analogous to LP_{11} modes of FMF) with Gaussian mode of orthogonal circular polarizations [21].

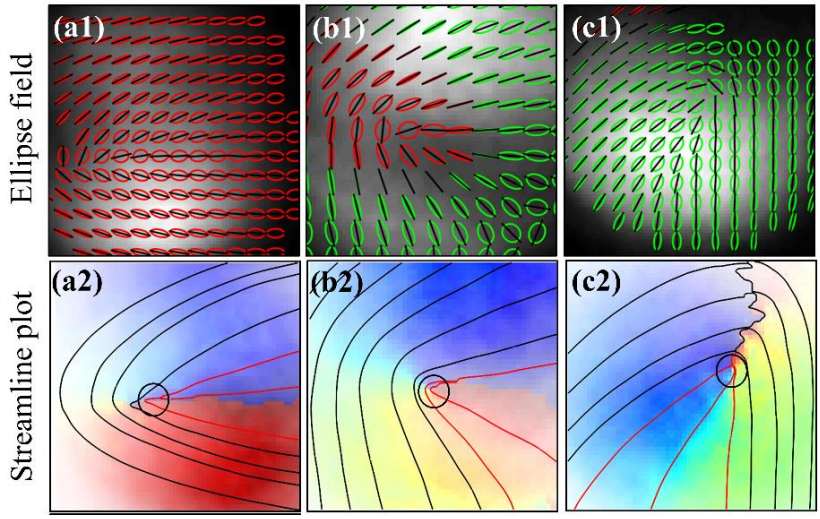

Fig. 6.5. Monstar singular topologies generated for different coupling conditions; (a1)-(c1) ellipse fields, (a2)-(c2) corresponding streamline plots.

Iconic monstar patterns with three radial lines encountered for different coupling conditions are shown in Fig. 6.5. Utmost care has been taken while exciting such complex mode combinations. Stokes polarimetry is carried out for the modes whose spatial intensity distribution looks like HG_{01} or HG_{10} mode with non-zero intensity between the adjacent lobes, which is nothing but the combination of an anisotropic vortex with Gaussian mode. Unlike lemon and star patterns, these patterns can hardly be identified with the spatial polarization map, but streamlines give effective visualization of such complex polarization topologies. It can be observed from Fig. 6.5 (a1) that the amplitude of one of the combining modes with right circular polarization is dominating. Similarly in Fig. 6.5 (c1) the amplitude of mode with left circular polarization is dominating while in Fig. 6.5 (b1), a right circular Gaussian mode is embedded in left circular anisotropic vortex mode. Hence, it can be stated that the relative amplitudes and relative phases of the combining modes are purely dependent on the input coupling conditions of FMF. The corresponding streamline plots are shown in Fig. 6.5 (a2) – (c2), where the black circles enclose the C-point and the red solid lines indicate the radial lines.

6.4.3 Formation of dipoles

The presence of two C-point polarization singularities of opposite topological index in the modal field is generally referred to as dipole i.e., star-lemon, star-monstar etc. In some

cases, two isolated C-points of the same index also can be found in the modal field such as star-star and lemon-lemon depending on the topology of phase and polarization of the interfering modes [29]. In the previous section, we explained that a combination of LG and Gaussian modes of orthogonal circular polarization forms a single isolated C-point (star or lemon), but the same modes in linear polarization basis (horizontal and vertical) results in the formation of dipoles as shown in Fig. 6.6 and the field distribution of dipoles is given by

$$E = \hat{e}_{H(V)} r e^{-r^2/w^2} e^{\pm i\varphi} e^{i\delta} + \hat{e}_{V(H)} e^{-r^2/w^2} \tag{8}$$

In the 4 digit notation mentioned on each dipole pattern, the first and third digits represent the topology of phase (l = 0, ±1) and the second and fourth letters represents the polarization basis (H-horizontal, V-vertical, R-right circular and L-left circular). Fig. 6.6 (a1) and (b1) are the star-monstar dipoles and Fig. 6.6 (c1) and (d1) shows the star-lemon dipole patterns.

Dipoles and a pair of isolated C-points can also be formed when two orthogonally polarized *LG* modes with slightly displaced vortex cores interfere.

$$E = \hat{e}_{R(H)} r e^{-r^2/w^2} e^{\pm i\varphi} e^{i\delta} + r_1 \hat{e}_{L(V)} e^{-{r_1}^2/w^2} e^{\pm i\varphi} \tag{9}$$

Equation (9) represents the combination of two vortex modes of orthogonal polarization with their cores slightly displaced ($r_1 = r + \Delta r$). Figures 6.6 (a2) and (d2) are the dipoles consisting of a star-lemon pair while Fig. 6.6 (b2) and (c2) are two isolated C-points with lemon and star topologies respectively. In this case the location of C-points is observed to coincide with the displaced vortex cores. In addition to the circular basis of the displaced vortex cores, the linear basis also can generate asymmetric dipole (Fig. 6.6 (a3) and (d3)) and double dipole (Fig. 6.6 (b3) and (c3)) patterns.

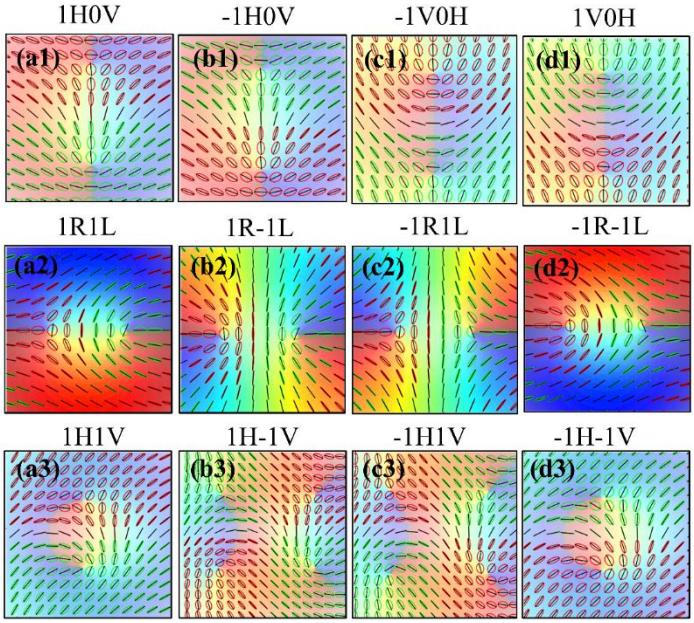

Fig. 6.6. Dipole topologies; (a1)-(d1) combination of a vortex mode and Gaussian mode in linear basis; combination of two vortex modes with displaced cores in (a2)-(d2) circular basis, (a3)-(d3) linear basis.

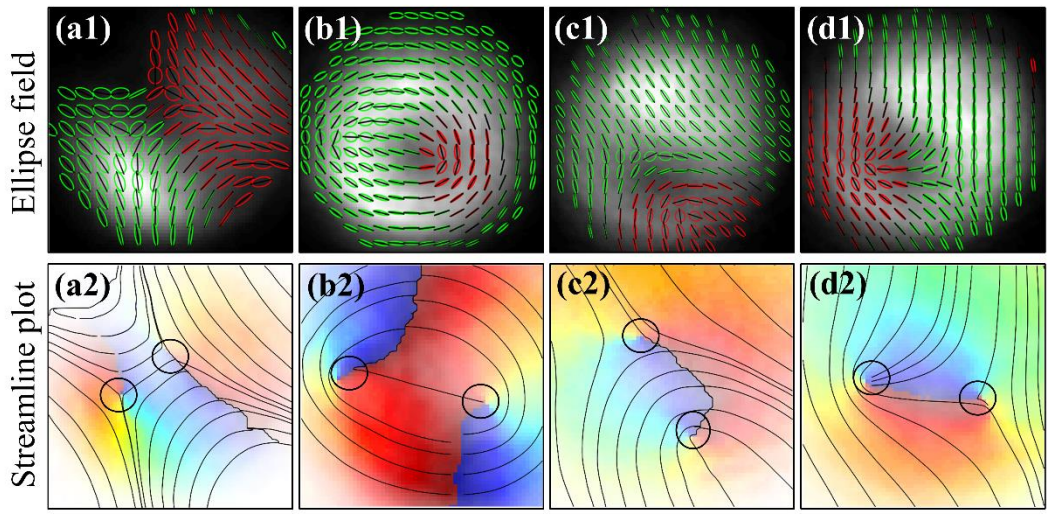

Fig. 6.7. Experimentally generated dipole patterns; (a) two isolated stars, (b) two isolated lemons (c) star-lemon dipole (d) monstar-star dipole.

Some of the experimentally generated dipoles and a pair of isolated C-points are shown in Fig. 6.7. During the excitation of dipoles, the output mode is observed to be a donut mode with near uniform intensity and in some cases with relatively large core area, which signifies two vortices separated by certain distance. By adjusting the coupling conditions of the fiber, we excited the combinations of two vortex modes of orthogonal circular polarization (Fig. 6.7 (a1) and (b1)) and the combinations of a vortex mode and a Gaussian mode of orthogonal linear polarization (Fig. 6.7 (c1) and (d1)). Figures 6.7

(a1) and (b1) show a pair of isolated C-points with star and lemon topologies facing each other and sharing a common radial line which are expected to be combinations of two vortex modes of opposite topological charge and orthogonal circular polarization with π relative phase difference. Figures 6.7 (c1) and (d1) show dipole patterns formed due to the combination of a vortex mode and a Gaussian mode of orthogonal linear polarizations as discussed above. Figures 6.7 (a2) - (d2) are the corresponding streamline plots.

6.4.4 Action of HWP and Cylindrical lens on C-points

The switching of C-point indices and transformation to their orthogonal states is of great scientific interest as these phenomena can be useful in polarization multiplexing and quantum computing [19,37]. Recent reports suggest that a HWP can be useful in switching the index of C-point singularity i.e., lemon to star and vice-versa [38] and a spiral phase plate (SPP) is capable of transforming a C-point to its orthogonal state [39]. Here, we investigate experimentally the effect of HWP and a CL in conversion of a C-point.

In the experimental setup, the generated C-points are allowed to pass through a HWP and CL that are inserted after the microscope objective lens L2 and Stokes polarimetry is carried out for the output mode in respective cases. Figure 6.8 shows the experimentally generated anisotropic lemon with right circular C-point and its transformations after passing through a CL and HWP. It can be observed from Fig. 6.8 (b1) and (c1) that the lemon has been transformed to a star type singularity of opposite index under the action of both CL and HWP individually. The radial lines are highlighted using a white solid line to guide the eye while C-point is enclosed in white circle. One interesting fact is that a CL has transformed lemon to star changing the index from +1/2 to -1/2, while leaving the SOP unaltered i.e., a lemon with right circular C-point converted to a star with right circular C-point as shown in Fig. 6.8 (b1). In contrast, a HWP converted both index and SOP i.e., a lemon with right circular C-point converted to a star with left circular C-point as shown in Fig. 6.8 (c1). Moreover, the radial lines of the star patterns converted using CL and HWP are orthogonal to each other. Figures 6.8 (a2) - (c2) are the corresponding ellipse orientation maps of Fig. 6.8 (a1) - (c1). The arrow on the black circle enclosing the C-point indicates the direction of ellipse orientation angle increment, which is anti-clockwise for lemon and clockwise for star patterns.

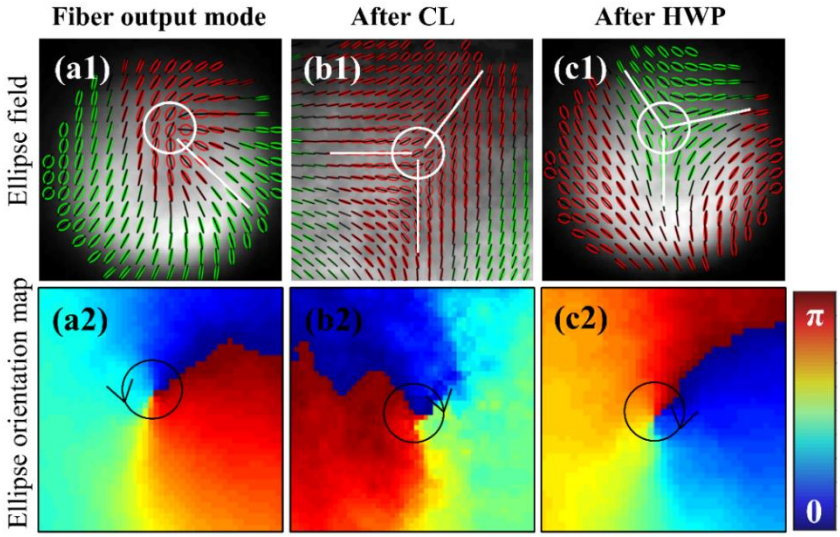

Fig. 6.8. Experimental results for generation and conversion of C-point from (a1) lemon to star using (b1) CL, (c1) HWP; (a2)-(c2) are corresponding ellipse orientation maps.

The same phenomenon is observed for a star pattern with right circular C-point as shown in Fig. 6.9. It is noteworthy to state that on conversion of C-point using a CL, only the index is changing but not SOP which means that the topological charge (l) of the vortex mode is changing from -1 to +1 in Fig. 6.8 and from +1 to -1 in Fig. 6.9. On the other hand, HWP has no effect on the phase of vortex mode but swaps the handedness of polarization. This phenomenon is useful in conditional switching of either phase (using CL) or polarization (using HWP) or both simultaneously using CL and HWP to get orthogonal C-point.

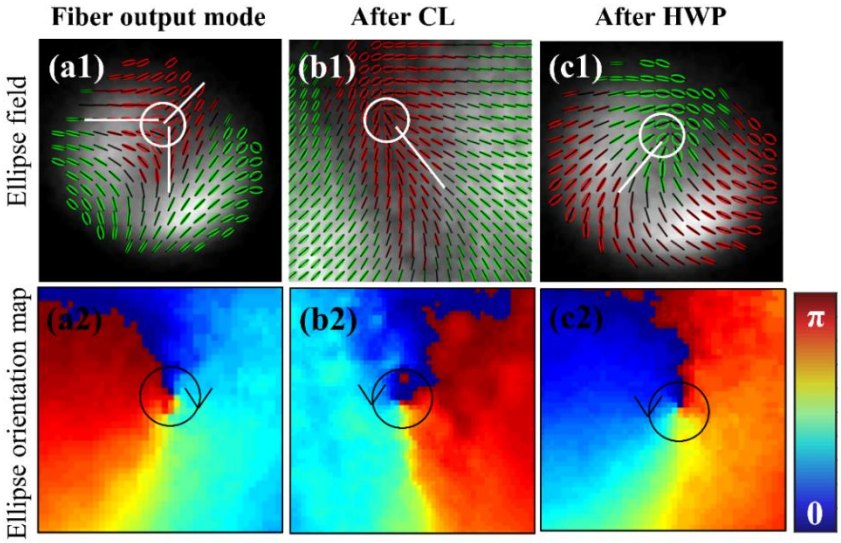

Fig. 6.9. Experimental results for generation and conversion of C-point from (a1) star to lemon using (b1) CL, (c1) HWP; (a2)-(c2) are corresponding ellipse orientation maps.

6.4.5 Stokes fields and Poincare vortices

The stokes parameters for a vector field distribution $E = E_x\hat{x} + E_y\hat{y}$ can be defined as follows

$$\begin{aligned} S_0 &= E_x E_x^* + E_y E_y^* \\ S_1 &= E_x E_x^* - E_y E_y^* \\ S_2 &= E_x E_y^* + E_y E_x^* \\ S_3 &= i(E_x E_y^* - E_y E_x^*) \end{aligned} \tag{10}$$

From these, complex Stokes fields (S_{ij}) and hence Stokes phases (Φ_{ij}) can be derived as follows [40]

$$S_{12} = S_1 + iS_2\ ,\ S_{23} = S_2 + iS_3, \text{ and } S_{31} = S_3 + iS_1 \tag{11}$$

$$\Phi_{12} = \arg(S_1 + iS_2),\ \Phi_{23} = \arg(S_2 + iS_3), \text{ and } \Phi_{31} = \arg(S_3 + iS_1) \tag{12}$$

Equation (12) represents Stokes phases, which gives information about Stokes vortices or Poincare vortices. The study of Stokes fields and Stokes vortices (singular points of Stokes field) is essential in exploring and understanding the topological aspects which are useful in many scientific fields as these are the signatures of most fundamental aspects of electromagnetic fields. These topologies are universal and very common in nature such as in fingerprints [41], liquid crystal arrangements [27,42,43], cosmic radiation [44], magnetic skyrmions [45] and biology [46]. The optical fields with π-symmetric topologies such as lemon, star and monstar with index ±1/2 and 2π-symmetric topologies such as spiral, saddle, radial and circulation with index ±1 are recently reported in vector-vortex beam fields and their poynting vector flow [47,48]. However, the studies related to these complex topologies are mostly theoretical and very few experimental evidence has been demonstrated using bulk optical setups that involve complex optical elements such as SPP and q-plates.

In this section, we discuss the complex topologies that are present around Stokes vortices which are derived from well patterned π-symmetric lemon and star topologies generated using FMF. Figures 6.10 (a1) – (d1) show the streamline plots for ellipse orientation angle ($\psi = \Phi_{12}/2$) of a lemon topology along with Stokes vortices. Here, only ψ is the π-symmetric vector field with half index whereas the vector field around all Stokes vortices is 2π-symmetric i.e., Φ_{12} has single vortex with radial topology while Φ_{23} and Φ_{31}have a pair of vortices (dipoles) with integer index. Corresponding

experimental results are shown in Fig. 6.10 (a2) – (d2). Slight deviation from the simulated patterns is observed in the experimentally generated topologies of Φ_{23} and Φ_{31} due to field asymmetry which may be caused due to slight variations in relative amplitudes and phase of interfering modes.

The simulated topologies around Stokes vortices for a star pattern are shown in Fig. 6.11 (a1) – (d1) and the corresponding experimental results are shown in Fig. 6.11 (a2) – (d2). Here, the topology of Φ_{12} is a saddle, that of Φ_{23} and Φ_{31} are dipoles as in previous case but with different topology, all are being of integer index. The topology of Φ_{12} changes from radial to spiral and then to circulation for a relative phase difference of 0, π/4 and π/2 between the interfering modes for a lemon but remains the same (saddle) for a star with a mere rotation in respective cases. This shows the strong dependency of topology of 2π-symmetric vector fields on that of their π-symmetric counter parts. Moreover, Φ_{ij} gives the information about the relative phase difference between the components of S_k $(i, j, k = 1,2,3$ in rotation) i.e., Φ_{12} gives the relative phase difference between components of S_3 (right circular and left circular polarizations), Φ_{23} between the components of S_1 (horizontal and vertical) and Φ_{31} between the components of S_2 (diagonal and anti-diagonal) [47].

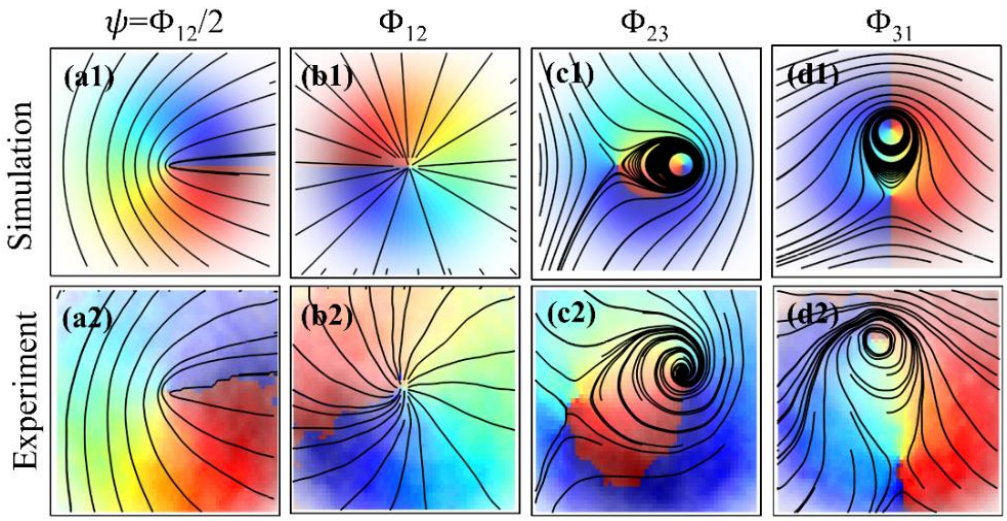

Fig. 6.10. (a1) – (d1) Simulated streamline plots for Stokes vortices of a lemon, (a2) – (d2) are the corresponding experimental results.

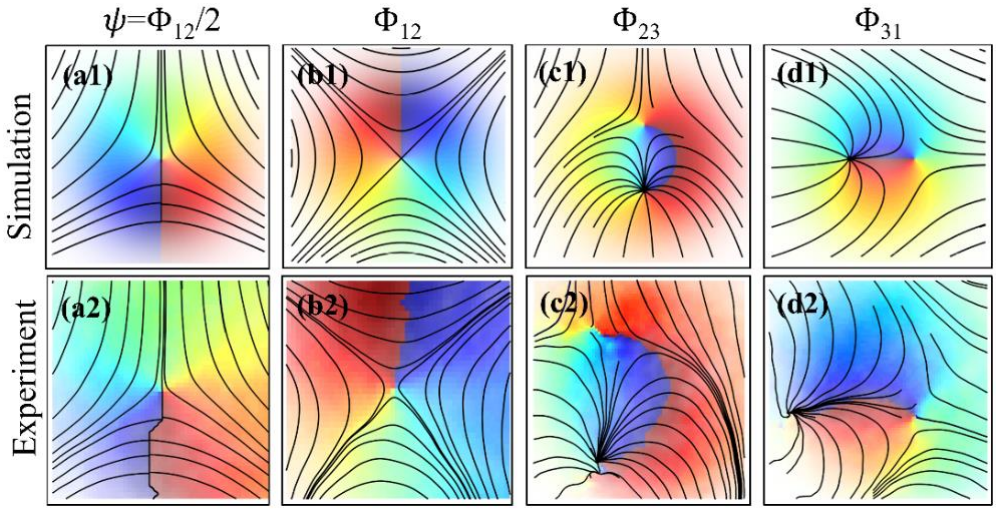

Fig. 6.11. (a1) – (d1) Simulated streamline plots for Stokes vortices of a star, (a2) – (d2) are the corresponding experimental results.

6.4.6 2π-symmetric vector fields of vector vortex modes

In the previous section, we discussed π and 2π-symmetric topologies in polarization ellipse orientation field and Stokes vortices (Φ_{12}) respectively. In this section, we discuss the direct realization of 2π-symmetric vector fields such as radial, spiral, circulation and saddle in the polarization ellipse orientation field by exciting the vector vortex modes of FMF. To the best of our knowledge, the topological aspects of vector modes of FMF have not been reported previously even though there are numerous reports on the controlled generation and manipulation of such inhomogeneously polarized fields. Figure 6.12 shows the simulated (row 1) and experimental (row 2) streamline plots for vector modes of FMF which are discussed in previous chapter and are excited by adjusting the coupling conditions. These vector modes, being 2π-symmetric in ellipse field, exhibit 4π-symmetry in Φ_{12} with topological index two. The vector modes with radial, azimuthal and spiral polarizations correspond to radial, circulation and spiral topologies in ellipse orientation field and all other hybrid modes correspond to saddle topology.

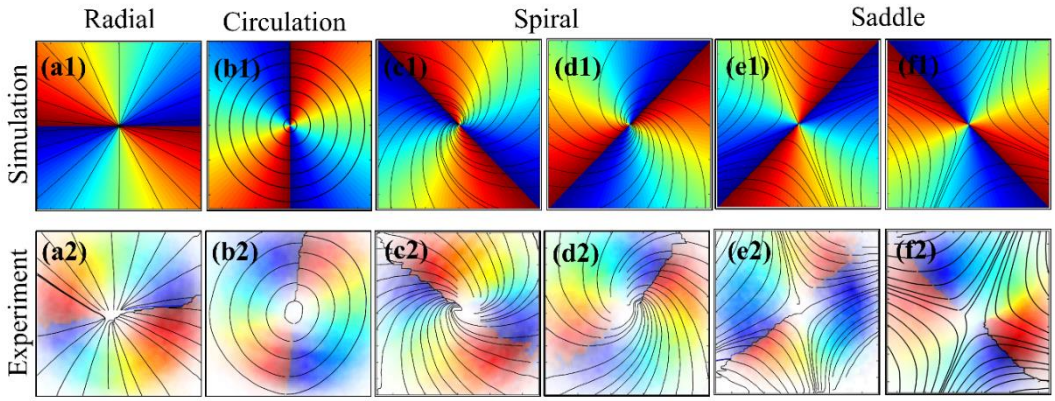

Fig. 6.12. Row 1: Simulated streamline plots for (a1) radial, (b1) azimuthal, (c1), (d1) spiral and (e1), (f1) hybrid vector modes of FMF; Row 2: (a2) – (f2) are the corresponding experimental results.

The optical fiber acts as a powerful tool to realize all complex polarization topologies by virtue of its inherent modal and polarization characteristics which otherwise is not possible without complex optical devices such as SPPs, SLMs and q-plates. Moreover, its cost effectiveness is one of the reasons for its usage to realize such complex optical phenomena. The only drawback in using fiber for this kind of studies is that it is possible to realize optical vortices of only first order with well-defined polarization behaviour and also it is a tedious job to control the excitation of desired modes if the number of supported modes increases in the fiber.

6.5 Conclusions

In this chapter, we have discussed polarization singularities, their origin and types with an experimental demonstration on their generation and characterization using Stokes polarimetry. We studied the generation of π-symmetric isolated C-points such as lemon and star and discussed the action of HWP and a cylindrical lens on them. We have successfully demonstrated the experimental generation of isolated monstar topologies by selective excitation of mode combinations with precise control over coupling conditions. The effect of relative phase differences between the interfering modes in generation of polarization singular topologies is studied. 2π-symmetric topologies are realized in Stokes vortices and also in the polarization ellipse orientation field of vector vortex mode fields.

References

[1] J. F. Nye, "Natural focusing and fine structure of light: caustic and wave dislocation," Institute of Physics Pub. 1999, London.

[2] M.V. Berry and J.H. Hannay, "Umbilic points on Gaussian random surfaces," J. Phys. A 10, 1809–1821 (1977).

[3] E.J. Galvez, B.L. Rojec, and K.R. McCullough, "Imaging optical singularities: Understanding the duality of C-points and optical vortices," *Proc. SPIE* 8637, 863706 (2013)

[4] M.R. Dennis, K. O'Holleran and M.J. Padgett, "Optical vortices and polarization singularities," Prog. Opt., 53, 293 – 363 (2009).

[5] M.R. Dennis, "Polarization singularities in paraxial vector fields: morphology and statistics," Opt. Comm., 213, 201–221 (2002).

[6] Dennis, M.R.; O'Holleran, K.; Padgett, M.J. Singular optics: Optical vortices and polarization
singularities. *Prog. Opt.* **2009**, *53*, 293–363

[7] M. S. Soskin and M. V. Vasnetsov, "Singular optics," Prog. Opt. 42, 219–276 (2001).

[8] Mokhun and M. S. Soskin, I. Freund, "Elliptic critical points: C-points, α-lines, and the sign rule," June 15, 2002 / Vol. 27, No. 12 / OPTICS LETTERS, 995-997.

[9] M. V. Berry, "Index formulae for singular lines of polarization," J. Opt. A: Pure Appl. Opt. 6 (2004) 675–678.

[10] F. Flossmann, U.T. Schwarz, M. Maier, and M.R. Dennis, "Stokes parameters in the unfolding of an optical vortex through a birefringent crystal," Opt. Express 14, 11402-11411 (2006)

[11] R. Botet, H. Kuratsuji, and R. Seto, "Novel aspects of evolution of the Stokes parameters for an electromagnetic wave in anisotropic media," Prog. Theor. Phys. 116, 285-294 (2006)

[12] Y.A. Kravtsov, B. Bieg, and K.Y. Bliokh, "Stokes-vector evolution in a weakly anisotropic inhomogeneous medium," J. Opt. Soc. Am. A 24, 3388-3396 (2007)

[13] K. Yu. Bliokh, Avi Niv, V. Kleiner and E. Hasman, "Singular polarimetry: Evolution of polarization singularities in electromagnetic waves propagating in a weakly anisotropic medium" Opt. Exp., 16, 695 – 709 (2008).

[14] S.M. Baumann, D. M. Klab, L.H. MacMillan, and E. J. Galvez, "Propagation dynamics of optical vortices due to Gouy phase," Opt. Exp., 17, 9818-9827 (2009).

[15] F. Ricci, W. Loffler, and M.P. Van Exter, "Instability of higher-order optical vortices analysed with multi-pinhole interferometer," Opt. Exp., 20, 22961-22975 (2012).

[16] Li Zhang, Xiaodong Qiu, Fangshu Li, Haigang Liu, Xianfeng Chen, and Lixiang Chen, "Second harmonic generation with full Poincare beams," Vol. 26, No. 9 | 30 Apr 2018 | OPTICS EXPRESS 11678-11684.

[17] I. Freund, "Second-harmonic generation of polarization singularities," Opt. Lett. 27(18), 1640–1642 (2002).

[18] L. G. Wang, "Optical forces on submicron particles induced by full Poincaré beams," Opt. Express 20(19), 20814–20826 (2012).

[19] B. Szafraniec, B. Nebendhal and T. Marshall, "Polarization demultiplexing in Stokes space" Opt. Exp., 18, 17928 – 17939 (2010).

[20] E.J. Galvez and S. Khadka, "Poincare modes of light," *Proc. of SPIE,* 8274, 82740Y 1-8 (2012)

[21] E. J. Galvez, B. L. Rojec, V. Kumar, and N. K. Viswanathan, "Generation of isolated asymmetric umbilics in light's polarization," Phys. Rev. A. 89, 031801 (2014)

[22] E. Otte, C. Alpmann, and C. Denz, "Higher-order polarization singularities in tailored vector beams," J. Opt. 18, 074012 (2016)

[23] V. Kumar, G.M. Philip and N.K. Viswanathan, "Formation and morphological transformation singularities: Hunting the monstar," J. Opt. 15, 044027, (2013)

[24] Filippo Cardano, Ebrahim Karimi, Lorenzo Marrucci, Corrado de Lisio, and Enrico Santamato, "Generation and dynamics of optical beams with polarization singularities," 2013, Vol. 21, No. 7 | OPTICS EXPRESS 8815- 8820

[25] E. Karimi, B. Piccirillo, L. Marrucci, and E. Santamato, "Light propagation in a birefringent plate with topological charge," Opt. Lett. 34, 1225–1227 (2009)

[26] Anouk de Hoogh, L. Kuipers, Taco D. Visser and Nir Rotenberg "Creating and Controlling Polarization Singularities in Plasmonic Fields," *Photonics* **2015**, *2*, 553-567

[27] A.D. Kiselev, "Singularities in polarization resolved angular patterns: transmittance of nematic liquid crystal cells," J. Phys.: Condens. Matter 19, 246102 (2007)

[28] Y. V. Jayasurya, V. V. G. Krishna Inavalli, and Nirmal K. Viswanathan, "Polarization singularities in the two-mode optical fiber output," 2011 / Vol. 50, No. 25 / APPLIED OPTICS E131-E137.

[29] V. Kumar and N. K. Viswanathan, "Polarization singularities and fiber modal decomposition," Proc. SPIE 8637, 86371A (2013)

[30] T. A. Fadeeva and A. V. Volyar, "Vectorial Topological Dipole in Output Radiation of a Fiber Optical Coupler," Technical Physics Letters, Vol. 30, No. 7, 2004, pp. 553–556

[31] M.R. Dennis, "Polarization singularity anisotropy: determining monstardom," Opt. Lett. 33, 2572–2574 (2008)

[32] Vijay Kumar, and Nirmal K. Viswanathan, "Is Monstar topologically same as lemon?," Complex Light and Optical Forces IX, Proc. of SPIE Vol. 9379, 937909 (1-4)

[33] Enrique J. Galvez1, and Behzad Khajavi, "Monstar disclinations in the polarization of singular optical beams," Vol. 34, No. 4 / April 2017 / J. Opt. Soc. A. A., 568-575.

[34] Ben A. Cvarch, Behzad Khajavi, Joshua A. Jones, Bruno Piccirillo, Lorenzo M Arrucci, and Enrique J. Galvez, "Monstar polarization singularities with elliptically-symmetric q-plates," Vol. 25, No. 13 | 26 Jun 2017 | OPTICS EXPRESS 14935-14943.

[35] F. Flossmann, U.T. Schwarz, M. Maier, and M.R. Dennis, "Polarization Singularities from Unfolding an Optical Vortex through a Birefringent Crystal," Phys. Rev. Lett. 95, 253901 1-4 (2005).

[36] F. Flossmann, K. O'Holleran, M.R. Dennis, and M.J. Padgett, "Polarization Singularities in 2D and 3D Speckle Fields," Phys. Rev. Lett. 100, 203902 1–4 (2008).

[37] E. Nagali, F. Sciarrino, F. De Martini, L. Marrucci, B. Piccirillo, E. Karimi, and E. Santamato, "Quantum information transfer from spin to orbital angular momentum of photons," Phys. Rev. Lett. 103, 013601 (2009)

[38] Sushanta Kumar Pal, Ruchi, and P. Senthilkumaran, "Polarization singularity index sign inversion by a half-wave plate," Appl. Opt., Vol. 56, No. 22, 6181-6190 (2017).

[39] B.S. Bhargava Ram, Ruchi, and P. Senthilkumaran, "Angular momentum switching and orthogonal field construction of C-points," Opt. Lett., Vol. 43, No. 9, 2157-2160 (2018).

[40] I. Freund, A. I. Mokhun and M. S. Soskin, O. V. Angelsky and I. I. Mokhun, "Stokes singularity relations," April 1, 2002 / Vol. 27, No. 7 / OPTICS LETTERS, 545-547.

[41] H. C. Lee and R. E. Gaensslen, Advances in Fingerprint Technology (CRC Press, 2001)

[42] X. Shi and Y. Ma, "Topological structure dynamics revealing collective evolution in active nematics," Nat. Commun. 4, 3013 (2013)

[43] I.O. Buinyi, V.G. Denisenko, and M.S. Soskin, "Topological structure in polarization resolved conoscopic patterns for nematic liquid crystal cells," Opt. Commun. 282, 143–155 (2010)

[44] J. M. Kovac, E. M. Leitch, C. Pryke, J. E. Carlstrom, N. W. Halverson, and W. L. Holzapfel, "Detection of polarization in the cosmic microwave background using DASI," Nature 420, 772–787 (2002)

[45] N. Nagaosa and Y. Tokura, "Topological properties and dynamics of magnetic skyrmions," Nat. Nanotechnol. 8, 899–911 (2013)

[46] L. S. Hirst, A. Ossowski, M. Fraser, J. Geng, J. V. Selinger, and R. L. B. Selinger, "Morphology transition in lipid vesicles due to in-plane order and topological defects," Proc. Natl. Acad. Sci. USA 110, 3242–3247 (2013).

[47] V. Kumar and N. Viswanathan, "Topological structures in the Poynting vector field: an experimental realization," Opt. Lett. 38, 3886–3889 (2013)

[48] Vijay Kumar and Nirmal K. Viswanathan, "Topological structures in vector-vortex beam fields," J. Opt. Soc. Am. B / Vol. 31, No. 6 / June 2014, A40-A45.

CHAPTER
7

Conclusions

Contents

CHAPTER 7

Conclusions

7.1 Conclusions

With the objective of controlled generation and characterization of vector modes in optical fiber, we started the work from an understanding of the fundamental aspects of wave propagation in an inhomogeneous dielectric optical waveguide with step-index profile. The electromagnetic vector wave equation that corresponds to light propagation in optical fiber is derived and general solutions are discussed in appendix. It is understood that the structural conditions of the optical fiber are responsible for the formation of vector modes of complex spatial polarization. Further, the vector wave equation is reduced to scalar wave equation by introducing the weakly guiding approximation. The linearly polarized modes are shown to be solutions under this approximation and the relation between vector modes and scalar modes is established.

The vector modes with radial, azimuthal and hybrid spatial polarization are generated using a few-mode optical fiber by precise control over the coupling conditions and are characterized using a rotating analyzer. A first order phase vortex is generated and is characterized by forming interferograms with a reference Gaussian mode. The presence of fork like structure in the interferogram is the significance of phase singularity (helicity of wave front) of the vortex mode. It has been observed that the input state of polarization is capable of switching the helicity or charge of the singularity of the generated vortex mode. The mechanism of switching phase vortices is expected to find potential application in particle tweezers. Further, the studies on higher order *LP* modes for the presence of phase singularities are presented in chapter 2. Apart from LP modes, few arbitrary modal fields are generated and the presence of phase singularities is identified. The generation of phase singularities of second order in fiber is found to be difficult as they are highly unstable and decompose into single charged vortices for small ambient perturbations. It is also observed that the number of singularities present in the modal field is directly proportional to the V-number of the fiber. This investigation helps to understand the fiber modal fields in terms of phase singularities present in them. As

the phase of the modal fields is highly sensitive to external perturbations on the fiber, the results may find applications in interferometric sensors.

A new approach for the generation of clockwise (CW) & counter-clockwise (CCW) spiral vector beams (SVBs) via combination of orthogonal LP_{11} modes with diagonal and anti-diagonal polarization vector has been demonstrated in chapter 3. The SVBs with polarization vector oriented in CW and CCW direction are experimentally generated using a few-mode optical fiber by controlling the coupling conditions and input state of polarization (SOP). It is observed that the orthogonal LP_{11} modes with diagonal and anti-diagonal polarization are excited for orthogonal linear input SOP, while the SVBs that are linear combinations of orthogonal LP_{11} modes are excited for an intermediate SOP. This shows the strong dependency of polarization of generated mode on the input SOP. Stokes analysis of the experimentally generated modes was found to be in excellent agreement with theoretically predicted results.

In chapter 4, we have presented an experimental demonstration on generating vector vortex modes (VVMs) in a few mode optical fiber by extending the basis of orthogonal LP_{11} modes with diagonal and anti-diagonal polarization vector. The VVMs are generated by controlling the coupling conditions of the fiber and input SOP. The clockwise and anti-clockwise orientations of half wave plate (HWP) from its mean position, before and after changing the coupling conditions, generated all VVMs of orthogonal polarization. Further, a Poincare sphere approach is presented for LP_{11} modes as well as VVMs generated from their linear combination. The location of regular and hybrid VVMs on the higher order Poincare sphere (HOPS) is justified by the positions of orthogonal LP_{11} modes on standard PS, which combine to generate respective VVMs. This approach is efficient and much useful in the representation of vector modes of a few-mode fiber.

From the results obtained in chapter 3 and chapter 4, it can be stated that any slight deviation in the ellipticity of the experimentally generated SVBs and VVMs may be attributed to the fiber birefringence and quality of optics used in the experiment. The SVBs with clockwise and anti-clockwise spiral spatial polarization which have sharper focusing properties next to radial and azimuthal vector modes are suitable for fields such as particle trapping, optical micro manipulation and lithography. And the VVMs with hybrid spatial polarization may also have considerable contribution towards imaging,

microscopy and polarization based data encryption by providing additional degree of freedom.

The vector modes discussed in the previous chapters are V-type polarization singularities, wherein the polarization vector is linearly polarized across the beam and the SOP is undefined at the center. In chapter 5, we have dealt with C-point polarization singularities that are more fundamental in nature. The origin and types of C-point singularities are discussed and π – Symmetric C-point topologies such as lemon, star and monstar are generated experimentally and analysed using Stokes polarimetry. The effect of HWP and cylindrical lens (CL) on the isolated C-points such as lemon and star is studied. It is observed that on conversion of C-point using a CL, only the index is changing but not SOP which means that the topological charge (l) of the vortex mode is changing from -1 to +1. On the other hand, HWP has no effect on the phase of vortex mode but swaps the handedness of polarization. This phenomenon is useful in conditional switching of either phase (using CL) or polarization (using HWP) or both simultaneously using a combination of CL and HWP to get orthogonal C-point. Further, 2π-symmetric topologies are realized in Stokes vortices and also in the polarization ellipse orientation field of vector vortex mode fields.

From all the above studies, we conclude that the optical fiber acts as a powerful tool to realize various VVMs and complex polarization topologies by virtue of its inherent mode mixing and polarization characteristics that arise from its structural model. Optical fiber makes it feasible to realize phase and polarization structured beams which is otherwise not possible without complex optical devices such as SPPs, SLMs and q-plates. Moreover, due to the cost effectiveness and flexibility in operation, optical fibers are being widely used in many applications. The main drawback in using fiber for this kind of studies is that the fibers are capable of generating vortices of first order only with well-defined polarization behaviour, while higher order vortices are unstable. Subsequently, it is a tedious job to control the excitation of desired modes if the number of supported modes increases in the fiber.

7.2 Scope of future work

In this thesis, attention was given to the generation and characterization of various VVMs and also the study of complex polarization singularities. We have successfully generated VVMs other than well-known zeroth order vector modes in few-mode optical fiber by

precise control over coupling conditions and taking advantage of inherent mode mixing phenomenon. As stated above, the fibers can only support vortices of first order with considerable stability and purity, while further studies related to more complex polarization phenomena are highly difficult. Though one may use custom designed optical fibers that support higher order vortices, it increases the cost of fabrication and yet suffer from certain limitations imposed by fiber geometry. Hence, we believe that fibers are useful in such studies only at the fundamental level and suffer from lack of mode stability at higher levels. For this reason, SLMs, SPPs, and q-plates are reliable sources for generating desired modes with good mode stability, which is essential in highly sensitive studies such as geometric phase and entanglement.

Based on current studies presented in this thesis, future work has scope in two possible ways. The first one is the study of fundamental phenomena such as geometrical phase of light beams, 3D polarization patterns, and spin-orbit interactions (SOI) and the second is application oriented i.e., optical tweezers, OAM multiplexing in fibers.

- It is always interesting to revisit the fundamental properties of physics, especially in optics and unleash the hidden aspects which may or may not have significant application but can surely change our view of science that we know today and also pave the path for better understanding of many scientific phenomena. Of late, SOI in light is gaining significant interest among researchers due to its fundamental nature and helps us in understanding light propagation in weakly anisotropic media [1-9]. Further studies may be extended in the direction to understand and explore SOI in light beams.
- Recent reports suggest that the propagation of polarization singular patterns form knots in 3D space, which are highly complicated topological structures. The study of these patterns helps us better understand the propagation characteristics of polarization singular beams. And also the observation of Mobius strips in polarization of light is significantly interesting and changes our regular views on the polarization of light [10-14].
- The light beams with OAM are significantly useful in free-space communication and also in advanced fiber optic communication. Recent investigations on OAM beams for their multiplexing capabilities in optical fibers show a new way to tackle ever expanding demand for high bandwidth. As these beams offer endless degrees of

freedom, the OAM mode multiplexing is of great research interest and yielding fruitful results [15,16].

In view of the numerous opportunities available for using structured beams, we are mainly focused in exploring and understanding the fundamental properties of light for which this thesis helps as a first step towards an endless journey of research.

References

1. Lorenzo Marrucci, Ebrahim Karimi, Sergei Slussarenko et al. "Spin-to-orbital conversion of the angular momentum of light and its classical and quantum application," *J. Opt.,* **13**, 064001 (1-13) (2011).
2. K. Yu. Bliokh, Avi Niv, V. Kleiner, et.al., "Singular polarimetry: Evolution of polarization singularities in electromagnetic waves propagating in a weakly anisotropic medium," *Opt. Exp.,* **16**, 695 – 709 (2008).
3. F. Flossmann, U.T. Schwarz, M. Maier, et.al., "Polarization Singularities from Unfolding an Optical Vortex through a Birefringent Crystal," *Phys. Rev. Lett.*, **95**, 253901 (1-4) (2005).
4. F. Flossmann, U.T. Schwarz, M. Maier, et.al., "Stokes parameters in the unfolding of an optical vortex through a birefringent crystal," *Opt. Express.,* **14**, 11402-11411 (2006).
5. L. Marrucci, C. Manzo and D. Paparo, "Optical spin-to-orbital angular momentum conversion in inhomogeneous anisotropic media," *Phys. Rev. Lett.,* **96**, 163905 (1–4) (2006).
6. C. Brosseau, "Evolution of the Stokes parameters in optically anisotropic media," *Opt. Lett.,* **20**, 1221-1223 (1995).
7. S.E. Segre, "New formalism for the analysis of polarization evolution for radiation in a weakly non uniform, fully anisotropic medium: a magnetized plasma," *J. Opt. Soc. Am. A.,* **18**, 2601-2606 (2001).
8. R. Botet, H. Kuratsuji and R. Seto, "Novel aspects of evolution of the Stokes parameters for an electromagnetic wave in anisotropic media," *Prog. Theor. Phys.,* **116**, 285-294 (2006).
9. Y.A. Kravtsov, B. Bieg and K.Y. Bliokh, "Stokes-vector evolution in a weakly anisotropic inhomogeneous medium," *J. Opt. Soc. Am. A.,* **24**, 3388-3396 (2007).

10. F. Flossmann, K. O'Holleran, M.R. Dennis, et.al., "Polarization Singularities in 2D and 3D Speckle Fields," *Phys. Rev. Lett.,* **100**, 203902 (1–4) (2008).
11. Freund I. "Optical Möbius strips in three-dimensional ellipse fields: I. Lines of circular polarization," *Opt. Commun.,* **283**, 1–15 (2010).
12. Freund I. "Optical Möbius strips in three-dimensional ellipse fields: I. Lines of linear polarization," *Opt. Commun.,* **283**, 16–28 (2010).
13. Freund I, "Möbius strips and twisted ribbons in intersecting Gauss Laguerre beams," *Opt. Commun.,* **284**, 3816–3845 (2011).
14. H. Kuratsuji and S. Kakigi, "Maxwell-Schrödinger equation for polarized light and evolution of the Stokes parameters," *Phys. Rev. Lett.,* **80**, 1888-1891 (1998).
15. G. Gibson, J. Courtial, M. Padgett, et.al., "Free space information transfer using light beams carrying orbital angular momentum," *Opt. Express.,* **12**, 5448–5456 (2004).
16. Jian Wang, "Advances in communications using optical vortices," *Photon. Res.,* **4**, B14-B28 (2016).

Appendix

Stokes Polarimetry

A.1 Polarization ellipse and Stokes polarization parameters [1-3]

A pair of plane waves that are orthogonal to each other at z=0 plane are represented by

$$E_x(t) = E_{0x}(t)\cos[\omega t + \delta_x(t)] = E_x \exp(i\omega t) \quad \text{(A.1)}$$

$$E_y(t) = E_{0y}(t)\cos\left[\omega t + \delta_y(t)\right] = E_y \exp(i\omega t) \quad \text{(A.2)}$$

Where $E_{0x}(t)$ and $E_{0y}(t)$ are the instantaneous real amplitudes, ω is the instantaneous angular frequency, $\delta_x(t)$ and $\delta_y(t)$ are the instantaneous phase factors and $E_x = E_{0x}\exp(i\delta_x)$ and $E_y = E_{0y}\exp(i\delta_y)$ are the complex amplitudes. The explicit removal of the term ωt from eq. A.1 and A.2 yields the equation for polarization ellipse, which is valid at a given instant of time.

$$\frac{E_x^2(t)}{E_{0x}^2(t)} + \frac{E_y^2(t)}{E_{0y}^2(t)} - \frac{2E_x(t)E_y(t)}{E_{0x}(t)E_{0y}(t)} cos\delta(t) = sin^2\delta(t) \quad \text{(A. 3)}$$

where $\delta(t) = \delta_x(t) - \delta_y(t)$ is the relative phase difference. For monochromatic radiation the amplitudes (E_{0x} and E_{0y}) and the phase (δ) are constants. Considering the time average of above equation, we get

$$\frac{\langle E_x^2(t)\rangle}{E_{0x}^2} + \frac{\langle E_y^2(t)\rangle}{E_{0y}^2} - \frac{2\langle E_x(t)E_y(t)\rangle}{E_{0x}E_{0y}} cos\delta = sin^2\delta \quad \text{(A. 4)}$$

Where $\langle E_i(t)E_j(t)\rangle = \lim_{T\to\infty} \frac{1}{T}\int_0^T E_i(t)E_j(t)\,dt; \qquad i,j = x,y$

Multiplying eq. (A.4) by $4E_{0x}^2E_{0y}^2$, we get

$$4E_{0y}^2\langle E_x^2(t)\rangle + 4E_{0x}^2\langle E_y^2(t)\rangle - 8E_{0x}E_{0y}\langle E_x(t)E_y(t)\rangle cos\delta = \left(2E_{0x}E_{0y}sin\delta\right)^2 \quad \text{(A. 5)}$$

On substituting the time average values derived from eq. (A.1) and eq. (A.2), we arrive at

$$2E_{0x}^2E_{0y}^2 + 2E_{0x}^2E_{0y}^2 - \left(2E_{0x}E_{0y}cos\delta\right)^2 = \left(2E_{0x}E_{0y}sin\delta\right)^2 \quad \text{(A. 6)}$$

Adding and subtracting $E_{0x}^4 + E_{0y}^4$ on left hand side of above equation results in perfect squares.

$$\left(E_{0x}^2 + E_{0y}^2\right)^2 - \left(E_{0x}^2 - E_{0y}^2\right)^2 - \left(2E_{0x}E_{0y}cos\delta\right)^2 = \left(2E_{0x}E_{0y}sin\delta\right)^2 \qquad (A.7)$$

Now, we introduce these quantities in terms of Stokes parameters as

$$S_0 = E_{0x}^2 + E_{0y}^2 = E_x^* E_x + E_y^* E_y$$

$$S_1 = E_{0x}^2 - E_{0y}^2 = E_x^* E_x - E_y^* E_y$$

$$S_2 = 2E_{0x}E_{0y}cos\delta = E_x E_y^* + E_y E_x^* \qquad (A.8)$$

$$S_3 = 2E_{0x}E_{0y}sin\delta = i(E_x E_y^* - E_y E_x^*)$$

$$and\ \ S_0^2 = S_1^2 + S_2^2 + S_3^2$$

Now, the polarization ellipse parameters such as ellipse orientation angle (ψ) and ellipticity (χ) can be expressed in terms Stokes parameters as follows

$$\psi = \frac{1}{2}tan^{-1}\left(\frac{2E_{0x}E_{0y}cos\delta}{E_{0x}^2 - E_{0y}^2}\right) = \frac{1}{2}tan^{-1}\left(\frac{S_2}{S_1}\right)$$

$$\chi = \frac{1}{2}sin^{-1}\left(\frac{2E_{0x}E_{0y}sin\delta}{E_{0x}^2 + E_{0y}^2}\right) = \frac{1}{2}sin^{-1}\left(\frac{S_3}{S_0}\right) \qquad (A.9)$$

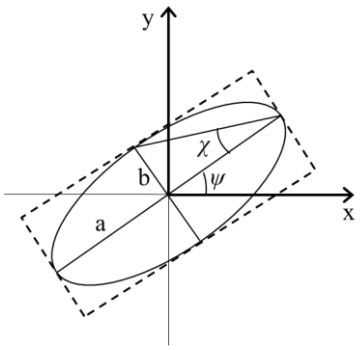

Fig. A.1. Polarization ellipse oriented at an angle ψ with respect to positive x-axis with an ellipticity$\chi = b/a$; a, b are the semi major and semi minor axes.

A.2 Stokes parameters in terms of intensity of images (Experimental determination)

The electric field that passed through a retarding element with retardation ϕ and a polarizer making an angle θ is given by

$$E = E_x e^{i\phi} cos\theta + E_y e^{-i\phi} sin\theta \quad (A.10)$$

The intensity of the light is then defined as

$$I = E.E^* \quad (A.11)$$

Substituting eq. (A.10) in eq. (A.11) and rearranging the terms we get

$$I = E_x E_x^* cos^2\theta + E_y E_y^* sin^2\theta + E_x^* E_y e^{-i\phi} sin\theta cos\theta + E_x E_y^* e^{i\phi} sin\theta cos\theta \quad (A.12)$$

From the definition of Stokes parameters from eq. (A.8) and using the trigonometric relations, the above equation can be reduced to

$$I(\theta, \phi) = \frac{1}{2}[S_0 + S_1 cos2\theta + S_2 cos\phi sin2\theta + S_3 sin\phi sin2\theta] \quad (A.13)$$

Equation (A.13) is the Stokes' intensity formula for measuring four Stokes parameters. The first three Stokes parameters (S_0, S_1, S_2) are measure using a single polarizer by rotating it to discrete angles 0°, 45°, 90° and 135°, which correspond to horizontal, diagonal, vertical and anti-diagonal polarizations respectively. The fourth Stokes parameter (S_3) is determined by placing a quarter wave plate at angle 90° before the polarizer and then the polarizer is rotated to 45°, and 135° for the measurement of right and left circular polarization content of the beam respectively. From eq. (A.13), the Stokes parameters in terms of measured intensities of the light beam for these discrete angles can be written as

$$\begin{aligned} S_0 &= I(0^o, 0^o) + I(90^o, 0^o) \\ S_1 &= I(0^o, 0^o) - I(90^o, 0^o) \\ S_2 &= I(45^o, 0^o) - I(135^o, 0^o) \\ S_0 &= I(45^o, 90^o) - I(135^o, 90^o) \end{aligned} \quad (A.14)$$

Thus, by measuring the intensities of images, Stokes parameters can be estimated.

References

[1] Dennis H. Goldstein, Polarized Light, CRC Press, London (2011)

[2] Max Born and Emil Wolf, Principles of Optics, Cambridge University Press (2003)

[3] C. Brosseau, Fundamentals of polarized light, John Wiley & Sons (1998)

List of Publications

International Journal Publications

1. C. Hari Krishna and Sourabh Roy, "**Analyzing characteristics of spiral vector beams generated by mixing of orthogonal LP_{11} modes in few-mode optical fiber**", *Appl. Opt.*, 57, 3853-3858 (2018).

2. C. Hari Krishna and Sourabh Roy, *"***Generation of inhomogeneously polarized vector vortex modes in a few mode optical fiber***", Opt Quant Electron*, 51: 41, 1-10 (2019).

3. C. Hari Krishna and Sourabh Roy, "**Poincare sphere representation for vector vortex modes of few-mode optical fiber**," *Opt. Eng*., 58(1), 016109, 1-6 (2019).

4. C. Hari Krishna and Sourabh Roy, "**Controlled generation of isolated C-points in few mode optical fiber**," communicated to *Optics Communications.*

International Conferences

1. C. Hari Krishna and Sourabh Roy "**Generation and Switching of Phase Vortices in Cylindrical Vector Beams**," Poster presentation in *Frontiers in Optics*, 17-21 Oct, 2016, Rochester, USA.

2. C. Hari Krishna and Sourabh Roy "**Optical Vortices in Higher Order LP modes of Few mode Optical Fiber**," Oral presentation in *Photonics 2016*, 04-08 Dec, 2016, IIT Kanpur, India.

3. C. Hari Krishna and Sourabh Roy "**Singularities in higher order modes of few mode optical fiber,**" Oral presentation in *FOTONICA*, 03-05 May, 2017, Padua, Italy.

4. C. Hari Krishna, VDR Pavan, and Sourabh Roy, "**Spirally polarized OAM beam generation in few-mode fiber**," Poster presentation in *SPIE Optics+Photoncs*, 19-23 Aug, 2018, San Diego, USA.

5. C. Hari Krishna, VDR Pavan, and Sourabh Roy, "**Generation of vector vortex modes from tilted polarized LP_{11} modes in a few-mode fiber**," Poster presentation in *Photonics 2018*, 12-15 Dec, 2018, IIT Delhi, India.